Muscle Activating Force Detection Using Surface Electromyography

表面筋電位を用いた筋活動力検出に関する研究

DOCTORAL DISSERTATION

Saran Keeratihattayakorn

Division of Human Mechanical Systems and Design
Graduate School of Engineering
Hokkaido University

Table of Contents

Chapter 1 Introduction

1.1 Background

Biomechanics is the science that deals with structure and function of living organism by combining mechanical engineering principles and biological knowledge. The role of biomechanical engineering is to implement the knowledge of biomechanics to help in improving the people's quality of life. The applications of biomechanics are including clinical application in treatment or prevention of injury, rehabilitation, ergonomic design and sport.

Muscle is vital to human life. The human strength is determined by the ability of muscle to exert force. There are more than 500 muscles in a human body which account for about 43% of the typical body mass. Each muscle has its own particular role in human movement. The primary purpose of muscle is to produce force. Skeletal muscles attached to bones by tendon and have the property of actively contracting and shortening. Human locomotion and muscle force is strongly correlated. The movement of human body is achieved by complex cooperation of muscles that cross the joint. The mechanics of muscle is concerned with the force created in a contraction and the factors that affect the level of force. The knowledge of "why" and "how" the muscle work is essential for improved human performance, preventing or treating injury, and development of effective rehabilitation procedure.

Study of human muscle is the main interest of scientist and biomechanical engineer for a long time. Muscle mechanics have been studied in vivo (within a living body), in situ (in the original biological location but with partial isolation) and in vitro (isolated from a living body). The early work of studying musculoskeletal system was made by Leonardo da Vinci, who spent much of his time in the analysis of muscles and their functions. Anatomical analysis provides the foundation knowledge of muscle. The bodies were dissected and studies as separate entities. Andreas Vesalius published his masterpiece work, the Fabrica, providing visual detail of human muscle. In the past, only basic anatomy was studied but their functional importance was overlooked. Until recently, the information of muscle could only be obtained

from cadavers or dead muscle rather than their active state due to the technical limitation and ethical restrains, not all measurements can be performed on living human muscle. Studying muscle in vivo requires tool that can observed muscle while it is still alive.

In the past decades, many researchers are interested in measuring muscle force during contraction. Direct measurement of muscle force in vivo is generally impractical and limited to invasive measurement (Ravary, et al., 2004) such as putting force transducers directly into tendons or ligaments (Fukashiro, et al., 1993; Finni, et al., 1998; Dennerlein, 2005). These techniques require surgery which is invasive and impractical. Thus, indirect method base on predictive model was get more attention from researchers. One of the most significant muscle research works belongs to A.V. Hill. With 50 years of details works on muscle mechanics resulting in a Nobel prize in physiology in 1922. The famous Hill's model describes the relationship between force-length-velocity relationships in muscle. His works provide groundwork for human muscle model which used widely in muscle research.

From a biomechanical standpoint, there is a relation between the internal muscle force that produces joint moments and the external force that is human body imparts on a work object. In order to determine the muscle force in a noninvasive manner, many method based on mathematical models were developed (Erdemir, et al., 2007). Inverse dynamic model based on linked body segment has been developed to estimate muscle force (Seireg and Arvikar, 1975; Amis, et al., 1980). With the help of advance computational technology, the calculation process can be done faster and these models can be used to estimate joint torque which is the result of all muscle forces acting on that joint. However, the limitation of inverse dynamic model is that the human joint is a redundant system with more unknowns than the equilibrium equations. Thus, the result is usually be total joint torque or total muscle force. To solve this problem the optimization method has been used to estimate muscle force (Raikova, 1992; Amarantini and Martin, 2004; Heintz and Gutierrez-Farewik,

2007). Inverse dynamic model and optimization have proved to be a potential tool for muscle force estimation. However, without muscle activity involve in the model it is impossible to specify which muscle generates force during movement.

The electromyography (EMG) signal was well known to be related to muscle force generation. The first observation of the relationship between electricity and muscle contraction was made by Luigi Galvani in 1791. His experiment showed that frog muscle contraction can be induced by electrical stimulation. This discovery was the starting point of neurophysiology. The first to report the detection of surface electrode with a primitive type of galvanometer was Raymond in 1849. In the last two decades, the method for detecting and processing EMG signal have been largely refined with the availability of better equipment, tool and computational techniques and becoming an important tool for research and clinical applications. Knowledge of the role of individual muscles in movement is founded on such analysis of the EMG signal. Using EMG as an indicator of the mechanical function of muscle is challenged due to the fact that the EMG reflects the electrical, not the mechanical event of a contraction. However, the application of current equipment for detecting and processing the signal remains the motivation for the use of EMG as a tool for measuring of muscle force.

Overused of muscle or disease can cause muscle dysfunction, limiting the ability of movement. Identifying the impaired muscle during contraction is important for effective treatment. However, sense of human is limited; sensor or scientific tool is required to improve the ability to observe muscle activity. One of the roles of biomechanical engineer is to provide tools for studying muscle function. Currently there is no practical tool ready for muscle force measurement. Development of method to estimate muscle force will be very useful in both biomechanical and medical fields.

1.2 Scope and aim of this study

To understand how muscles work together, it is required a tool that can "see" the activity of muscle and a method to "measure" individual muscle force. Using surface EMG signal which detected from skin surface is one way to measure muscle activity in a non-invasive manner. In recent years method for detecting and processing EMG signal have been improved considerably. The aim of this research is to develop methods to estimate muscle forces using surface EMG signal. In this thesis, a series of study and research were conducted to achieve the aim.

The main focus of this study is muscle force during human locomotion in daily activity such as carrying an object, using a hand tool and walking. Upper and lower limb are the important parts of the human body that defines the dexterity. The development of a method to estimate muscle force from EMG required knowledge of many aspects, starting from EMG detection technique, interpretation of the detected signals, and understanding the relationship between muscle force and EMG signal. A practicable muscle force estimation technique called EMG-driven model was developed and implemented to estimate muscle force during elbow and knee joint movement. EMG signal from the muscles were measured by pairs of bipolar electrode and used to estimate muscle force. The results show the effect of dynamic motion on the EMG signals. Increasing in muscle force or movement speed affects the amplitude of EMG signal. It seems that EMG-driven model is practical in estimate muscle force in major joint where surface EMG signals from muscles are detectable, like those of the upper arm and legs. However, in the human forearm, there are many muscles that are used to control the complex movement of fingers and hand. These muscles are relatively small and difficult to detect by conventional surface electrode. The problem of detecting unwanted signals or cross-talk is the main problem in assessing muscle activity in forearm region.

To overcome the cross-talk problem a novel method called electromyography computed tomography (EMG-CT) was developed to measure individual muscle activity within the deep forearm region using multi surface electrode (Nakajima, et al., 2014). This developed method provides a tool to visualize muscle activity within the forearm. The present study developed a method to estimate muscle stress i.e., force generated during contraction per unit area in the whole cross-section of the forearm during hand action using EMG-CT, the relationship between force and muscle activity during gripping was investigated. A model related muscle activity and force was developed. Muscle stress, was estimated during hand gripping. This method provides a new way of measuring muscle stress in the human forearm.

Chapter 2 Muscle Physiology and Electromyographic Phenomena

2.1 Muscle physiology

An understanding of musculoskeletal systems and their mechanical properties is important in biomechanics study. Anatomy study provides essential information for musculoskeletal structures and joint motions relate to human movement. Skeletal muscle varies in shape, size, and function. The role of skeletal muscle is to act as motor that move the bones about joint. Muscles are attached to bones by tendons. When muscle contracts, force transmit from one bone to another through joint and generate motion. The human body can be represented as a system of articulated segments in static or dynamic balance. Mechanically, there are three main types of muscle contractions: isometric, isotonic, and isokinetic. During isometric contraction, muscle develops tension without shortening. Isotonic refers to muscle developing a constant tension, and isokinetic is a muscle contraction at a constant velocity. A concentric action occurs when the torque that muscle group makes is larger than the torque of a resistance, resulting in muscle shortening. An eccentric muscle action is the lengthening of an activated muscle.

Skeletal muscle is hierarchically organized, as shown in Fig. 2.1. Muscle is composed of a large number of muscle fibers. Each fiber also contains many myofibrils. The myofibril contains a series of sarcomeres that make the striated appearance of skeletal muscle. The active tension of whole muscles based on the interaction of two contractile proteins in sarcomeres i.e. actin and myosin. Cross-bridges between myosin and actin are attached and detached with chemical energy stored in adenosine triphosphate (Huxley and Hanson, 1954). This mechanism generates tension within a muscle fiber.

The tension created by a muscle contraction also depends on the length of the muscle, and the velocity of contraction. A muscle produces the maximum amount of tension when it is lengthened slightly beyond resting length. In concentric muscle contractions, a muscle can produce less tension as shortening velocity increases. In eccentric muscle contraction, the maximum tension a muscle can produce increases as the speed of lengthening increases.

Motor unit (MU) is the basic building block for the production of force and movement, both in reflex and voluntary contractions. MU is defined as a set of muscle fibers innervated by the same motoneuron as shown in Fig 2.2. MU can vary in size considerably. The MUs are distributed throughout the cross-sectional area of the muscle. The amount of force and power generated by muscle is directly related to the type, number, and size of motor units in the muscle. There are two type of muscle fiber in mammalian skeletal: slow twitch motor unit (Type I) which are recruited for light to moderate intensity activity and fast twitch motor unit (Type II) which capable of high force production and fast contraction speed.

The force and velocity of body movement is controlled by motor unit recruitment and rate coding. Slow twitch motor units are recruited first and the fast twitch fatigable units are recruited only when fast powerful movement is required. Each time a contraction is repeated, a particular motor unit is recruited at the same force level. At high force levels after every motor units have been recruited, additional force is generated by increasing the firing frequencies of the motor units.

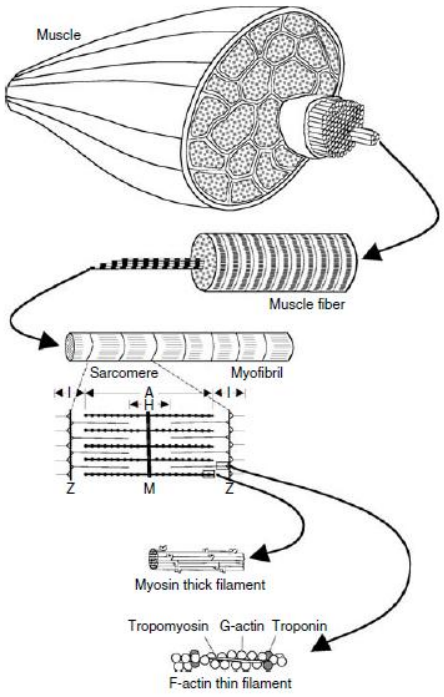

Figure 2.1 Organization of skeletal muscle from the muscle fibers to the protein filament (Freivalds, 2011).

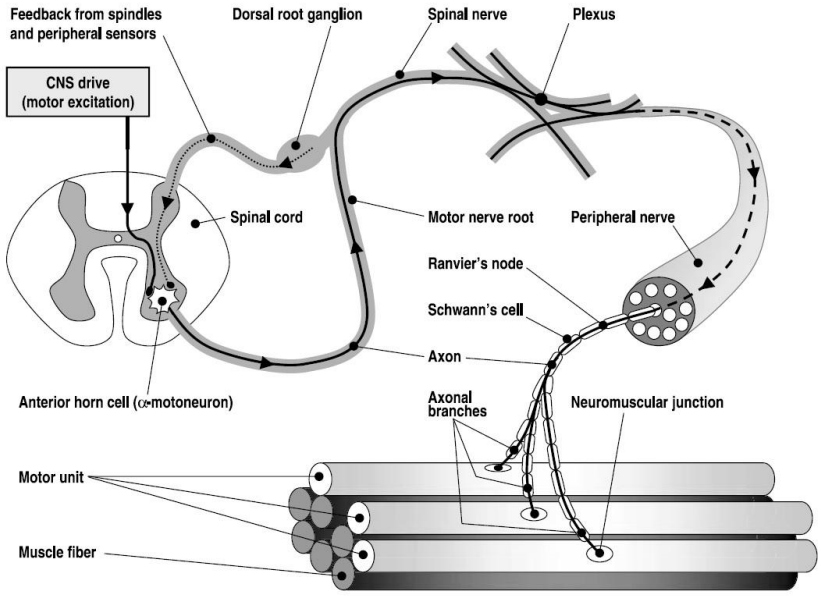

Figure 2.2 Motor unit structure. The motoneuron innervates a certain number of muscle fibers by the neuromuscular junctions (Roberto, et al., 2003).

2.2 Electromyographic phenomena

Electromyography (EMG) is the study of muscle function through the electrical signal that the muscles emanate. EMG has been used in studying of muscle function and in clinical application such important topics as musculoskeletal injury, carpal tunnel syndrome, and muscle fatigue. Modern instrumentation has been developed to facilitate easy acquisition of EMG data. Surface electrode is usually used to measure EMG signal from skin surface due to its non-invasive and ease of use. In the past decades, EMG study progress significantly. However, the interpretation of EMG signals stills has many issues unresolved.

2.2.1 Origin of EMG signal

Muscle fibers are active by the central nervous system through electric signals transmitted by motoneurons. A chain of events occur before a muscle fiber contracts. Each muscle fiber is surrounded by a plasma membrane called the sarcolemma. The excitability of muscle fibers through neural control can be explained by a model of a semi-permeable membrane describing the electrical properties of the electrical properties of sarcolemma. Central nervous system activity initiates a depolarization in the motoneuron. The depolarization is conducted along the motoneuron to the muscle fiber's motor endplate. At the endplate, a chemical substance is released causing a rapid depolarization of the muscle fiber under the motor endplate. Resulting in depolarization of the muscle fiber membrane which triggers muscle contraction (Lucas, 1909). This rapid depolarization, and the subsequent repolarization of the muscle fiber, is an action potential. The propagated action potential spreads along the sarcolemma and into the muscle fiber. The EMG signal is based on action potentials at the muscle fiber membrane resulting from depolarization/repolarization processes.

In order to study EMG signal generated from muscle fiber. EMG technique is based on the fact that local electrophysiological processes result in a detectable flow of the transmembrane current at a certain distance from the

active sources (i.e., muscle fiber). This flow of current in the tissue (i.e., the volume conduction), allows EMG measurements to be made at a distance from the sources. The principle of volume conductivity is important. In general, the simplest model used to interpret extracullular action potentials of muscle is the dipole concept (R, 1947; Plonsey, 1974). The basis of surface EMG is the relationship between the action potentials of muscle fibers and the extracellular recording of those action potentials at the skin surface. Electrodes external to the muscle fiber can be used to detect action potentials.

2.2.2 Surface EMG detection technique

When muscle generates force, there are electric signals that generated and propagate along muscle fiber; these signals can be detected by placing electrode on the skin surface (Fig. 2.3). Surface electrodes are generally used in the bipolar configuration. In bipolar electrode configuration, two electrodes are used at the detection site and a third common-mode reference, or ground electrode is placed distally in a neutral electrical environment. This arrangement of electrodes is dictated by the use of a differential preamplifier as the means of signal amplification. The differential preamplifier increased the amplitude of the difference signal between each of the detecting electrodes and the common mode reference. Signals that are common to both detection electrode sites are termed common mode signals and produce a nearly zero preamplifier output. This desirable characteristic of differential preamplifiers significantly improves the signal-to-noise ratio of the measurement and allows the detection of low level EMG potentials in noisy environment.

The observed EMG signal is filtered by the tissue and the electrode in the process of being detected, it is necessary to amplify it. This might affect the frequency characteristics of the signal. It is important to note that the characteristics of the observed EMG signal are a function of the apparatus used to acquire the signal as well as the electrical current which is generated by the muscle fibers.

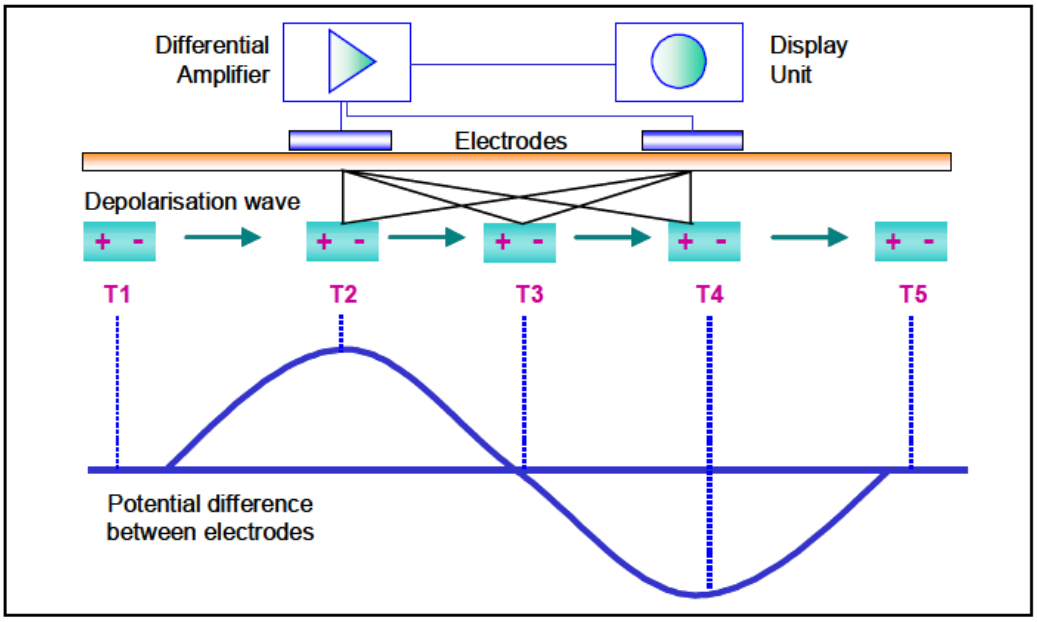

Figure 2.3 The model of wandering electrical dipole on muscle fiber membrane. The surface electrodes are attached to skin surface to detect EMG signal (Kumar and Mital, 1996).

The relationship between muscle force and EMG signal is the main focus in EMG study. It is desirable to estimate muscle force by using surface EMG signal which can be detected easily by surface electrode. During muscle contraction, electrical and mechanical events occur simultaneously. Muscle fiber starts the process of contraction when depolarization releases calcium ions. The amount of force is controlled by changes in the number of recruited MUs or by changes in the frequency of recruitment (Adrian and Bronk, 1929). The muscle action potential is the temporal and spatial summation of individual action potentials of all fibers of a MU which detected by surface electrode on skin surface. The detected signals usually contain activity of more than one muscle.

The relationship between muscle force and EMG during voluntary contraction is not yet well understood. Many studies report the relationship between the EMG and force (Messier, et al., 1971; Pruim, et al., 1980; Metral and Cassar, 1981). The greater the ability of recruit MUs simultaneously, the greater the force produced by the muscle. Many studies have found that surface EMG signal change in proportional to the increasing of muscle force for isometric contraction but others claim that this relationship is not linear (Hof, 1984; Karlsson and Gerdle, 2001; Del Santo, et al., 2007).

There are many factors that influence the relationship between EMG and force. The acquisition procedure, the kinematics of the body movement, and the processing methods used, all have an effect on the muscle force-EMG relationship. The cross-talk problem is the main factor when detecting signal from smaller muscles where the surface electrodes must be placed close to the adjacent musculature. In general, it is difficult to identify precisely the source of contamination of the physiological signal. The problem of cross-talk from adjacent muscles is the major concern of using surface electrode to detect muscle activity especially, in forearm region where many muscles are packed together. The amount of cooperative activity can also change the contribution of muscle strength, thus affect the relationship between force and EMG signal.

The activation patterns of individual muscles are not representative of all muscles in the same functional group, and there are differences in how muscles within a muscle group respond to training. Even individual muscle is quite sophisticated, with different motor unit activation depending on the task or muscle action. Type of contraction either isometric or anisometric and either isotonic or anisotonic also affect the relationship between EMG and muscle force. The used of EMG as a tool for determining the force is challenging due to complexity and variability in biological signals.

Chapter 3 An EMG-Driven Model for Estimating Muscle Force

3.1 EMG-driven model

In order to determine the muscle forces in a noninvasive manner, many methods based on mathematical models were developed (Erdemir, et al., 2007). The electromyography (EMG) signal was well known to be related to muscle force generation. EMG-to-force processing was well described by Hof and Van Den Berg (1981) and thus, EMG was introduced into the model to estimate the muscle force. The advantage of the EMG-driven model is that the processed EMG signal reflects the activation of each muscle crossing the joint, thus facilitating the accurate estimation of the individual muscle force. Interest in the EMG-driven model has grown recently after it was proven to be a powerful tool to estimate the muscle force in various movements (White and Winter, 1992; Feng, et al., 1999; Lloyd and Besier, 2003; Shao, et al., 2009).

An important part of the EMG-driven model is the musculotendon model, which indicates that, the change in length of muscle during contraction affects the potential force that a muscle can generate. The popular Hill-type muscle model is usually used to describe the contraction mechanism of the muscle. Muscle model parameters such as maximum isometric force (F_0), optimum muscle length (L_{FOPT}), and maximum shortening velocity (v_0) represent muscle force-length-velocity relationships. The accuracy of the estimated muscle force in the EMG-driven model depends on how well we estimate these parameters. However, muscle model parameters vary among individuals. Thus, a tuning process is required to estimate the appropriate value. Some researchers obtained these parameters by using calibration trials and optimization processes to tune the parameters (White and Winter, 1992; Lloyd and Besier, 2003; Shao, et al., 2009). The tuning process provides a set of muscle model parameters that account for a limit movement conditions. It has never been examined whether they can be applied to estimate the muscle force with respect to a different speed than that used in the calibration trials. As the knowledge of the manner in which muscle parameters respond to the change of

movement velocity is still limited, using the same set of parameters for different conditions can be problematic.

The influence of changing movement velocity on the muscular activity has been investigated. During repetitive movement such as cycling and walking, muscles in lower-limb increased their EMG activity level as the movement rate increased (Neptune, et al., 1997; Hof, et al., 2002). High-speed muscle contractions have been showed to enhanced EMG activities in the shoulder and leg muscles (Carpentier, et al., 1996; Laursen, et al., 1998; Brindle, et al., 2006). These finding demonstrate that there is a velocity effect on muscle force generation. Therefore, it is expected that changing the movement velocity or rate-effect would have an effect on muscle model parameters. Change in velocities has very important implication in sports, rehabilitation, ergonomics and treatment of motor unit disorders. In addition, the ability to change the velocity of ongoing movement is important feature to perform a proper daily activity. Thus, to confidently use the EMG-driven model, validation of the rate-effect on the muscle model parameters is required.

In the present study, we aimed to develop an EMG-driven model to estimate the muscle force during elbow and knee flexion/extension movement, and to determine the influence of the rate-effect on the model parameters of the Hill-type muscle model. The muscle model parameters were estimated using an EMG-driven model technique in combination with experimental measurements and an optimization process. The optimization process was used to minimize the difference between the estimated and the experimental results, by fitting the value of muscle parameters at various movement frequencies. We believe that the information derived from this study will be useful in modeling the dynamic performance of muscles and improving the existing model.

The muscle-tendon unit is composed of muscle fiber in series with the tendon, following the musculotendon model as described by Zajac (Zajac, 1989). The Hill-type model is composed of a contractile element (CE) in parallel with a passive element (PE) that is in series with the tendon (Fig. 3.1a). Thus, the force in the musculotendon unit, F_{MT} can be represented by:

$$F_{MT} = F_t = F_M cos(\varphi) = (F_{CE} + F_{PE}) cos(\varphi) \tag{3.1}$$

where F_t is the tendon force; F_M is the sum of forces in the CE (F_{CE}) and the PE (F_{PE}); the pennation angle, φ is the angle between the lines of action of the tendon and the muscle fiber. F_{CE} can be estimated by the generalized function:

$$F_{CE} = F_0 \cdot \alpha_l(l_M) \cdot \alpha_v(v_M) \cdot \alpha_{EMG}(t) \tag{3.2}$$

where $F_0 = PCSA \times \sigma_m$, F_0 is the maximum isometric force that the model can generate, which is a function of the physiological cross-section area (PCSA) and maximum muscle stress, σ_m. $\alpha_l(l_M)$ is the fraction of the F_0 that the muscle can produce at the current length, l_M (Figure 3.1b). $\alpha_v(v_M)$ is the fraction of F_0 that the muscle can produce at the current velocity v_M (Figure 3.1c). $\alpha_{EMG}(t)$ is the muscle activation measured from the EMG signal. The normalized force-length relationship, $\alpha_l(l_M)$ was calculated as described by Gallucci and Challis (2002), and is shown below:

$$\alpha_l(l_M) = 1 - \left(\frac{l_M - L_{FOPT}}{w \cdot L_{FOPT}} \right)^2 \tag{3.3}$$

where L_{FOPT} is the optimum length of muscle fiber and w is a parameter specifying the width of the force-length relationship. For the force-velocity relationship, Hill proposed a relationship between tension and muscle velocity

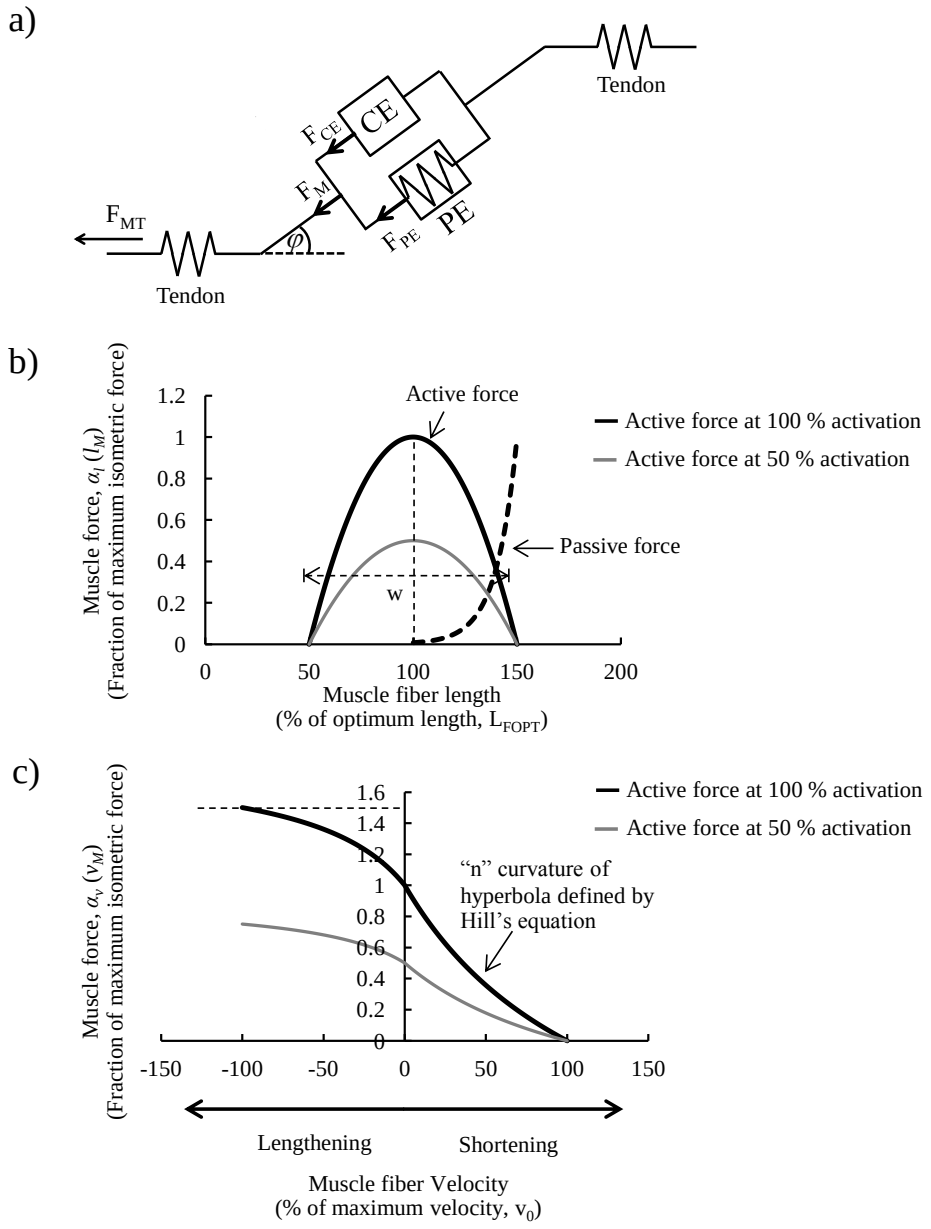

Figure 3.1 Hill type muscle model a) The muscle model is composed of a contractile element (CE) in series with a tendon and parallel to a passive element (PE). b) The force-length relationship of the CE element. Values are normalized by maximum isometric force (F_0) and optimum muscle length (L_{FOPT}). *w* is the width of the parabola in the force-length curve. c) The force-velocity relationship of the CE. Values are normalized by F_0 and maximum shortening velocity (v_0).

and described it by the equation (Hill, 1938):

$$(F_M + a)(v_M + b) = (F_0 + a)b \tag{3.4}$$

where a and b are Hill's constants normalized to F_0 and maximum shortening velocity v_0 respectively. The shape parameter in Hill's equation can be described by the ratio $n = a/F_0 = b/v_0$. The value of n ranges between 0.2 and 0.8 (White and Winter, 1992) thus, for concentric condition Hill's equation was rewritten in the form:

$$\alpha_v(v_M) = \frac{n(v_0 - v_M)}{(n \cdot v_0 + v_M)}, \text{ concentric} \tag{3.5}$$

for eccentric form of the force-velocity relationship the equation was presented by FitzHugh (1977) as:

$$\alpha_v(v_M) = 1.5 - 0.5\frac{n(v_0 - v_M)}{(v_M - 2 \cdot n \cdot v_0)}, \text{ eccentric} \tag{3.6}$$

These relationships indicate that the muscle force from muscle fiber contraction depends on the length and velocity of the muscle fiber. The muscle length and variable moment arms during flexion/extension were estimated using a musculoskeletal model. The model was scaled to fit the specific-subject model using the software OpenSim (version 3.2, Standford, USA) [Fig. 3.2] based on the length of the upper arm and forearm of each subject.

EMG is a measure of the depolarization of muscle fibers; the properly processed EMG signals can be used as an indirect measure of muscle activity. The "muscle activation dynamic" is used to transform raw EMG signals to muscle activation (Zajac, 1989), and this can then be used as input in the EMG-driven model. Raw EMG signals were processed to obtain normalized, rectified, filtered EMG, *emg(t)* and then a recursive filter (Buchanan, et al., 2004) was

used to determine the neural activation value, *u(t)*. This process can be approximated by a discrete eqaution:

$$u(t) = \alpha_t \cdot emg(t-d) - \beta_1 \cdot u(t-1) - \beta_2 \cdot u(t-2) \tag{3.7}$$

where d is the electromechanical delay, α_t, and β_1 and β_2 are coefficients that define the second-order dynamics. In the present study, the relationship between EMG and muscle activation was defined by an exponential relationship (Lloyd and Besier, 2003), where A is a non-linear shape factor constrained to $-3<A<0$, and is described as:

$$\alpha_{EMG}(t) = \frac{\left(e^{A \cdot u(t)} - 1\right)}{\left(e^{A} - 1\right)} \tag{3.8}$$

The passive force from PE (F_{PE}) can be represented by the exponential relationship described by Schutte (1993):

$$F_{PE}(l_m) = F_0 \frac{e^{10(l_M / L_{FOPT} - 1)}}{e^5} \tag{3.9}$$

Muscle force from each muscle can be calculated by muscle model described above.

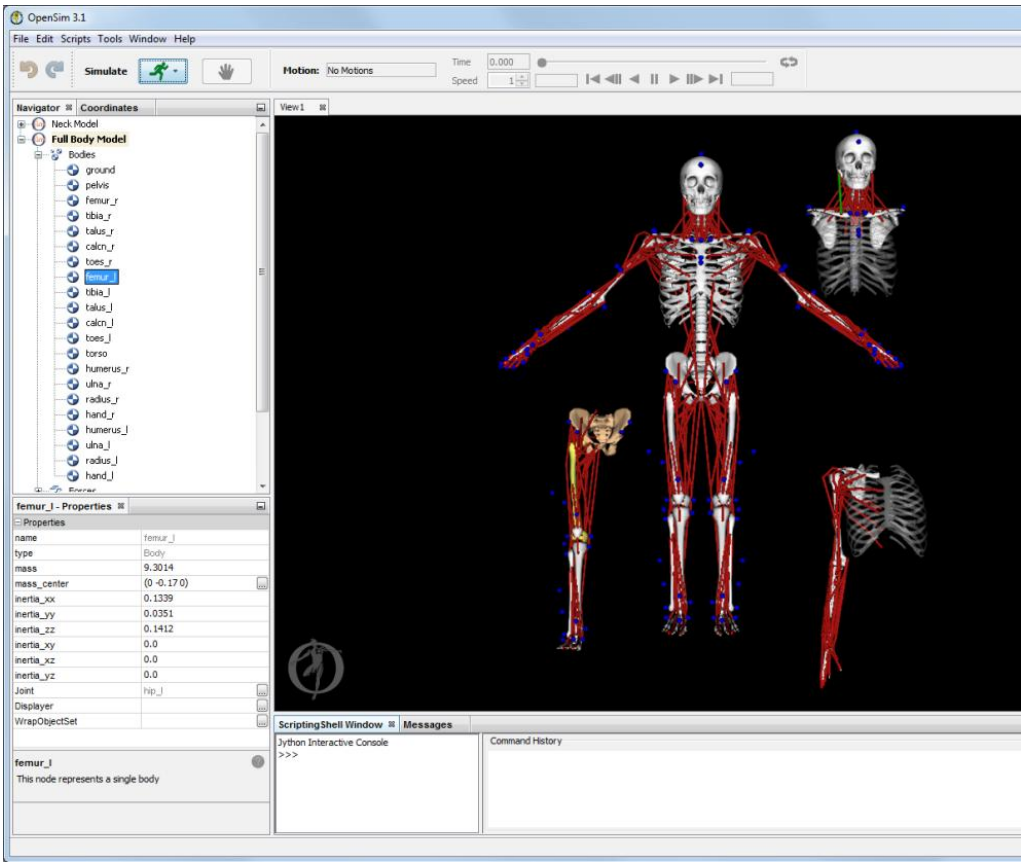

Figure 3.2 Opensim, a computational musculoskeletal model used to estimate muscle length and moment arm during joint movement (Delp, et al., 2007).

3.2 Muscle force estimation during elbow joint movement

Upper-limb motion is essential for performing daily activities, such as eating, drinking, washing of the face, brushing of the teeth and pushing/pulling objects. Any disability of the upper limb will limit the activities that a person can perform, thus making it difficult of an individual to lead a normal life. The elbow is an important mechanical link in the upper limb. The flexion/extension motion of the elbow primarily results from the reaction forces generated by the biceps and triceps. Knowledge of muscle mechanics is required for designing effective exercise training programs and developing rehabilitation procedures. In order to enhance our understanding of the muscle mechanics during elbow joint movement, the estimation of muscle force of the biceps and triceps in vivo is necessary.

3.2.1 Elbow joint model

In the present study, the elbow flexion/extension movement in the sagittal plane was described as a two-bar linkage with the biceps and triceps working as an agonist and antagonist pair of muscles (Fig. 3.3), while treating the forearm and hand as a rigid body with the elbow axis fixed. The equation of motion can be described by:

$$I_f \ddot{\theta}_e = F_M^b R^b - F_M^t R^t - m_f g d_f \cos\theta_e - TR \tag{3.10}$$

where I_f is the mass moment of inertia of the forearm and hand with respect to the elbow axis. θ_e and $\ddot{\theta}_e$ are the elbow flexion angle and angular acceleration, respectively. F_M^b is the force of the biceps and F_M^t is the force of the triceps. R^b and R^t are the moment arm of the biceps and triceps, respectively. m_f is the mass of the forearm and hand, and g is the gravitational acceleration. d_f is the length between the center of mass of the forearm and the elbow joint axis. T is the external load applied to the forearm and R is the distance between the position of applied load to the elbow joint axis.

3.2.2 Experiment procedure

Four healthy subjects (aged between 25 and 30 years) participated in this study. All the subjects volunteered to take part in the study and provided informed consent.

The subject was seated comfortably with the upper dominant arm laid vertically and supported by an adjustable stand. Surface EMG signals were acquired using 30-mm diameter electrodes (Ag/AgCl, Vitrode M, NIHON KOHDEN, Japan). The subject's skin was cleaned with alcohol before attaching the electrodes. Pairs of bipolar surface electrodes were aligned parallel to the muscle fiber and positioned on the mid-belly regions of the biceps and triceps of the subject's upper arm, according to the recommended position (Zipp, 1982). The raw EMG signal data were collected using surface EMG sensor (Biolog, DL-500, S&ME, Japan) at a sampling rate of 1000 Hz and were processed off-line by using the MATLAB software (Mathworks, USA). First, the raw EMG signals were filtered using the Butterworth bandpass filter (10-500 Hz), followed by full-wave rectification and filtering using a fourth-order Butterworth low-pass filter (3 Hz) for conversion to linear envelope profile (LE). Maximum voluntary contraction (MVC) exercises were performed against static resistance, for each muscle separately and used to normalize the processed EMG signals.

Elbow flexion angles were measured by using an electrogoniometer (SG75, Biometric, USA) which was attached on the subject's elbow. The external load was measured by the load cell (DTG-20, DigiTech Co.,LTD, Japan) that was fixed to the ground (Fig. 3.4). The electrogoniometer data and force data were sampled at 1000 Hz.

Before the test was initiated, the subjects were instructed to relax and practice moving their arm in a synchronized manner with a digital metronome (TU-80, Roland Corporation, USA); prior to beginning the test, the subjects were asked to maintain an initial position with the elbow at full extension (flexion angle = 0^{o}). Each subject performed two trials of elbow flexion and extension with movement frequencies of 0.2, 0.4, 0.6, 0.8, 1.0, and 1.2 Hz. For

each trial, a set of 4 cycles of elbow flexion/extension was performed. Each cycle start from full extension position to reach a stopper at 120^{o} of flexion. An adequate rest period was provided between each trial in order to avoid fatigue. Elbow joint angular velocity was obtained by numerical differentiation of the position joint angle that was measured using the electrogoniometer. The raw data for each trial were processed as described above and then averaged across 4 cycles for each subject.

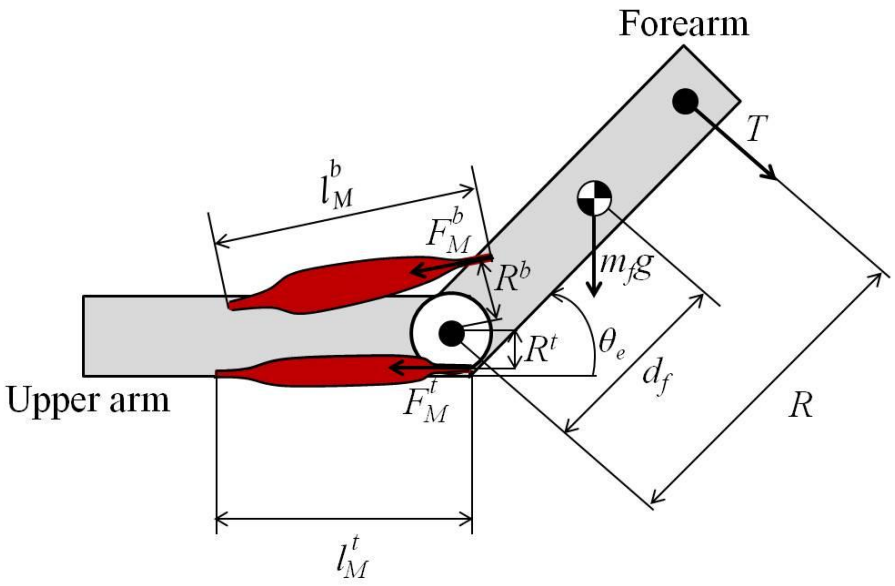

Figure 3.3 A schematic of a simple two-bar linkage model represents the arm with the biceps and triceps working as an agonist and antagonist pair of muscles.

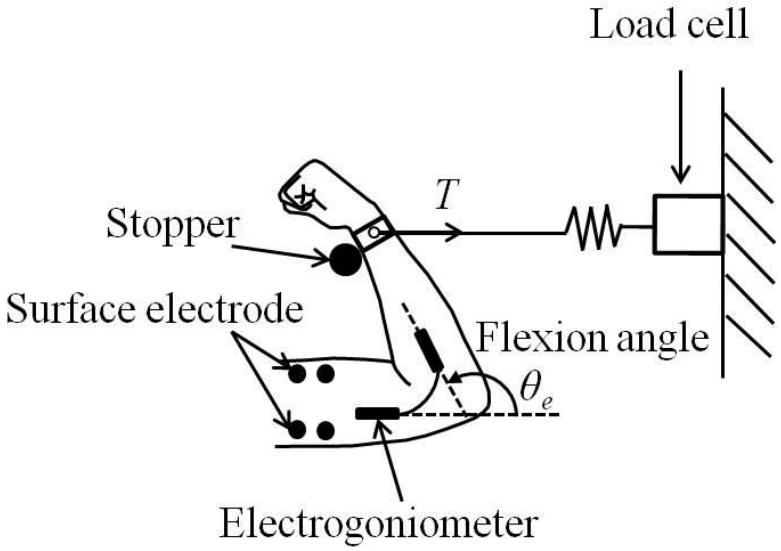

Figure 3.4 Schematic drawing of the experimental set-up. Pairs of surface electrodes were attached to the biceps and triceps to detect the EMG signal. The eletrogoniometer was attached to the elbow joint to measure the elbow flexion angle. A load cell was attached to the subject's wrist to measure the external force.

3.2.3 Optimization process

From the muscle model (Fig 3.1), the muscle model parameters to be optimized included F_0, $L_{FOPT,}$ w, v_0 and n. The specific set of muscle parameters for each movement condition was determined using an optimization method (Fig. 3.5). We have assumed that the external force applied to the body's limb estimated by the model should match those measured from the load cell. A simulated annealing algorithm was used to tune the model parameters by minimizing the objective function, (J) given by:

$$J = \sum_{1}^{n} \left(T_m - T_c\right)^2 \tag{3.11}$$

where n is the number of samples during the entire movement in each trial, T_m is the measured external force from the load cell and T_c is the estimated external force calculated from the model. The initial estimation of the muscle parameters was based on literature data (An, et al., 1981; Winters and Stark, 1985; Murray, et al., 2000; Hale, et al., 2011), and the values were allowed to vary within the physiological range. The optimization was calculated using the Optimization Toolbox in MATLAB (Mathworks, USA).

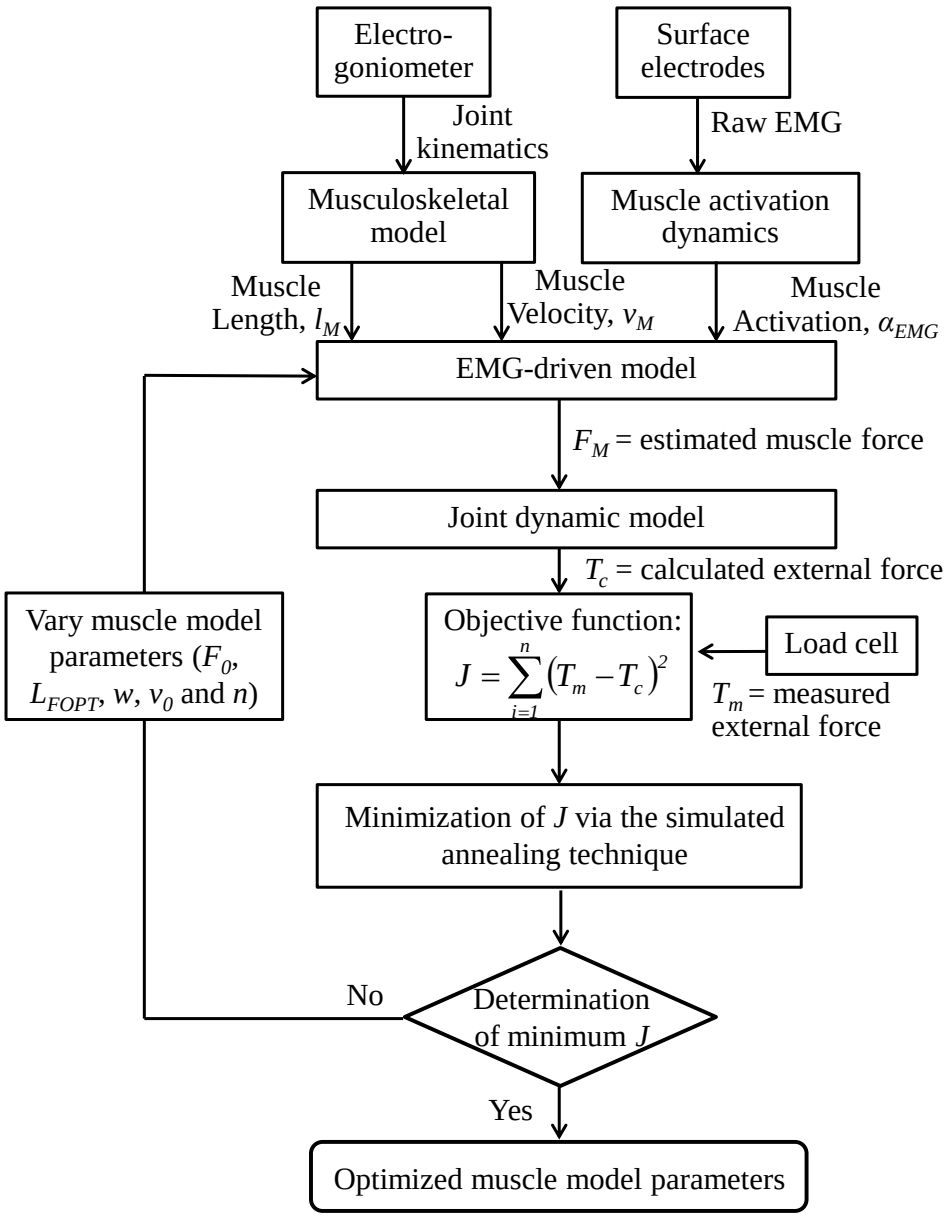

Figure 3.5 Optimization process to estimate muscle model parameters. The specific set of muscle parameters for each movement frequency was determined. The muscle model parameters to be optimized included maximum isometric force (F_0), optimum muscle length (L_{FOPT}), width of the force-length relationship (w), the maximum shortening velocity (v_0) and the curvature of the hyperbola defined in Hill's equation (n).

3.2.4 Results

There was a velocity effect for EMG activities of both biceps and triceps (Fig. 3.6a). As movement frequency increase from a slow speed (0.2 Hz) to faster speed (1.2 Hz), the profile of EMG activities change with considerably shortened in duration and increase in amplitude. The peak EMG magnitude values were calculated by scaling all the value with the MVC value of each subject. Both biceps and triceps demonstrated increase in peak EMG magnitude as movement frequency increase (Fig. 3.6b).

Table 3.1 shows the boundary of muscle model parameters in optimization process and optimized muscle model parameters. Figure 3.7 shows an example of a comparison between the measured external forces from the load cell (red solid line) and external force calculated from the model (blue dot line); the calculated force from the model appears to correspond to the measured force. The average coefficient of determination (R^2) and the normalized root mean square errors (RMSE) values between the measured external force and the estimated external forces were calculated at various movement frequencies (Table 3.2). We noted that the estimated force fits very well with the measured force, with the R^2 value ranging from 0.91 to 0.99 and the %RMSE value ranging from 5.56% to 16.13%.

The optimized values of the model parameters for biceps changed with the movement frequency (Fig 3.8). All the data were averaged for each subject and then across all subjects to obtain a group average. Thus, these results show that the muscle parameters changed according to movement frequency. This relationship was described as a linear relationship. The maximum isometric force of the biceps ($F_{0,b}$; y=117.84x+213.05, R^2=0.922) and the maximum velocity of shortening of the biceps ($v_{0,b}$; y=0.7113x+1.3193, R^2=0.9832), increased with increasing movement frequency, whereas the Hill's equation curvature of the biceps (n_b; y=-0.1962x+0.6992, R^2=0.8831) decreased with increasing movement frequency.

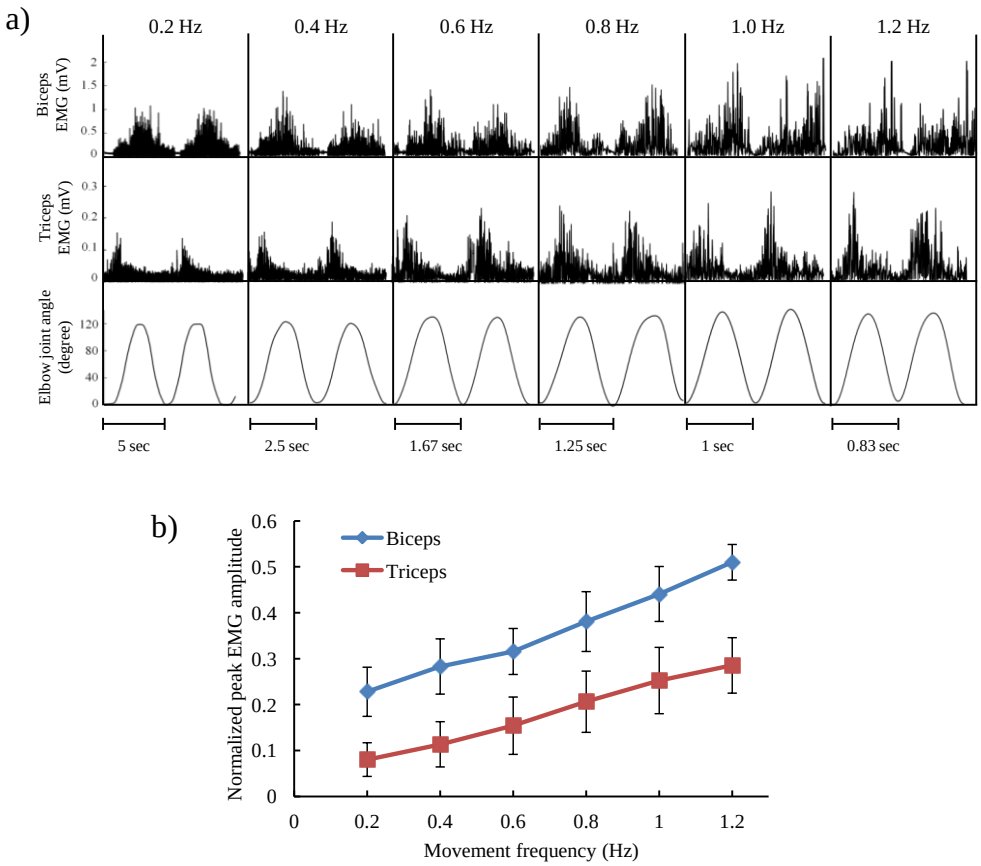

Figure 3.6 a) A representative recording of the biceps EMG (upper trace), triceps EMG (middle trace) and joint angle (lower trace) during elbow flexion/extension movement at various movement frequency (0.2-1.2 Hz). b) Relationship between the normalized peak EMG amplitudes of the biceps and triceps and movement frequency (0.2-1.2 Hz).

Table 3.1 Optimized muscle model parameters

Muscle model parameters	Boundary		Optimized value (SD)
	Min	Max	
Biceps			
$F_{0,b}$ (N)	180	475	295.54(45.92)
$L_{FOPT,b}$ (cm)	13.1	23.4	15.22(4.55)
w_b	0.4	1.44	0.83(0.04)
$v_{0,b}$ (m/s)	1	5	1.82(0.26)
n_b	0.2	0.8	0.56(0.08)
Triceps			
$F_{0,t}$ (N)	864	2320	1272.42(117.57)
$L_{FOPT,t}$ (cm)	9.90	36	30.91(1.30)
w_t	0.4	1.44	0.79(0.04)
$v_{0,t}$ (m/s)	1	5	2.69(0.53)
n_t	0.2	0.8	0.46(0.05)

Table 3.2 The average coefficient of determination (R^2) and the normalized Table root mean square errors (RMSE) expressed as differences between the measured external force and estimated external force calculated by the model.

Movement frequency	R^2	%RMSE
0.2 Hz	0.98 ± 0.01	5.56 ± 1.77
0.4 Hz	0.99 ± 0.01	6.77 ± 1.55
0.6 Hz	0.97 ± 0.03	6.55 ± 3.12
0.8 Hz	0.96 ± 0.04	9.75 ± 1.68
1.0 Hz	0.94 ± 0.06	12.09 ± 4.43
1.2 Hz	0.91 ± 0.08	16.13 ± 6.73

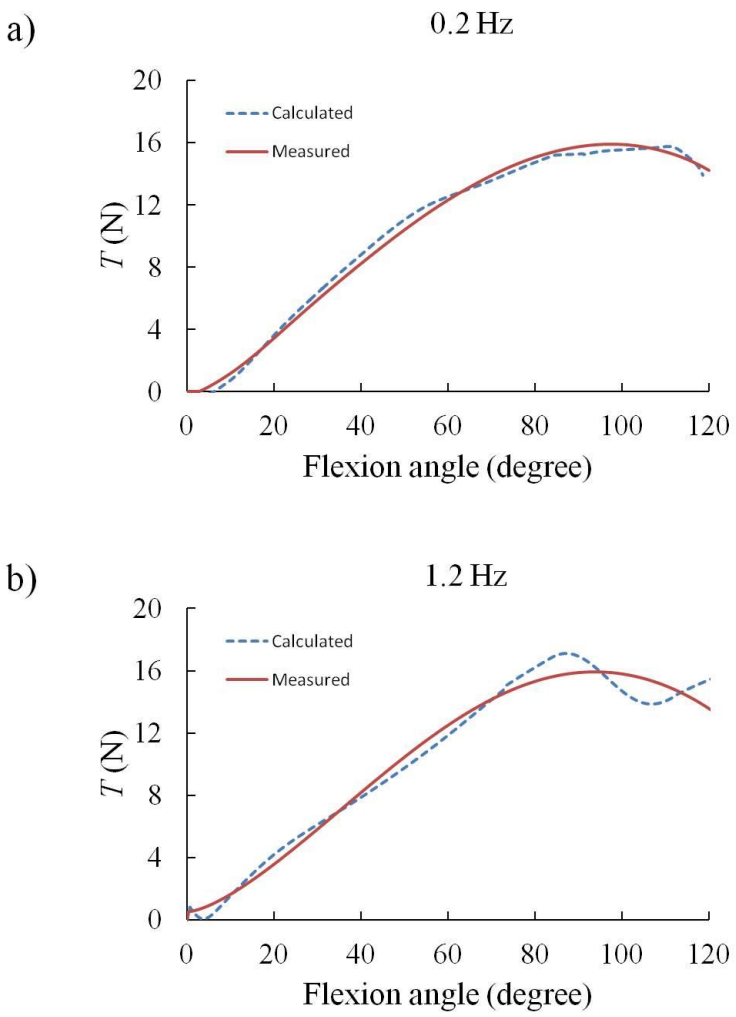

Figure 3.7 An example of comparison of the external force, *T* between measured force (red solid line) and estimated external force calculated from the model (blue dot line) in a) movement frequency 0.2 Hz and b) movement frequency 1.2 Hz.

Biceps

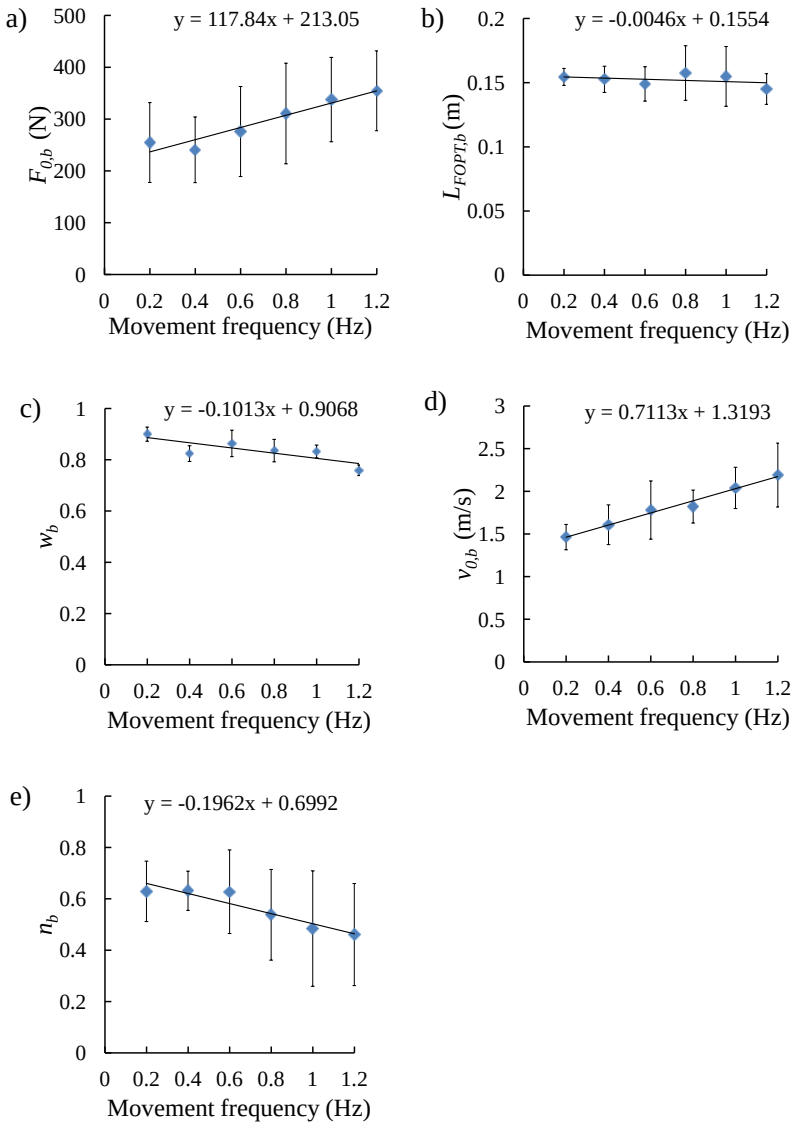

Figure 3.8 (continue)

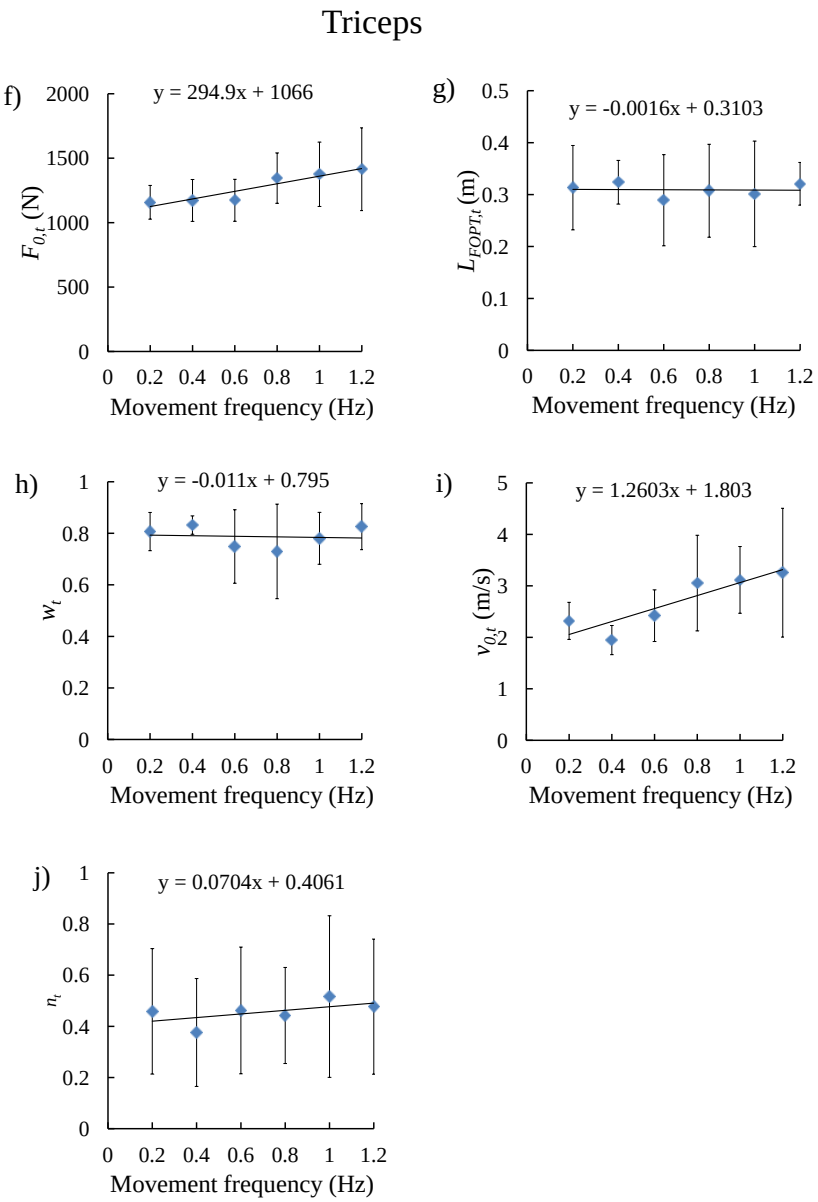

Figure 3.8 Mean optimized muscle parameters of the biceps and triceps according to the movement frequency a) $F_{0,b}$: maximum isometric force of the biceps, b) $L_{FOPT,b}$: optimum biceps length, c) w_b: the width of the force-length relationship of the biceps, d) $v_{0,b}$: maximum shortening velocity of the biceps, e) n_b: Hill's equation curvature of the biceps. f) $F_{0,t}$: maximum isometric force of the triceps, g) $L_{FOPT,t}$: optimum triceps length, h) w_t: width of the force-length relationship of the triceps, i) $v_{0,t}$: maximum shortening velocity of the triceps, and j) n_t: Hill's equation curvature of the triceps.

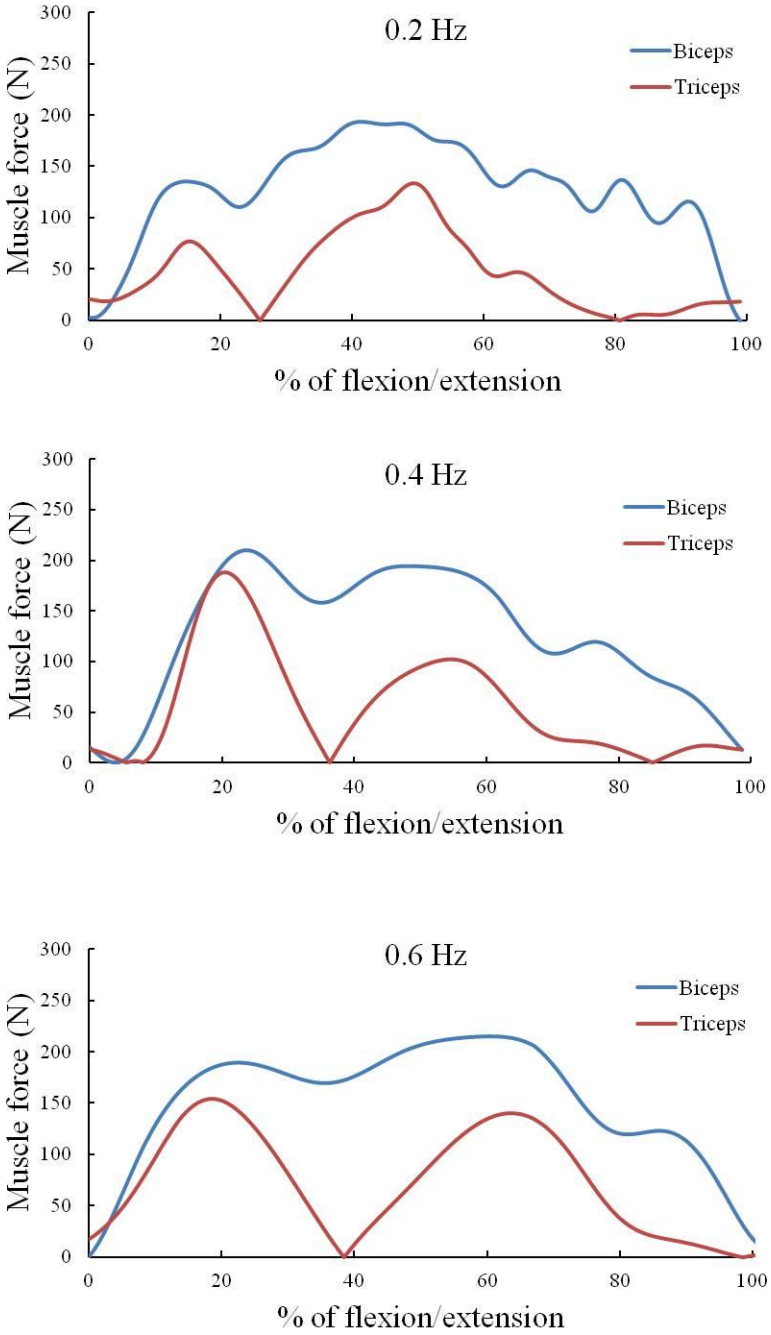

Figure 3.9 (continue)

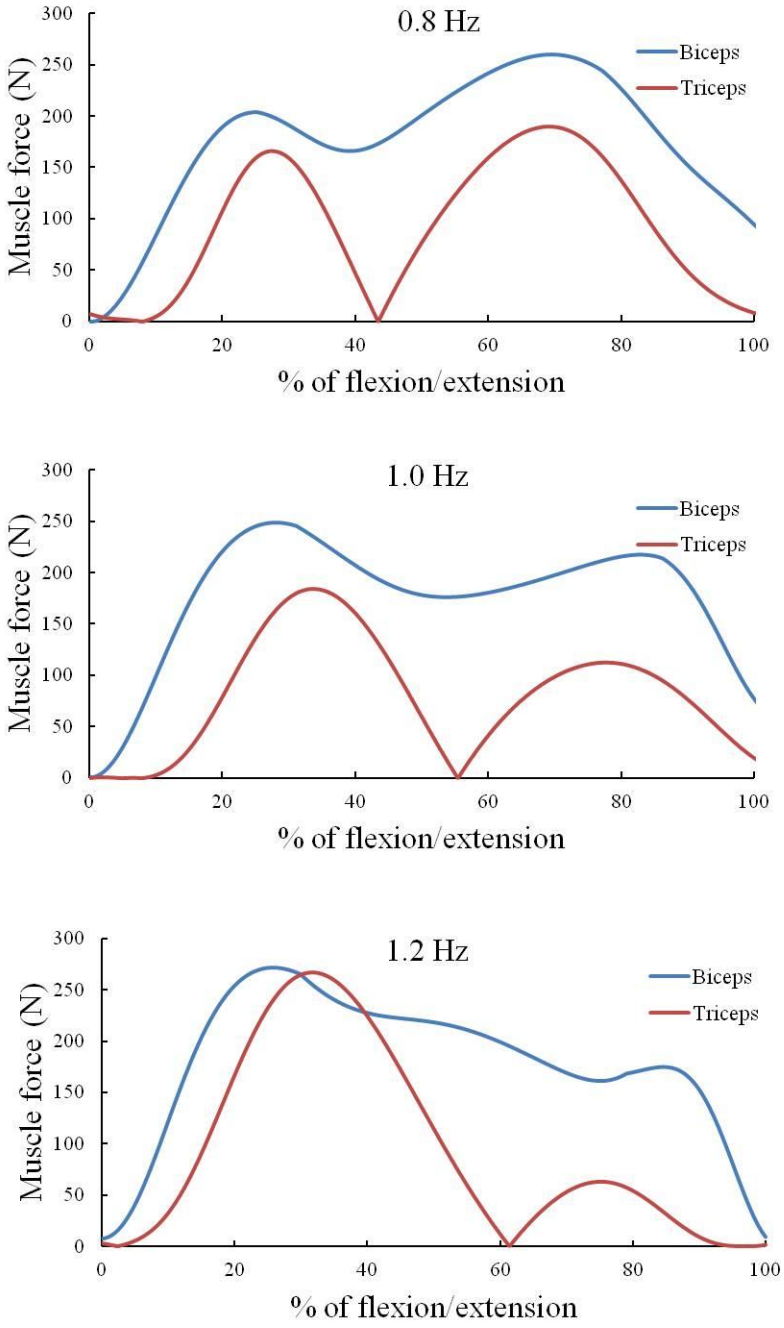

Figure 3.9 Muscle forces estimation during elbow flexion/extension, biceps (blue solid line) and triceps (red solid line) at various movement frequencies.

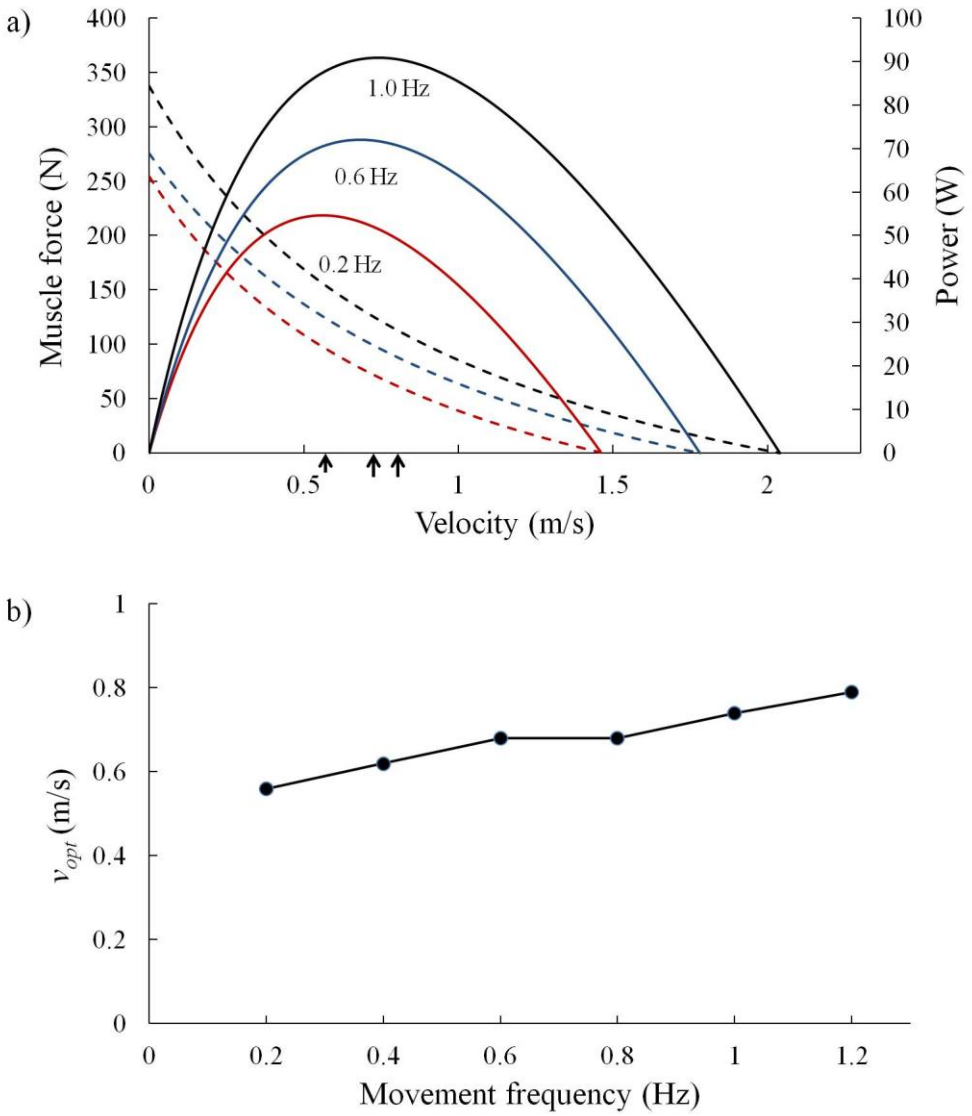

Figure 3.10 Examples of the force-velocity curve and power-velocity curve of the biceps a) Average force-power curves of biceps at movement frequencies of 0.2, 0.6 and 1.0 Hz are represented by solid lines, whereas the corresponding average force-velocity curves are represented by dashed lines. Small arrows on the abscissa indicate the velocity of shortening (v_{opt}) at which maximum power (W_{max}) is reached. b) A histogram showing the optimal velocity value of the biceps at various movement frequencies (0.2-1.2 Hz).

however, the optimum biceps length ($L_{FOPT,b}$;y=-0.0046x+0.1554, R^2=0.1433) and the width of the force-length relationship of the biceps (w_b;y=-0.1013x+0.9068, R^2=0.6541) changed minimally with increasing movement frequency. The optimized model parameters for the triceps also changed with the movement frequency. The relationship was also described as a linear relationship; The maximum isometric force of the triceps ($F_{0,t}$;y=294.9x+1066, R^2=0.882), and the maximum velocity of shortening of the triceps ($v_{0,t}$; y=1.2603x+1.803, R^2=0.796) increased with increasing movement frequency, whereas there was minimal change in the optimal triceps length ($L_{FOPT,t}$;y=-0.0016x+0.3103, R^2=0.002), width of the force-length relationship, (w_t; y=-0.011x+0.795, R^2=0.0099), and Hill's equation curvature of the triceps (n_t; y=0.0704x+0.4061, R^2=0.3248) with increasing movement frequency.

Biceps and triceps forces were estimated during elbow flexion/motion at various moving speeds (Fig. 3.9). The muscle contributions changed during the motion. The muscle force of the biceps and triceps increased as movements frequencies increased. The change in biceps and triceps force pattern can be observed at every movement frequencies.

The average power-velocity curves were calculated using the information from the force-velocity curve. As noted in Fig. 3.10a, the muscle can generate greater maximum power output (W_{max}) at a higher movement frequency. The optimal velocity (v_{opt}), where W_{max} is reached is shown in Fig. 3.10b. Moreover, the v_{opt} value increases as the movement frequency increases.

3.2.5 Discussion

In this study, an EMG-driven model was developed and used to estimate muscle force during elbow flexion/extension movement. The optimization process used data from various movement frequencies. The change in muscle force contribution can be observed non-invasively.

During elbow flexion/extension movement, both biceps and triceps generate force to move forearm as shown in Fig. 3.9. Level and timing of muscle force generation change with movement speed. As movement speed increase more force is required to generate faster movement. During flexion (0-50% of flexion/extension movement), biceps works as agonist muscle and triceps works as antagonist muscle. While during extension (50-100% of flexion/extension) triceps work as agonist and biceps works as antagonist muscle. The results seem consistent with the anatomical information. The cooperative activity of biceps and triceps was presented. The pattern seems similar in every movement speed (Fig. 3.9). The maximum biceps force occur at about 20% of flexion/extension cycle which required to move forearm and the maximum triceps force occur later at about 40% of flexion/extension cycle to break the forearm movement.

Another finding of the present study is that muscle model parameters depend on the movement frequency. The impact of the rate-effect on the muscle parameters is shown in Fig. 3.8. When the forearm moves with a higher movement frequency, greater power is required to generate the movement. The change in shortening velocity of muscle directly affects the operating point in the force-velocity relationship. The force-velocity relationship dictates that a muscle's ability to produce force decrease with increasing speeds of contraction, and hence there is an optimum shortening velocity which maximal power is produced. It is well known fact that human muscle is non-homogeneous, and is composed of two muscle fiber types, type I (slow) and type II (fast), which have different roles and properties (Close, 1972). Both fiber types contribute to muscle force generation during muscle contraction. The properties of muscles might change according to the movement velocity of

the task, since muscles tend to operate in vivo at a velocity and load condition at which maximum power is developed (Rome, et al., 1988). The recruitment strategy of both muscle fibers during dynamic contraction is not yet fully understands due to the limitation of conducting in vivo experiment in human. However, Rome et al. (1988) demonstrated that in carp, fast and slow fibers shorten at different velocities which develops their maximum power output. This indicates that there is a mechanism to optimize mechanical power and efficiency at different movement speeds by selective recruitment of the suitable fiber type. Assuming that the same mechanism also holds true in human, the muscle tends to operate at a point of optimum velocity where speed and power are most efficiently utilized. We noted that the F_0 and v_0 values increased with higher movement frequency. An increase in the F_0 and v_0 values in the force-velocity relationship facilitates the generation of greater maximum power output (W_{max}) in the muscle (Fig. 3.10a). The F_0 and v_0 values depend on the muscle fiber composition since the properties of the entire muscle lump is determined by the properties values of the combined fast fibers and slow fibers (Zajac, 1989). Both fiber types contribute to muscle force generation during muscle contraction. Properties of the whole muscle lump during contraction can be changed depend on the recruitment of both slow and fast fibers. Walmsley et al. (1978) shown that during locomotion in cat, over a wide range of walking speeds (0.6–3 m/s), soleus (100% slow muscle fibers) developed approximately the same peak force while the average medial gastrocnemius (mixed muscle fibers) force varies over a threefold range. Many studies report that fast fibers have higher F_0 and v_0 values as compared to slow fibers (Larsson and Moss, 1993; Harridge, et al., 1996; Bottinelli, et al., 1999). In addition the change in F_0 could be regarded to be proportional to change in maximum muscle stress (σ_m). Many studies in cat and human muscle reported that the value of σ_m in fast fiber is higher than in slow fiber (Burke, et al., 1973; Dum, et al., 1982; Bodine, et al., 1987; Bottinelli, et al., 1996). At a higher speed, fast fibers play an important role in generating force, since fast fibers can produce much greater power as compared to slow fibers (Bottinelli, et al., 1999). In addition, at high

movement frequency, the velocities at which the muscle shortens can be faster than the v_0 of its slow fiber. Therefore, when the shortening velocity increases, the properties of the entire muscle lump should shift toward and reflect the values of the fast fibers. An increase in the F_0 and v_0 values also facilitates the generation of optimum power output at a higher shortening velocity in the muscle. The change in the v_{opt} (Fig. 3.10b) indicates that during dynamic contraction, the muscle tends to tune its properties to extent at which the muscle can work efficiently. Therefore, varying the F_0 and v_0 values with the movement frequency enable to better reflect the underlying mechanism in the muscle. At first a simple linear relation between these parameters and movement frequency can be implemented. The relationship can be extracted from the results of this study (Fig. 3.8).

In the force-length relationship, the parameters that describe the relationship are the L_{FOPT} (defined as the muscle length at which the muscle generates maximum force) and w. The results show that both L_{FOPT} and w slightly changed with increasing movement frequency. The effective operating range of muscle is approximately between $0.5L_{FOPT}$ and $1.5L_{FOPT}$ (Zajac, 1989) ($w \approx 1$). Many studies report operating range of muscle in ascending or plateau region of the force-length curve (Loren, et al., 1996; Murray, et al., 2000; Hale, et al., 2011). It seems that slightly change in these parameters does not have much effect on this region of force-length curve. Muscle still operates at the optimum point at which the muscles work most efficiently in the force-length relationship. Thus, the impact of the rate-effect on these parameters appears to be minimal.

In order to improve the accuracy of the EMG-driven model when using in a wide range of speed movement, muscle model parameters should be adjusted according to the movement speed. Muscle model parameters should be tuned at the slowest and fastest movement condition to form a linear relationship.

A limitation encountered when developing an EMG-driven model is that the muscle force cannot be measured directly. To evaluate the accuracy of the

estimated muscle force, it is necessary to compare the calculated external force with the measured force. The accuracy of the estimated muscle force depends on the proposed mechanical model. The lumped model being used in the present study consists of the combination, of all of the elbow flexors as a single "biceps" and all the extensors as a single "triceps" (Bouisset, 1973; Winters and Stark, 1985). This basic approach of lumping synergistic muscles is useful when assessing tasks involving motion of a single joint such as the elbow joint. However, it should be noted that there are more than two muscles at every joint. For studies of certain specific tasks, separation of synergistic muscles is necessary. By adding more muscle models into the mechanical model, we can study a system that exhibits a wide range of human movement.

In present study, there are five muscle model parameters to be adjusted. These parameters are enough for describing the mechanism of the force-length-velocity relationship. Adding more muscle model parameters to be optimized might help in fit more between the estimated force and measured force. However, this should be carefully performed as the added complexity can make interpretation of results more difficult. Buchanan et al. (2004) suggested that the fewer optimization variables that are adjusted, the more assured the physiological meaning of the model. Good agreement between the external forces calculated from the model and the measured ones (Fig. 3.7) showed the feasibility of this approach to estimate muscle model parameters.

The EMG signals recorded with surface electrodes is dependent on several factors, such as skin thickness, the distance of the electrode from the active muscle area, and the quality of contact between the electrode and skin. The EMG signals from the muscles that are near the skin surface, such as the biceps and triceps, can be easily measured. However, we did not succeed in obtaining a stable isolated EMG signals from the branchialis muscle because it is deeply located under the biceps. Thus, if the brachialis muscle with inaccurate EMG signal is included into the mechanical model, a significant error may be obtained. Therefore, we did not include the brachialis in our model.

Increase in the movement frequency affects the accuracy of the estimated muscle force of the Hill-type muscle model. In the present study, we noted that the model estimated the force with good accuracy (%RMSE<10%) within a range of 0.2-0.8 Hz, which is the range of normal movement. The error of the estimated force increased with higher movement frequency (at 1.0 and 1.2 Hz.). This limitation may be attributed to the lack of the force-acceleration relationship in the CE. The Hill's muscle model is generally based on the force-velocity relationship in isotonic contractions, and thus it appears to be suitable for slow movements with constant force. However, during rapid movement, the force generated rapidly by muscle changes during the acceleration phase, may induce an error in Hill's muscle model. Moreover, the force acceleration relationship in such cases is not well known. Certain studies have indicated that muscle respond differently to all three kinematic parameters, including velocity, acceleration and jerk (Le Bozec, et al., 1987; Fee Jr, et al., 2009). Thus, we believe that a better understanding of the force-acceleration relationship in vivo could be useful for developing an EMG-driven model for rapid movement.

For accurately estimating muscle force using the EMG-driven model, the change in the muscle model parameters according to movement frequency should be considered. The EMG-driven model with adjusted muscle model parameters is effective in estimating the muscle force during normal movements (frequency: 0.2-0.8 Hz). To further improve the muscle model, we suggest that the relationship between acceleration and muscle force should be investigated and this should be included into the muscle model.

3.3 Muscle force estimation during knee joint movement

Knee motion is required during most of daily activities, such as walking, ascending/descending stairs, cycling and sitting up/down. Human knee has an ability to move in various speeds by adjusting muscle force that generated from each muscle within the lower limb. The ability to adjust the speed is an important mechanism that provides adaptation to change in locomotion activity, e.g. change from walking to running or to enhance stability during the movement. The evaluation of the muscle force at knee joint is of importance in many areas of biomechanics research such as improving rehabilitation program, design of better implant systems and development of training program for athletes. However, direct measurement of muscle force is difficult and invasive, thus indirect measurement and mathematical model is required to estimate the muscle force. Many study developed an inverse dynamics model to estimate joint moment from external forces and kinematics of body movement (Kingma, et al., 1996; Silva and Ambrósio, 2002; Erdemir, et al., 2007). Many studies reported the change in EMG activities of several muscles in lower limbs when movement speed increase (Hwang and Abraham, 2001; Hof, et al., 2002; den Otter, et al., 2004). Understanding muscular contributions to knee flexion/extension is of important in studying muscle mechanism and developing a better rehabilitation program. Therefore, we were interested in determining how individual muscles contribute to knee flexion/extension when the movement speed change using EMG-driven model.

3.3.1 Knee joint model

The knee flexion/extension movement in the sagittal plane was described by a segmental model where the shank and thigh were considered to be two rigid bodies, connected by a hinge-type joint, as shown in Fig. 3.11. The model considered the rectus femoris (RF), vatsus lateralis (VL), biceps femoris (BF) and gastrocnemius (GaS) muscles. These muscles generate forces that drive the knee joint to move. The equation of motion can be described by

$$I_s\ddot{\theta}_k = \sum F_{flexor} R_{flexor} - \sum F_{extensor} R_{extensor} + m_s g d_s \cos\theta_k - T_s R_s \qquad (3.12)$$

where I_s is the mass moment of inertia of the shank and foot with respect to the knee axis. θ_k and $\ddot{\theta}_k$ are the knee flexion angle and angular acceleration, respectively. F_{flexor} is the force of the flexors, and $F_{extensor}$ is the force of the extensors. R_{flexor} and $R_{extensor}$ are the moment arms of the flexors and extensors respectively. m_s is the mass of the shank and foot. d_s is the length between the center of mass of the shank, and the knee joint axis. T_s is the external load applied to the shank, and R_s is the distance between the position of the applied load to the knee joint axis.

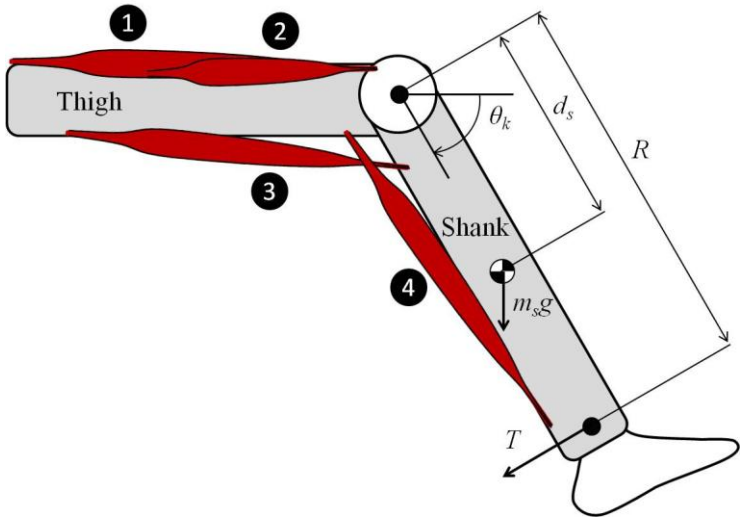

Figure 3.11 Biomechanical model of knee joint. A schematic of a two-bar linkage model represents the human leg segment with lower limb muscles. Knee extensors: (1) rectus femoris and (2) vastus lateralis. Knee flexors: (3) bicep femoris and (4) gastrocnemius.

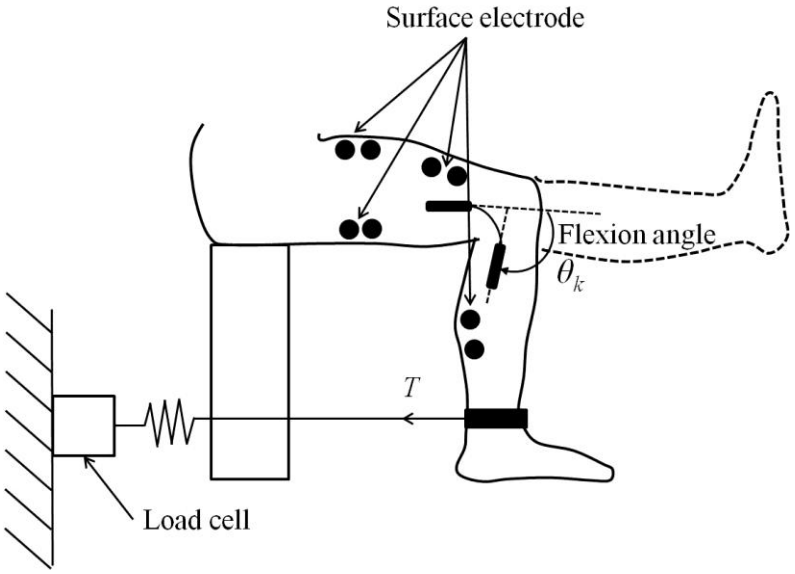

Figure 3.12 Schematic drawing of the experimental set-up. Pairs of surface electrodes were attached to the rectus femoris, vastus lateralis, bicep femoris and gastrocnemius to detect the EMG signals. An electrogoniometer was attached to the knee joint to measure the knee flexion angle. A load cell was attached to the subject's leg to measure the external force.

3.3.2 Experiment procedure

Two healthy subjects participated in this study. The subjects sat comfortably in an upright position and performed a series of knee joint flexion and extension movements with predetermined movement frequencies ranging from 0.2 Hz to 1.0 Hz. Knee flexion angles were measured with an electrogoniometer (SG75, Biometric, USA) that was attached to the subject's leg. The external load was measured by a load cell (DTG-20, DigiTech Co.,Ltd., Japan) that was fixed to the ground (Fig. 3.12). The raw EMG signals from the RF, VL, BF and GaS were collected with bipolar surface electrodes at a sampling rate of 1000 Hz (Biolog, DL-500, S&ME, Japan) and processed offline with the MATLAB software (Mathworks, USA). First, the raw EMG signals were filtered using the Butterworth bandpass filter (10-500 Hz); this was followed by full-wave rectification and filtering using a fourth-order Butterworth low-pass filter (3 Hz) for conversion to a linear envelope profile. MVC exercises were performed against static resistance for each muscle separately in order to normalize the processed EMG signals.

Before the test was initiated, the subjects were instructed to relax and practice moving their leg in a synchronized manner with a digital metronome (TU-80, Roland Corporation, USA). Each subject performed two trials of knee flexion and extension with movement frequencies of 0.2, 0.4, 0.6, 0.8, and 1.0 Hz. For each trial, a set of 20 cycles of knee flexion/extension movements was performed. The range of motion executed at the knee was between 0^o and 90^o. An adequate rest period was provided between each trial in order to avoid fatigue. The knee joint angular velocity was obtained by numerical differentiation of the position joint angle that was measured by the electrogoniometer. The raw data for each trial were processed as described above and then averaged across 20 cycles for each subject.

3.3.3 Results

Figure 3.13 shows EMG recordings of the RF, VL, and BF muscles and the knee flexion angle during extension/flexion. The amplitude and timing changed when the movement speed increased. This shows the influence of the movement speed on the muscle force generation mechanism. As the movement frequency increased from a slow speed (0.2 Hz) to a faster speed (1.0 Hz), both RF and BF EMG activities changed with a substantial decrease in duration and increase in amplitude. The peak RF EMG activity appeared at full extension. The peak BF EMG activity at low speed (0.2 Hz) appeared late in the extension, and the timing and amplitude changed when the speed increased. In contrast, changing the movement speed had little influence on the VL. The VL EMG activity seemed comparatively stable when the movement speed increased.

The muscle force of each muscle was estimated using EMG data and the joint angle as inputs for the developed EMG-driven model. The predictive ability of the model was validated by the fitness between the external forces calculated by the inverse dynamic model and the measured values during the experimental trials. Figure 3.14 shows an example comparison between the measured external forces from the load cell (red solid line) and external force calculated from the model (blue dotted line); the calculated and measured forces appear to correspond. The average coefficient of determination (R^2) and the predicted external forces were calculated at various movement frequencies. The R^2 values ranged from 0.91 to 0.97 and, the %RMSE ranged from 3.68% to 6.68%; thus, the predicted and measured forces showed good correspondence.

Individual muscle forces were estimated during knee flexion/motion at various moving speeds (Fig. 3.15). The muscle contributions changed during the motion. The muscle force of the VL showed a minimal change in muscle force when the movement speed increased. In contrast, the RF and BF generated more force when the movement speed increased. During slow movement (e.g., 0.2 and 0.4 Hz), the VL was the main muscle that contributed

to generating knee extension. For faster movements, the RF was the main muscle that accelerated the body segment to achieve the desired speed. The increased co-contraction of the RF and BF was observed at higher speeds (e.g., 0.8 and 1.0 Hz). The peak force of the VL occurred at about 60% of the extension/flexion time and stayed the same for all speeds. The GaS provided only a small contribution during knee flexion/extension movements.

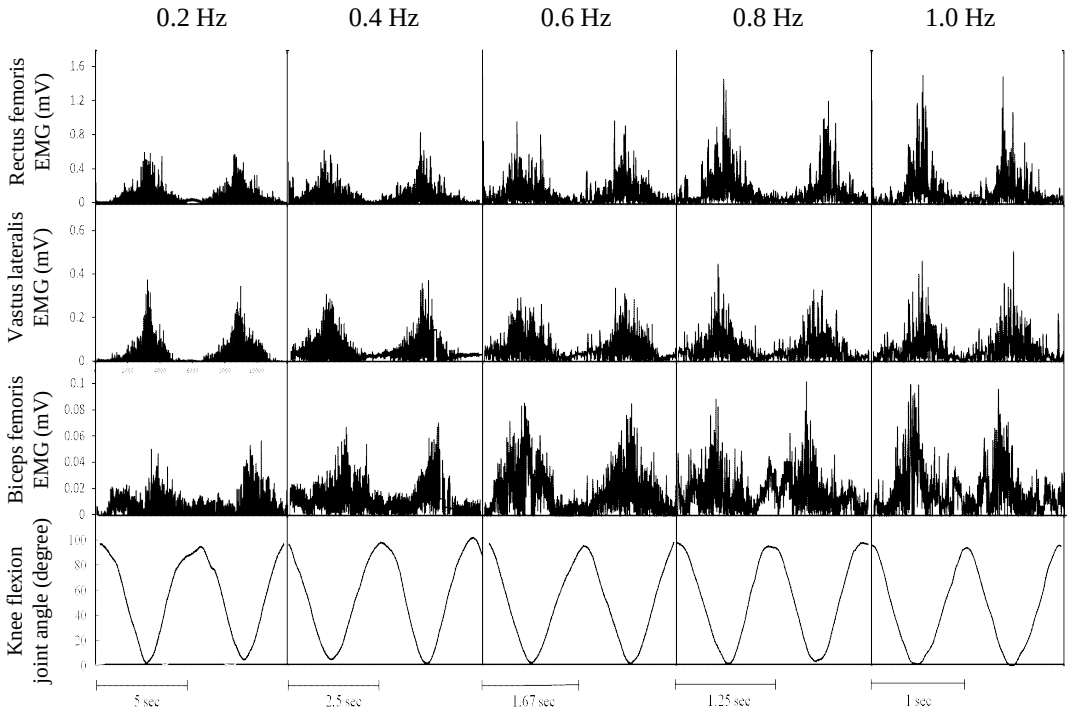

Figure 3.13 Representative recording of EMG profiles of lower limb muscles and knee joint angle during knee extension/flexion movement at various movement frequencies (0.2-1.0 Hz).

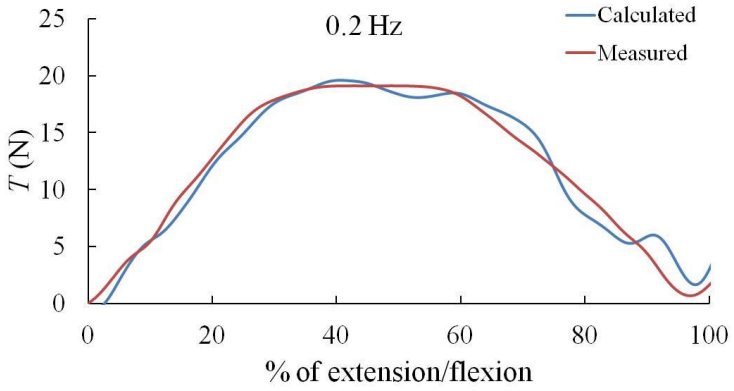

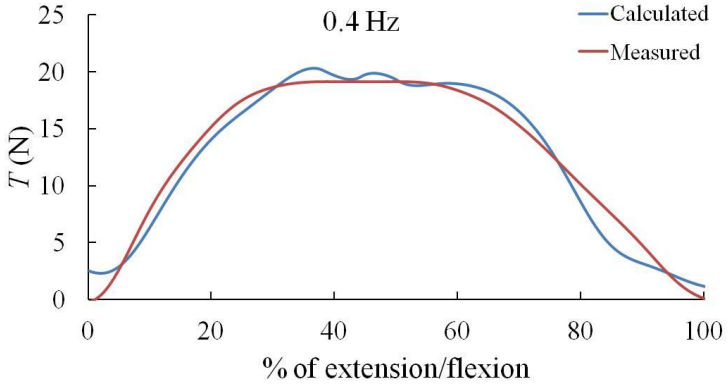

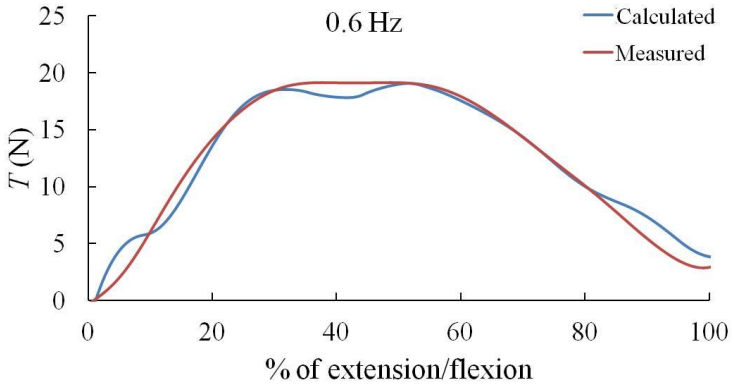

Figure 3.14 (continue)

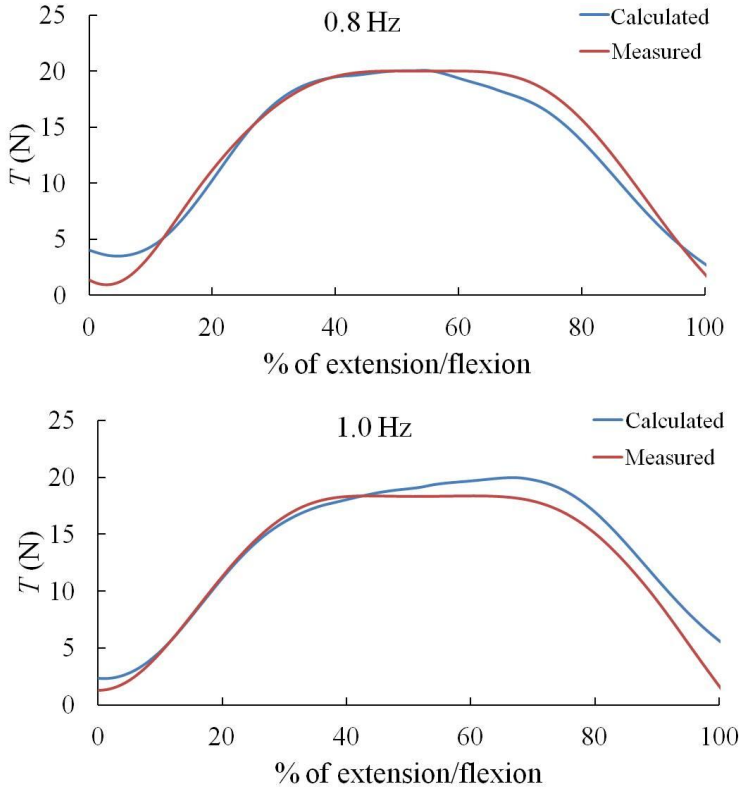

Figure 3.14 An example of comparison of the external force, *T* between measured force (red solid line) and estimated external force calculated from the model (blue dot line) during knee extension/flexion movement a) 0.2 Hz, b) 0.4 Hz, c) 0.6 Hz, d) 0.8 Hz, and e) 1.0 Hz.

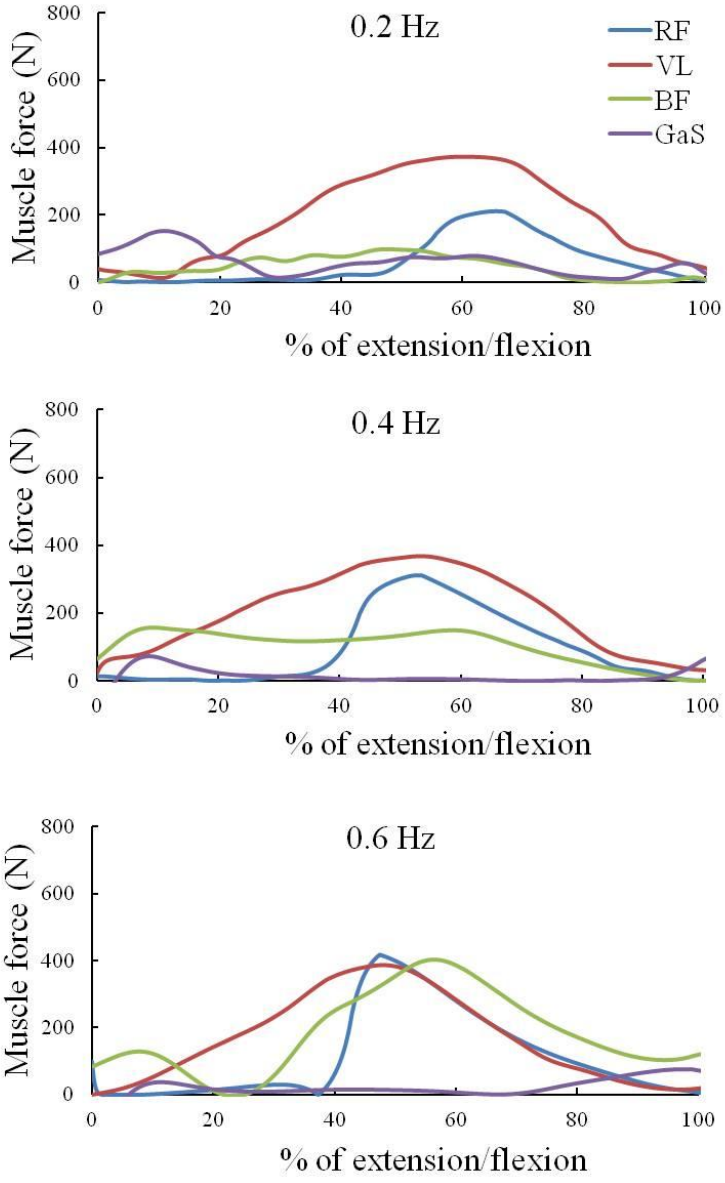

Figure 3.15 (continue)

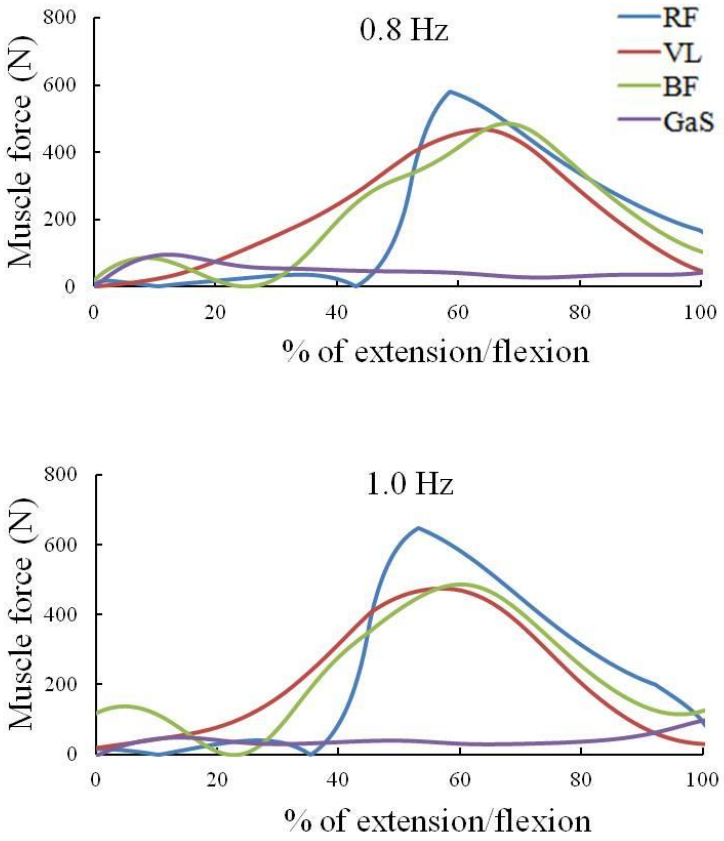

Figure 3.15 Example of estimated muscle force: rectus femoris (RF), vastus lateralis (VL), biceps femoris (BF) and gastrocnemius (GaS) during knee extension/flexion at various movement frequencies (0.2-1.0 Hz).

3.3.4 Discussion

Figure 3.13 shows EMG activities during human knee flexion/extension under different speed conditions. The EMG activity reflects the electrical state of a contracting muscle and can be related to the muscle force. The changes in the EMG signals show the influence of speed on the muscle mechanism. Each muscle reacts to a change in speed differently. The EMG signals from the RF and BF changed significantly when the movement speed increased. A marked change appeared in the BF EMG initiation relative to the knee angle with the phase advanced, which led to a co-contraction phase with the RF. The co-contraction of the RF and BF increased with the movement speed. For repeated cycling movements, Suzuki et al. (1982) reported on the changes in the RF and BF activities as the pedaling speed increases. The movement speed seems to have a strong influence on the RF and BF muscles. This may be due to the increase in muscle co-contraction to increase stability and accelerate/decelerate a body segment. Muscle co-contraction is the simultaneous activity of agonists crossing the same joint and acts as a stabilizer (Busse, et al., 2005). Based on the results, studying the timing of this co-contraction may help in developing stability control of lower limbs.

Figure 3.15 shows individual muscle forces during knee extension/flexion at different movement frequencies; the results provided additional insight into how muscles react to changes in speed. The role of muscles in knee extension/flexion motion is to control the accelerating and decelerating forces of the shank segment. The amplitude of the muscle force increases with the movement speed because of the need for a larger force output. For low movement speeds (e.g., 0.2, 0.4, and 0.6 Hz), the VL is the main muscle that generates the extension force and changes in the movement speed seem to have a low influence on VL activity. During the braking phase (50% extension/flexion time) at higher speeds, the RF generates more forces. Many studies on muscle activity during walking have reported that the RF activity increases with the walking speed (Shiavi, et al., 1987; Nene, et al.,

1999; den Otter, et al., 2004). The results of this study confirm that the role of RF is to accelerate the leg at higher movement speeds.

Some specific limitations of the presented technique and results must also be addressed. In this study, the biomechanical model of the knee joint did not consider the smaller muscles with small contributions to the total plantar flexion torque. Several other muscles act synergistically for plantar flexion and can be activated to stabilize the knee joint in the frontal plane. However, any production should be based on muscle activity analysis for a given task. Since these smaller muscles are deep, surface EMG access is difficult. Considering more muscles may improve the model accuracy but the instability of EMG signals from deep muscles should also be considered.

In this study, an EMG-driven model for predicting muscle forces in lower limbs was developed and used to examine the contributions of individual muscles to knee flexion/extension motion. The changes in muscle force when the movement speed increased was observed and analyzed. This system provides insight into muscle force generation during knee motion, which can lead to better understanding of the muscle mechanisms and development of a rehabilitation program.

3.4 Summary

It was demonstrated that the developed EMG-driven model can be used to estimate muscle force in elbow and knee joint during flexion/extension motion. Body kinetic and EMG signals were used as inputs to the model. Individual muscle force of each joint during dynamic movement was estimated. The results show that there is the relationship between movement speed and EMG signal. The EMG-driven model using conventional surface EMG is very useful in estimating muscle force in elbow and knee joint which are moved by large muscles. However, the limitations of conventional surface EMG signal to access deep muscle, preventing the possibility of using this system to estimate force in human forearm. To estimate muscle force within the forearm, the development of a method to detect muscle activity in deep forearm muscle is necessary.

Chapter 4 An EMG-CT Method for Detection of Multi Muscle Activity in the Forearm

4.1 EMG-CT method

The human hand is an excellent end-effector of the upper limb capable of innumerable actions, from fine operations to heavy-duty tasks. A complex movement of the hand is generated by the coordination of many muscles and tendons in the forearm. There are 19 muscles reside within the human forearm. List of forearm muscle is shown in Fig. 4.1 and Table 4.1. Mechanically, there are four joints in each finger, from the proximal to distal: carpometacarpal (CMC), metacarpophalangeal (MCP), proximal interphalangeal (PIP), and distal interphalangeal (DIP) joints as shown in Fig. 4.2. The complex movement of fingers and hand is generated by cooperative activity of muscles within the forearm.

For best understanding of hand and finger function, individual muscle activity in the forearm must be observable. Electromyography (EMG) has been widely used as a standard tool for studying the kinesiology of muscles. An intramuscular needle electrode is usually employed to detect the activity of deep muscles in the forearm. However, using the needle electrode is a painful procedure and not appropriate for clinical application. Surface EMG is preferable because of its ease of use and noninvasive nature. The drawback of surface EMG is that signals in a region where a large number of muscles lie close together are superimposed, it is so called "crosstalk problem" The crosstalk is highly complicated in a small volume such as the forearm (Perry, et al., 1981; De Luca and Merletti, 1988; Winter, et al., 1994). This makes obtaining individual muscle activities in the forearm difficult, limiting the usefulness of surface EMG. A method to overcome this problem would allow accurate observation of individual muscle activity.

In previous attempts to extract motor information from surface EMG, the relationship between the muscle action potential (MAP) of a motor unit (MU) and surface conduction has been established using a scanning EMG method (Stalberg and Antoni, 1980), and the position of the activated single MU in the biceps has been estimated with surface electrodes placed around the

upper arm (Roeleveld, et al., 1998). The activities of MUs in forearm muscles have been estimated from surface EMG signals using an array electrode and blind-deconvolution techniques (Nakamura, et al., 2004; Garcia, et al., 2005). However, these methods do not work well when many MUs in many muscles are activated at the same time (e.g., in heavy work using the forearm) [Buchthal and Schmalbruch, 1980]. Recently, surface EMG equipment using a multi-electrode array has been employed (Blok, et al., 2002; Merletti, et al., 2003). But the analysis of single MU firing patterns and MU characteristics is still complicated and time-consuming (Drost, et al., 2006).

This chapter describes a novel EMG technique, the electromyography computed tomography (EMG-CT) method, as a tool for investigating muscle activities in the forearm based on the distribution of surface EMG on the skin surface (Nakajima, et al., 2014). Muscle activities are calculated by comparing the measured surface EMG to simulated results from the mathematical model. To verify the reverse estimation method, physical work experiments were carried out for three subjects applying a flexion load with three kinds of weights to the proximal PIP joint of the middle finger. The activation of individual muscles is estimated by the obtained surface EMG. The development of EMG-CT will be very useful in studying muscular strategies and mechanisms of muscles in the forearm, which may potentially be used for evaluation of neuromuscular rehabilitation.

a) Anterior muscles of the right hand

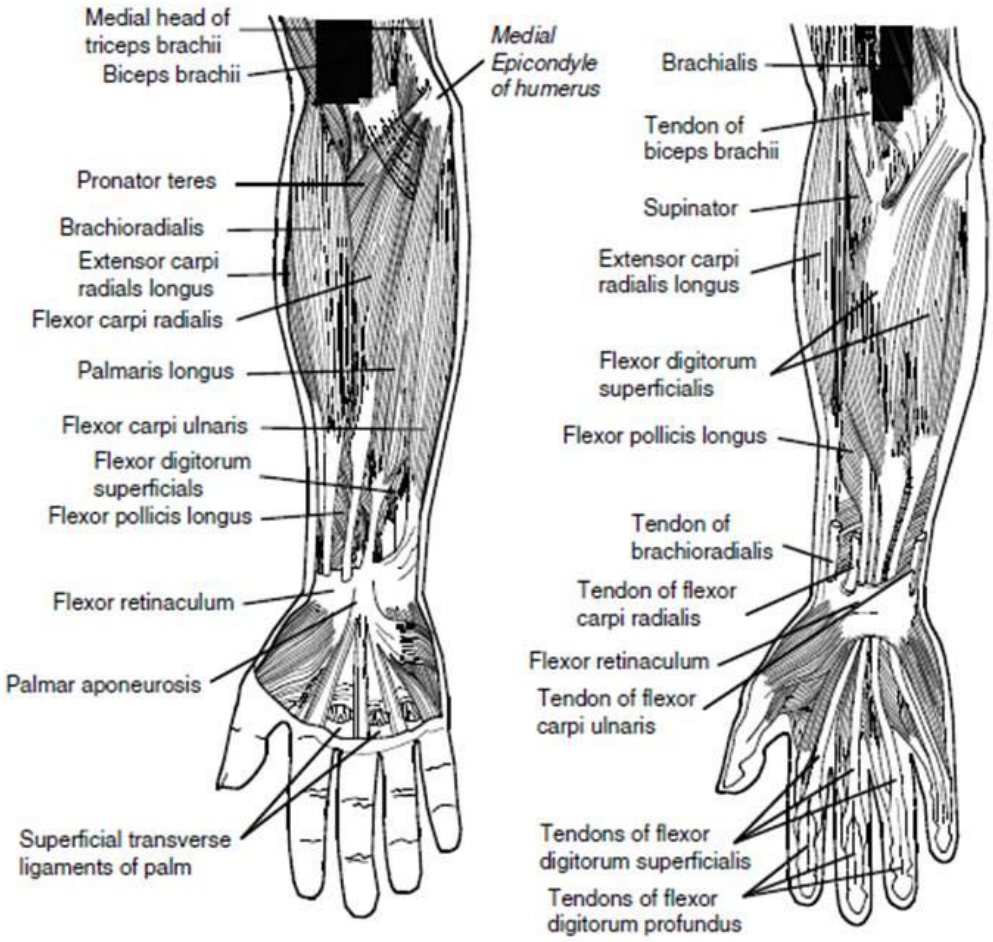

Figure 4.1 (continue)

b) Posterior muscles of the right hand

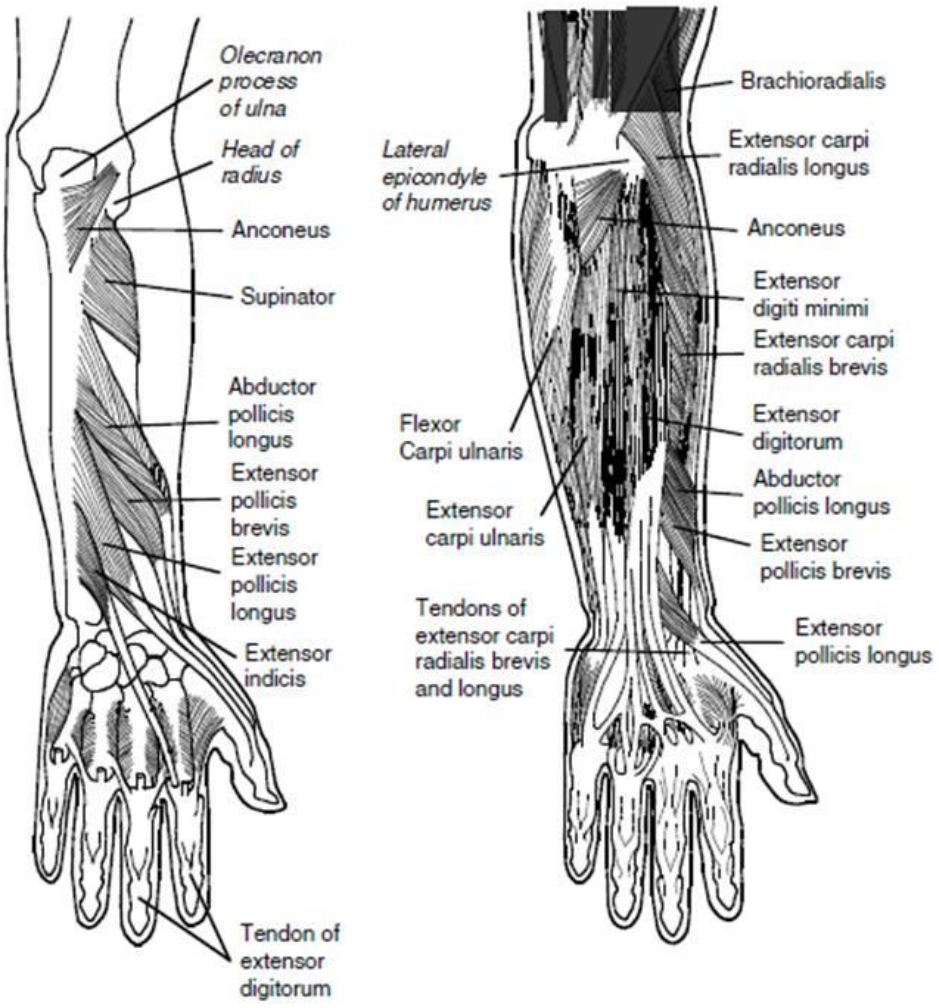

Figure 4.1 Muscles in the right arm a) Anterior muscles, superficial layer (left) and middle layer (right). b) Posterior muscle, deep layer (left) and superficial layer (right) [Freivalds, 2011].

Table 4.1 List of muscles in forearm (Stone and Stone, 2003)

Name	Action
1)Pronator teres	Pronates and flexes forearm
2)Flexor carpi radialis	Flexes hand, synergist in abduction with extensor carpi radialis longus and brevis
3)Palmaris	Flexes the hand
4)Flexor carpi ulnaris	Flexes hand, synergist in adduction of hand with extensor carpi ulnaris
5) Flexor digitorum superficialis	Flexes the middle phalanges of the finger
6) Flexor digitorum profundus	Flexes distal phalanges
7) Flexor pollicis longus	Flexes the thumb
8) Pronator Quadratus	Pronates forearm and hand
9) Brachioradialis	Flexes forearm
10) Extensor carpi radialis longus	Extends hand, synergist in abduction of hand with flexor carpi radialis
11) Extensor carpi radialis brevis	Extends hand, synergist in abduction of hand with flexor carpi radialis
12) Extensor digitorum communis	Extends the fingers and wrist
13) Extensor digiti minimi	Extend fifth finger (Little finger)
14) Extensor carpi ulnaris	Extends hand, synergist in adduction of hand with flexor carpi ulnaris
15) Supinator	Supinates forearm
16) Abductor pollicis longus	Abducts, laterally rotates and extends thumb; abducts wrist
17) Extensor pollicis brevis	Extends thumb, abducts hand
18) Extensor pollicis longus	Extends thumb
19) Extensor indicis	Extends index finger

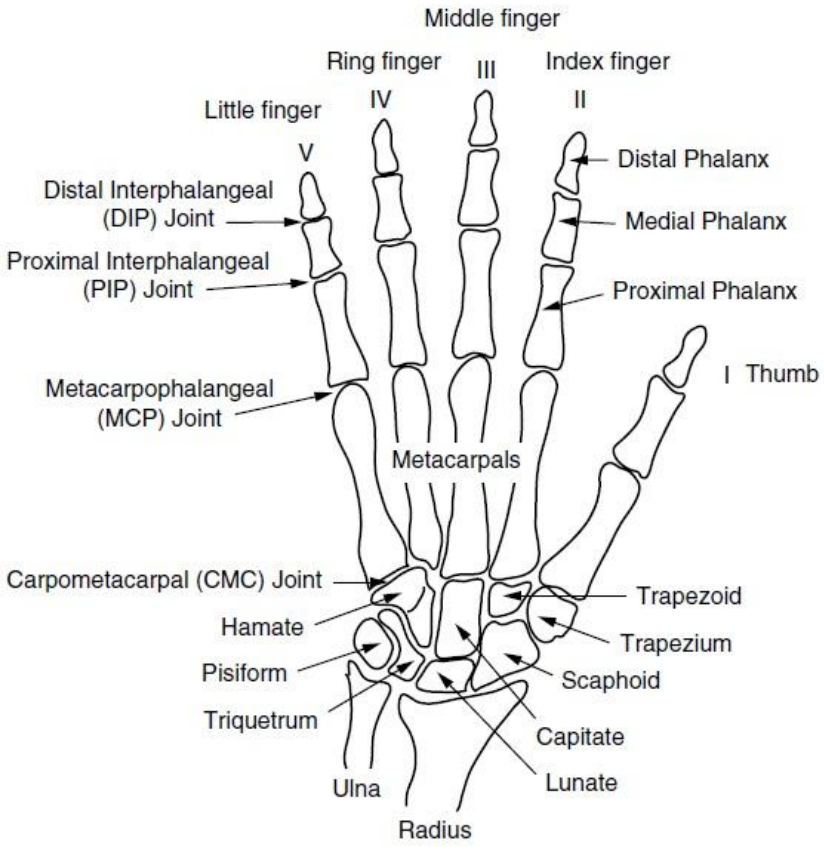

Figure 4.2 Bones and joints of the right hand (palmar view) [Freivalds, 2011].

4.1.1 EMG conduction model in human forearm

Surface EMG technique is based on the fact that local electrophysiological processes result in a detectable flow of the transmembrane current at a certain distance from the active sources (i.e., muscle fiber). This flow of current in the tissue (i.e., the volume conduction), allows EMG measurements to be made at a distance from the sources. When a muscle fiber depolarizes and generates current, a change in the electrical potential distribution can be detected by a bipolar surface electrode on the skin. In previous study, characteristic of surface EMG conduction in the forearm was analyzed (Nakajima et al., 2008). The relationship between detected surface EMG signal and the distance between the electrode and the source of muscle action potential was estimated and validated using experimental phantom-forearm filled with finely ground specimens of muscle (Nakajima et al., 2009). The activity and position of the source in the model can be calculated from the surface EMG power of the surface electrode. Based on these studies, EMG conduction model with dipole sink and source was formulated to reverse estimation of muscle activity (Fig 4.3).

The cross-sectional area of muscle region in the forearm was divided into small elements for calculation (Fig 4.4). The mathematical model have been formulated in term of the mean square value of the muscle action potential changes in proportion to the power exponent of attenuation (PEA) *b*;

$$\bar{V}_{ik}^2 = V_0(d_i)^2 f_k I_k^2 \left(\frac{l_{ik}}{l_0} \right)^{2b(d_i)} \tag{4.1}$$

where d_i is the distance between the pair of bipolar electrode i (mm), I_k is the strength of the current dipole in muscle fiber k (mA),V_0 is a transformation coefficient (mV/mA), f_k is the firing rate of muscle fiber k, l_{ik} is the conduction distance, and l_0 is the unit length (1 mm). The previous study also showed that V_0 and b are functions of inter electrode distances (IED) of the bipolar electrode d (Fig 4.5 and Table 4.2) [Nakajima et al.,2008].

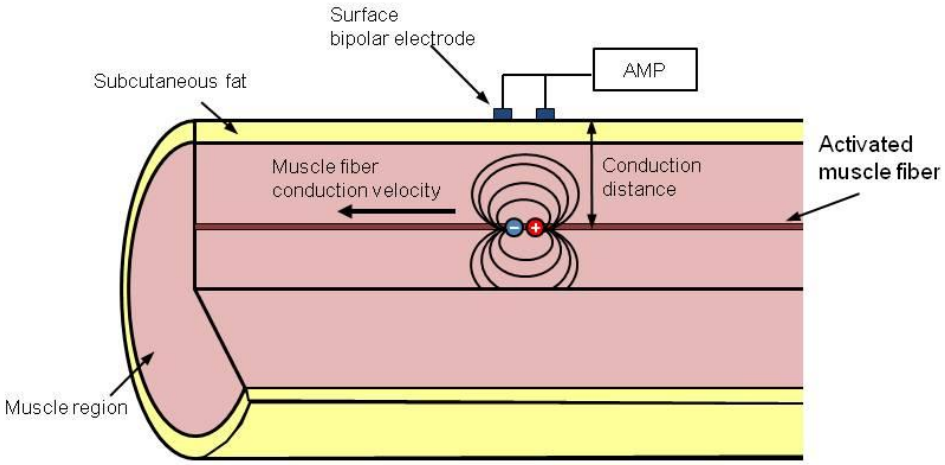

Figure 4.3 EMG conduction model of the forearm. A dipole source action potential propagates along muscle fiber. Surface bipolar electrode was attached to the skin surface to detect surface EMG signal.

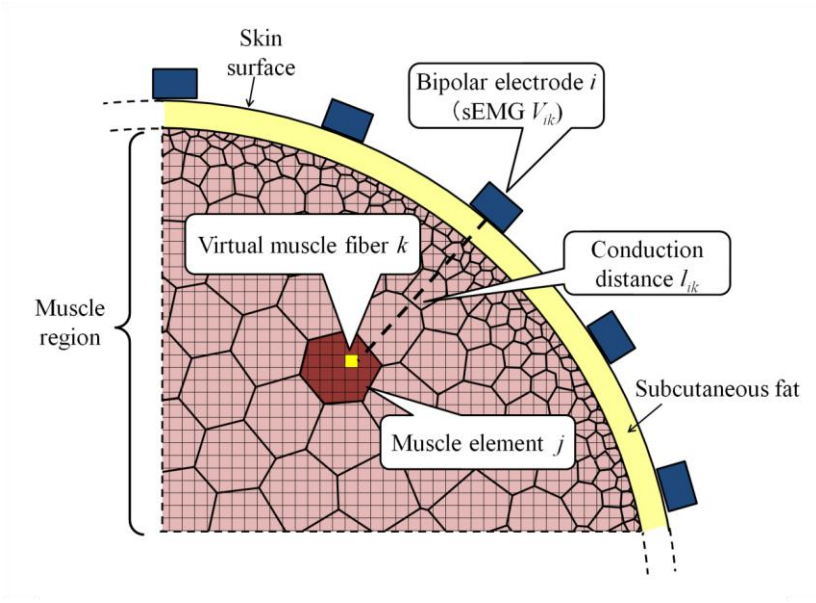

Figure 4.4 Representation of EMG conduction model for calculation. Virtual muscle fiber *k* is a part of the muscle element *j*. l_{ik} is the distance between the muscle fiber *k* and the bipolar electrode *i*. V_{ik} is the surface electromyography (surface EMG) from muscle fiber *k* detected by a bipolar electrode (reprinted from Nakajima, et al., 2014).

From the macroscopic point of view, we considered that MUs in any muscles fiber independently. Thus, the statistical summation of power of the MAP from each muscle fiber is possible. The muscle activation from all muscle fibers *k* detected by a bipolar electrode *i* (V_i) can be simply expressed as

$$\overline{V_i}^2 = \sum_k \overline{V_{ik}}^2 = V_0(d_i)^2 \sum_k f_k I_k^2 \left(\frac{l_{ik}}{l_0} \right)^{2b(d_i)} \tag{4.2}$$

for simplicity, let $m_k{}^2 = f_k I_k{}^2$ be the mean square muscle action current of activated fiber *k*. The equation can then be rewritten as

$$\overline{V_i}^2 = V_0(d_i)^2 \sum_k m_k^2 \left(\frac{l_{ik}}{l_0} \right)^{2b(d_i)} \tag{4.3}$$

The MAP from element *j* is a superposition of the contributing action potentials from all the fibers within the element. By summation of all muscle activation of muscle fiber *k* in element *j* ($k \in muscle\ j$) gives

$$\overline{V_i}^2 = \sum_j \left\{ V_0(d_i)^2 \sum_{k \in muscle\ j} m_k^2 \left(\frac{l_{ik}}{l_0} \right)^{2b(d_i)} \right\} = \sum_j \overline{V_{ij}}^2 \tag{4.4}$$

Here, the mean square muscle action current in muscle element *j* (m_j^2) can be calculated as

$$m_j^2 = \frac{1}{n_j} \sum_{k \in muscle\ j} m_k^2 (k \in muscle\ j) \tag{4.5}$$

The mean square muscle activation of element *j*, $\overline{V_{ij}}^2$ can then be rewritten as

$$\overline{V}_{ij}^{\,2} = V_0(d_i)^2 m_j^2 \sum_{k \in muscle\ j} \left(\frac{l_{ik}}{l_0} \right)^{2b(d_i)} \tag{4.6}$$

the mean square surface EMG detected by bipolar electrode *i* is considered to be the summation of muscle activation from all elements *j*. Letting L_{ij} be the transfer coefficient simplifies the equation to

$$\overline{V}_i^{\,2} = \sum_j \overline{V}_{ij}^{\,2} = \sum_j L_{ij} m_j^2 \tag{4.7}$$

where

$$L_{ij} = V_0(d_i)^2 \sum_{k \in muscle\ j} \left(\frac{l_{ik}}{l_0} \right)^{2b(d_i)} \tag{4.8}$$

The surface EMG signal from each bipolar electrode pair can be calculated from the EMG conduction model described above.

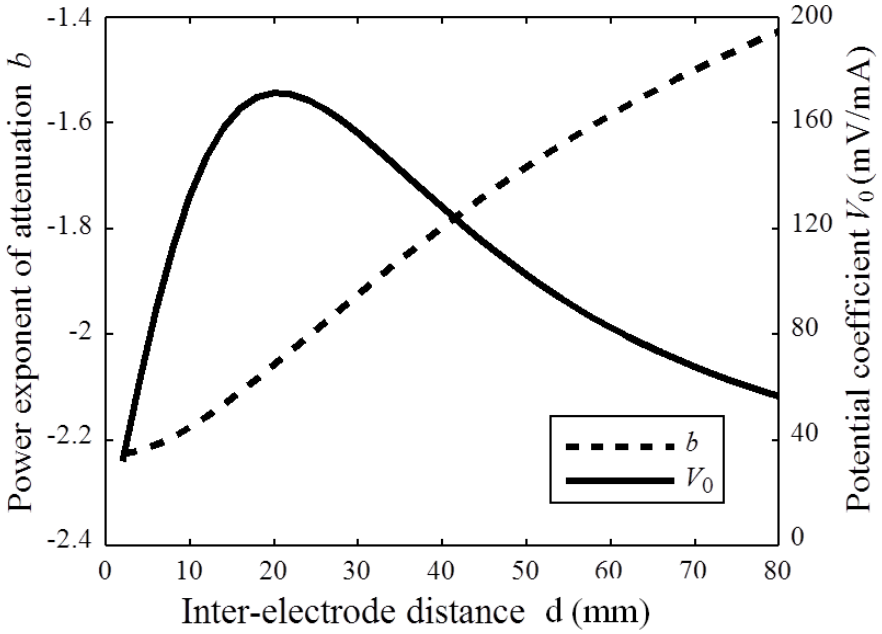

Figure 4.5 Power exponent of attenuation of the coefficient resulting from the difference in inter-electrode distance (IED). The strength of surface EMG is affected by IED of the bipolar electrode (reprinted from Nakajima, et al., 2014).

Table 4.2 Power exponent of the attenuation (PEA) and coefficient values at various inter electrode distances (IED) [Nakajima et al., 2008].

IED (mm)	PEA *b*	Coefficient V_0(mV/mA)
15	-2.12	162
45	-1.74	115

4.1.2 Muscle elements

The cross-section area of human's forearm was modeled as a circular region. The circumferential length of the circular region was equal to the measured subject's forearm circumferential length. Forearm muscle region was divided into many small elements. The base points of muscle elements were placed using the finite element algorithm. Muscle element nodes were distributed across the entire cross-sectional with an element size of 1 mm at the surface and 4 mm for the inside region. The area of each muscle element was divided using Voronoi tessellation (Du, et al., 1999; Sukumar, 2003). Given a set N of muscle element nodes n on a plane, the Voronoi cell $C(n_I)$ for a node n_I is composed by all the nodes closer to node n_I than any other node $n_J \in N$ ($J \neq I$). Thus, the Voronoi cell $C(n_I)$ in plane $\Re^2$ can be described by the following equation:

$$C(n_I) = \left\{ x \in \Re^2 : d(x, x_I) < d(x, x_J), \forall I \neq J \right\} \tag{4.9}$$

where $d(x_I, x_J)$ is the Euclidean distance between x_I and x_J. The boundary of each muscle element was drawn using the perpendicular bisectors of the lines connecting each node within the Voronoi cell $C(n_I)$. This approach was used to construct a forearm EMG conduction model (Fig. 4.6) which was subsequently used to calculate muscle activation of each muscle element.

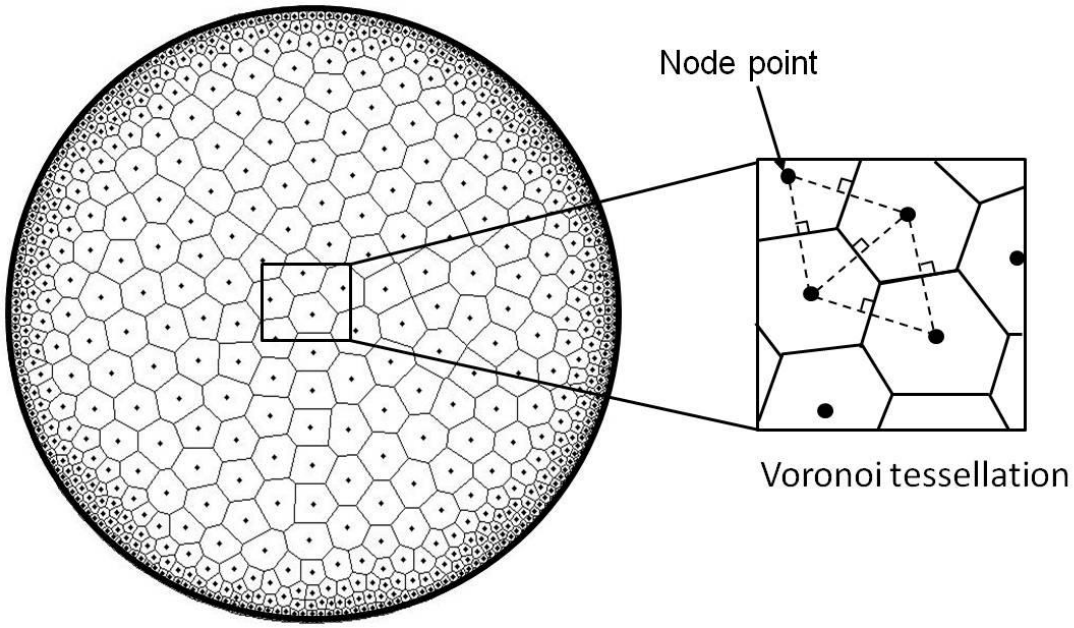

Figure 4.6 Forearm model. Muscle region within forearm cross-sectional area was divided into small elements using Voronoi tessellation.

4.1.3 Calculation process

To estimate the muscle activation of each muscle element, sequential quadratic programming (SQP) was used to optimize the value (Fig. 4.7). SQP is generally used to solve non-linear equations. The objective function f is given by

$$f = \sum_i (V_i - V_{Mi})^2 \tag{4.10}$$

where V_i is the calculated surface EMG from Equation (4.7) and V_{Mi} is the measured surface EMG from the experiment. The search direction in which the gradient ∇f of the objective function vanishes can be expressed as the function

$$min_{[D_j]}\left\{\nabla f^T[D_j] + \frac{1}{2}[D_j]^T \nabla^2 f[D_j]\right\} \tag{4.11}$$

where D_j is the search direction. When the optimization process becomes unstable, when there is a large difference in the weight of the contribution of each of the muscles, the power conduction matrix is filtered so that the value of elements smaller than 1% of the maximum value in the same row is set to zero, as

$$L_{ij} < 0.01 \max_j(L_{ij}) \quad on\ row\ i \rightarrow L_{ij} = 0 \tag{4.12}$$

The optimization was calculated using the Optimization Toolbox in MATLAB (version 8.5, Mathworks, USA).

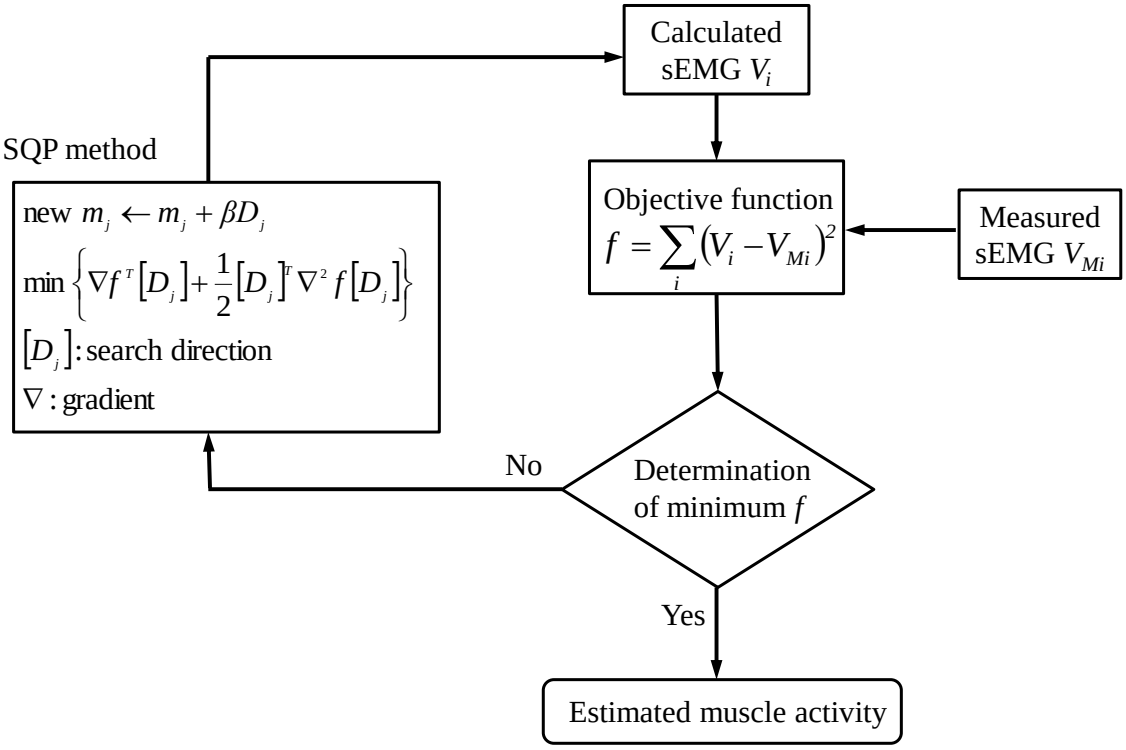

Figure 4.7 Optimization process for estimating muscle activity. Calculated and experimentally measured surface electromyography activities were compared. Sequential quadratic programming (SQP) was used to optimize the value (reprinted from Nakajima, et al., 2014).

4.1.4 Experimental procedure

For validation of the method, isometric contractions of finger muscles were examined for three subjects. Table 4.3 shows the subject's specific data. The subjects sat on a chair with their forearm placed on a horizontal table. The upper arm was at 0° of abduction, the elbow joint flexed at 90° and the wrist placed at 0° of flexion, palm up (Fig. 4.8a). The wrist, palm, and proximal phalanx of the middle finger were fixed to the table (Fig. 4.8b). A weight was hung on the middle phalanx of the middle finger with a cotton thread, at a position 10 mm distal from the PIP joint. The load was applied for 5 seconds and repeated thrice with 5-second rest intervals. The weights of the load were 0.50, 0.75, and 1.00 kg.

The surface EMG signals from the forearm were recorded with 20 custom-built electrode plates. The electrode plate was composed of an 8×60 mm polyvinyl chloride plate of and four aligned stainless steel 3mm diameter electrodes (Fig. 4.9). IED of the differential bipolar electrodes were 15 and 45 mm, with the middle points coinciding. Surface EMG recording using a bipolar electrode with wide IED can detect distant muscle activation because of low attenuation, whereas a bipolar electrode with narrow IED can detect activation only at short distances. Bipolar electrode pairs can detect muscle activation at different depths.

The electrode plates were bound around the subject's forearm, with the middle point at 1/3 of the forearm length from the radial styloid process, parallel to the axis of the radius. Before binding the electrode plates, their forearm skin was shaved by a razor and cleansed by alcohol swab; the electrodes were pasted with conductive gel. The surface EMG signals were obtained with a custom-built amplifier connected to the electrodes with a >1GΩ input impedance, a >100dB common mode rejection ratio (CMRR) and a <100nV/$\sqrt{\text{Hz}}$ signal noise ratio (SNR). The surface EMG signals were processed with the amplifier: (1) amplified 1000 times; (2) filtered using fourth-order Butterworth high-pass filter with a 10-Hz cutoff frequency and low-pass

filter with a 300-Hz; (3) A/D-converted and recorded on a PC with a sampling rate of 2 kHz/channel using 16-bit, ±10V input range A/D converter (ADA16-32/2(CB)F, CONTEC Co., Ltd. JAPAN). The recorded signals were filtered in the PC using 7th-order Butterworth high-pass digital filter with a 10-Hz cutoff frequency and low-pass digital-filter with a 200-Hz. The root mean square (RMS) value and mean power of each channel were calculated from the recorded signals in 500 ms windows.

To quantify each muscle activity, it was necessary to determine the location of each muscle in the cross-sectional area. The arrangement of muscles in the forearm was reconstructed by tracing the muscle boundary from an MR image (Fig 4.10). There are thirteen muscles in the cross section: the extensor carpi ulnaris (ECU), extensor digiti minimi (EDM), extensor digitorum communis (EDC), extensor pollicis longus (EPL), abductor pollicis longus (APL), extensor carpi radialis longus (ECRL), extensor carpi radialis brevis (ECRB), flexor digitorum profundus (FDP), flexor pollicis longus (FPL), brachioradialis (BR), flexor carpi ulnaris (FCU), flexor digitorum superficialis (FDS), and flexor carpi radialis (FCR).

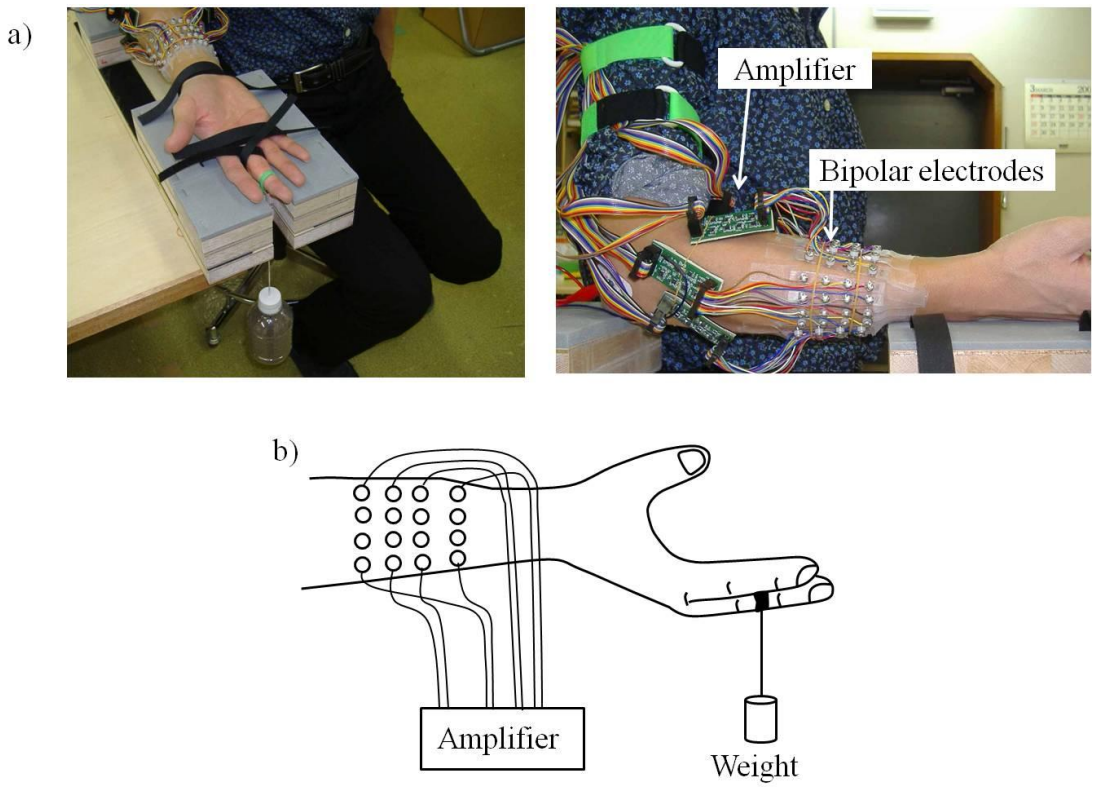

Figure 4.8 Experimental setup a) Arm posture during testing. The upper right arm of a subject was at 0° of abduction, the elbow joint flexed at 90° and the wrist placed at 0° of flexion, palm up. A total of 40 bipolar electrode pairs were placed around the forearm, with the middle points at 1/3 of the forearm length from the radial styloid process, parallel and in the axis of the radius. b) A weight was suspended with cotton thread from the middle phalanx of the middle finger, 10 mm from the PIP joint (reprinted from Nakajima, et al., 2014).

Table 4.3 Subjects specific data.

	Age (year)	Height (cm)	Weight (kg)	Circumference of forearm (mm)	Forearm length (mm)	Thickness of skin (mm)
Subject 1	32	180	63	210	280	2.5
Subject 2	37	172	71	201	260	3.0
Subject 3	37	174	60	194	240	2.5
Average*	35.3±2.4	175.3±3.4	64.7±4.6	201.7±6.5	260.0±16.3	2.7±0.2

* Mean±SD

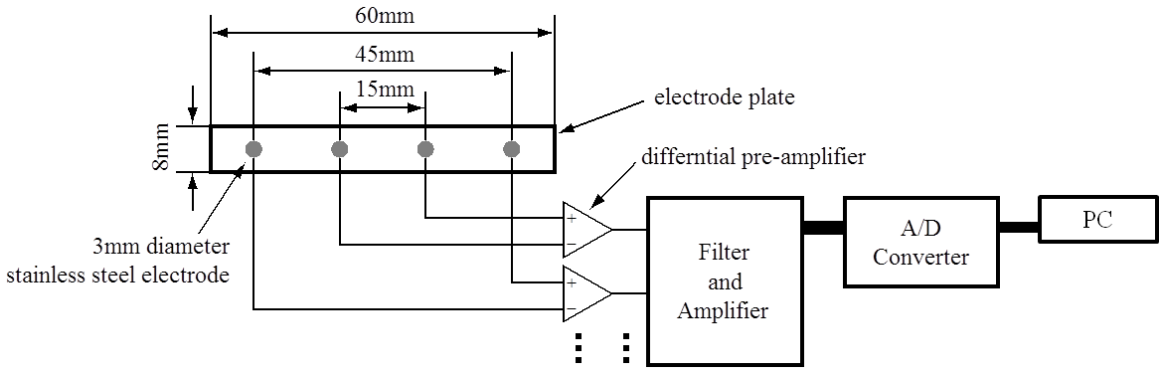

Figure 4.9 Schematic diagram of the electrode plate on which two bipolar electrode pairs were constructed. A pair of electrodes is connected to a differential pre-amplifier (reprinted from Nakajima, et al., 2014).

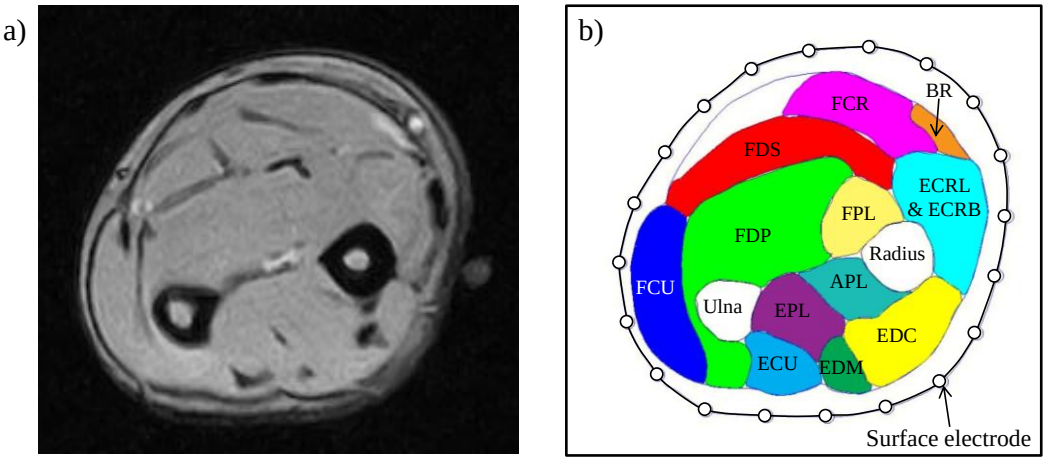

Figure 4.10 a) MR image of cross-section of a right forearm b) The arrangement of muscles in the forearm trace from the cross-sectional area of MR image at 1/3 forearm length from the processus styloideus radii, palm up. There are thirteen muscles in the cross section: the extensor carpi ulnaris (ECU), extensor digiti minimi (EDM), extensor digitorum communis (EDC), extensor pollicis longus (EPL), abductor pollicis longus (APL), extensor carpi radialis longus (ECRL), extensor carpi radialis brevis (ECRB), flexor digitorum profundus (FDP), flexor pollicis longus (FPL), brachioradialis (BR), flexor carpi ulnaris (FCU), flexor digitorum superficialis (FDS), and flexor carpi radialis (FCR) [reprinted from Nakajima, et al., 2014].

4.2 Results

Figure 4.11 shows the EMG tomography results for all subjects. The muscular activity of each muscle element was estimated by inverse calculation. The results show the position and level of activation of forearm muscle during the contraction. It can be seen that the muscle activities are unevenly distributed, with the positions of activated muscle consistent with the position of the muscle area from MRI. High muscle activities were found in the FDS and EDC areas. The area and intensity of the high-amplitude region in the tomographic image increased with load. Coactivation of the FDS and EDC areas when a load was applied to the PIP joint is apparent. A flexion load to the PIP joint of the middle finger caused activation of the FDS muscle, reflected in the estimation results. The total muscle activity s_m is defined as the summation of muscle action current (m_j) within the forearm area calculated by

$$s_m = \sum_j \left(m_j \times A_j \right) \tag{4.13}$$

where A_j is the area of muscle element j. Figure 4.12 shows the total muscle activities of all three subjects, which appear to increase monotonically with load.

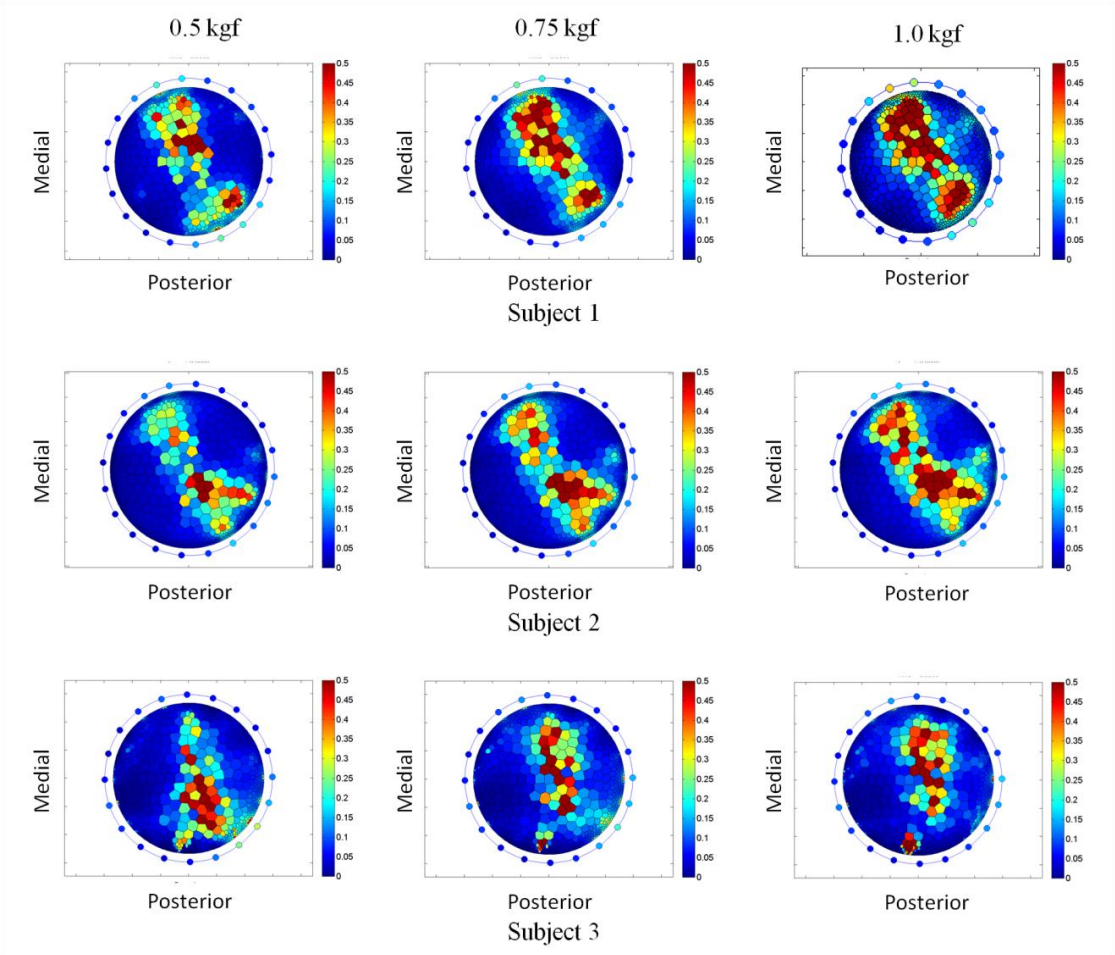

Figure 4.11 Electromyography computed tomography of all subjects when the flexion load (4.9, 7.4 and 9.8 N) was applied to the PIP joint of the middle phalanx (reprinted from Nakajima, et al., 2014).

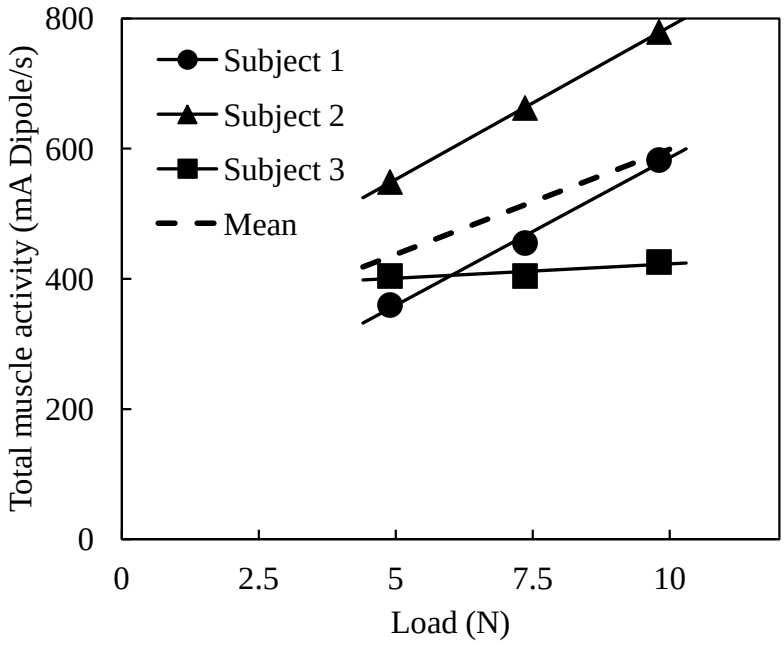

Figure 4.12 The relationship between the total muscle activation within forearm and load applied to the PIP joint of the middle phalanx of all subjects (reprinted from Nakajima, et al., 2014).

4.3 Discussion

To our knowledge, this is the first study to estimate EMG-CT in human forearm by using multi surface electrode, providing a new view in EMG study. Muscle activity of each element was computed from surface EMG signals that detected from the skin surface around the forearm. One novelty of this method is that we can locate the active muscle area during the contraction non-invasively.

Physical experiments were performed to verify the results. The positions of active muscle (Fig. 4.11) were validated by comparing the area of active elements with the outlines of muscle area (Fig.4.10b). During PIP joint contraction of the middle phalanx, the areas of activate muscle are of the FDC and EDC which is the main flexor and extensor in a middle finger. Kinesiologically, a flexion load to the PIP joint of the middle finger causes activation of the FDS muscle, and this is reflected in the estimated results. When load increases, force production requires more recruitment of MUs, the increase in muscle activation area and amplitude seem consistent with the results. The activations of muscle are of the FDS, FDP and EDC, which are the primary flexor and extensor of the fingers. Many studies which used intramuscular electrodes to detect muscle activity confirmed that during finger flexion, these muscles were active (Johanson, et al., 1990; Maier and Hepp-Reymond, 1995; Butler, et al., 2005). In addition, when load increases from 4.9 N to 9.8 N, the mean of total muscle activity of all subjects increase from 437.6 mADipole/s to 595.6 mADipole/s (Fig. 4.12). It seems that EMG-CT can investigate muscle activities in the forearm properly.

Muscle activation pattern of Subject 1 and Subject 2 seem to be similar. Both subjects used the same muscle, i.e., the FDS, FDP and EDC to generate muscle force when a load was applied to the middle finger. The slight different in the activation area and amplitude might due to the different in individual muscle structure. It is noted that Subject 3 seems to use a bit more of the FCR, this might cause by unintentional movement of wrist during the task.

The advantage of surface EMG tomography compared to the frequently-used intramuscular electromyography is that it provides the method to locate the activated MUs non-invasively from the skin surface. Give ability to gain a more comprehensive insight into the individual muscle activity of the whole cross-sectional area. In principle surface EMG tomography allows us to detect pathological changes at the MU level, providing a novel tool for studying MU function and strategies. In clinical application aspect, it can be used as diagnostic tool for neurogenic disorder or MU disorder.

The forearm conduction model which was used in the reverse-estimation considered only muscle tissue, to reduce the computational load. However, there are subcutaneous fat and skin which may influence the estimation in a real forearm. Lowery et al. have reported the influence of subcutaneous fat and skin on the crosstalk of the myoelectric potential, using a cylindrical conduction model consisting of muscle tissue, bone, as well as subcutaneous fat and skin (Lowery, et al., 2003). They concluded that increases of the thickness of subcutaneous fat causes increases in the crosstalk. The estimation method proposed in this paper is basically an analysis of the crosstalk. Therefore, it has possibility that the subcutaneous fat would affect the estimation. Since the thickness of subcutaneous fat in the forearm of the subjects was less than 3 mm, the influence on the estimates may be small. However, this factor must be considered in estimating deep muscles which generate weak surface EMG signals.

In addition, subcutaneous fat also causes decreases in the mean power frequency of the surface EMG spectrum, similar to a low-pass filter, because of the permittivity of the fat (Stoykov, et al., 2002). The low-pass filter effect is also caused by the spatial dispersion of the surface EMG distribution (Lindström et al., 1977). The effect is stronger with increases in the distance between an activated muscle fiber and the surface. Therefore, the surface EMG power in high frequency is easily reduced. To avoid the influence of the low-

pass filter effect on the reverse estimation, using only the low frequency components of the surface EMG for the calculation would be effective.

The anisotropic conductivity of muscle tissue and muscle alignment from previous studies was used in the estimation (Schwan et al., 1953; Burger and van, 1961; Geddes and Baker, 1967; Gabriel, et al., 1996; Faes, et al., 1999). However, in actual measurements, these parameters may be highly dependent on the individual being measured. To increase the precision of the estimates, calibration of these parameters for each subject is necessary. Electrical impedance tomography (EIT) can measure the conductivity distribution in the forearm (Cheney et al., 1999). EIT is the method to reconstruct the conductivity distribution in a volume conductor from electrical potential distribution of the surface causing by the current through the surface electrodes around the conductor. The current is loaded through a pair of the electrodes and simultaneously measured potentials at other electrodes, and then it is repeated at whole electrodes. The conductivity distribution is reconstructed to compare the measured potential distributions to the simulated those using the finite element model and an optimization method. Since the alignment of electrodes in EIT is approximately that of the estimates, it is useful to measure the conductivity distribution in a sequence on an experiment.

Furthermore, the surface electrode position on the forearm should be also calibrated. The estimation method has sensitivity to the circumferential electrode positions because many of muscles in the forearm are thin. The positions are certainly misaligned even with extreme caution. However, it is impractical to claim fine accuracy to the measurers. To calibrate the electrode position, detecting the closest electrodes from activated index muscles would be useful. Firstly, the measurer activates the index muscle. Then the electrode detecting the strongest surface EMG power can be considered as the closest to the activated muscle. To repeat the detection by some index muscles, the correct alignment of the electrode can be found.

From this study, it is demonstrated that EMG-CT tomography allows the investigation of the activity of the MU within the muscle region. This makes the activated MUs to be located non-invasively from the skin surface possible. This method opens a new window to EMG study in the forearm which could be potentially used for studying of muscle mechanism and diagnostic tool for rehabilitation evaluation in the future.

Chapter 5 Muscle Stress Distribution in the Forearm Using EMG-CT Method

5.1 Stress estimation method

Measuring muscle stress defined as force generated in the muscles per unit cross-sectional area of the forearm is of great importance because it could help to understand how internal load is shared within the forearm muscles and to provide more insight into muscle mechanics.

Some researchers have attempted to measure muscle force using force transducers implanted into the forearm (Schuind, et al., 1992; Dennerlein, et al., 1998). Direct measurement of forces in forearm muscle is impractical and invasive. The muscle function and condition can be determined by electromyography (EMG) signals. Surface electrode is usually used to measure EMG signal from skin surface due to its non-invasive and ease of use. Many studies related EMG signals to muscle force generation (Buchanan, et al., 1993; Duque, et al., 1995; Hoozemans and van Dieen, 2005; Vigouroux, et al., 2007; Disselhorst-Klug, et al., 2009). However, conventional surface EMG cannot assess individual muscle activity due to high distortion of signals from noise generated by nearby muscles, making it difficult to estimate stress distribution within the forearm muscles.

It was demonstrated that the EMG–CT method can measure muscle activity distribution in the whole cross-section of the forearm in a non-invasive manner. The muscle activity distribution identified by EMG–CT has high potential to estimate muscle stress in the forearm muscles.

Therefore, this study proposes a novel method to estimate muscle stress generated in the forearm during hand gripping, using muscle activity data obtained by EMG–CT. For calculation of the stress, the cross-sectional geometry of the forearm should be measured. Recently, fast and low-cost handy 3D scanning technologies have been increasingly accepted as an efficient approach to collecting body segment data (Stančić, et al., 2013; Van den Herrewegen, et al., 2014). A forearm model was constructed from subjects' forearm geometry obtained with a handy 3D scanner. The stress distribution within the forearm during gripping loads was estimated and visualized in tomographic images. The developed method has many practical applications

such as determining the effectiveness of surgical or rehabilitation procedures by monitoring muscle recovery progress, or used as a diagnostic tool for detecting diseased or injured muscle within the patient forearm so it can be treated more accurately.

In this study, muscle stress generated in the forearm during hand gripping was performed as a trial. Hand gripping requires forces exerted by the fingers and the thumb, which are mainly controlled by the muscles of the forearm; thus, the gripping abilities of the hand are directly related to the strength of the forearm muscles. During performing a hand grip as shown in Fig. 5.1, maximum gripping force F was defined as the force required by the subject's hand to keep a hand grip at full grip position, as described by the following equation:

$$F \equiv \int_{x_1}^{x_2} w_f \, dx \tag{5.1}$$

where w_f is the force distributed along the handle of the hand grip during full grip position. x_1 and x_2 are the distances from the center of rotation of the hand grip to the respective ends of the handle. In static equilibrium, torque generated by the hand grip is equal to torque exerted by w_f, as described by the following equation:

$$T_{max} = \int_{x_1}^{x_2} w_f \, x dx \tag{5.2}$$

where $T_{\max}$ is the maximum torque generated by the hand grip at the full grip position. It was assumed that at the full grip position, the subject's hand exerted a uniformly distributed force (constant w_f) on the handle of the hand grip. Thus, F can be calculated by the following equation:

$$F = \frac{2T_{max}}{(x_2 + x_1)} \tag{5.3}$$

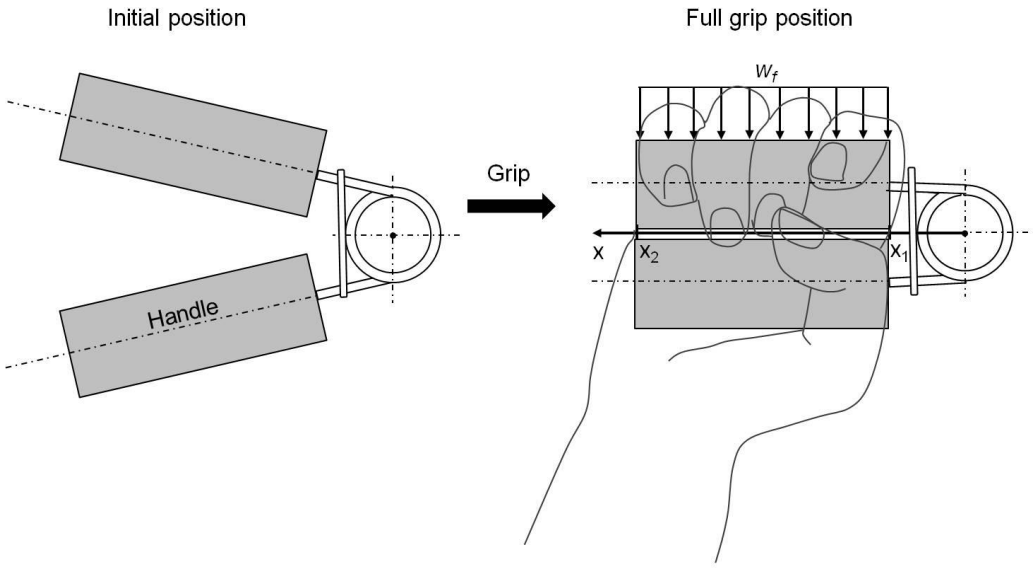

Figure 5.1 A hand grip used in the experiment. The subject exerted a uniformly distributed force w_f along the handle to keep the hand grip in the full grip position.

5.1.1 Real shape forearm model construction

The realistic geometry of forearm is an important factor especially in stress estimation in which the area of muscle affects the result. Using average geometry such as circular shape to construct forearm model might yield inaccurate results due to the individual difference. In this study, the procedure to obtain the outline of forearm cross-sectional area using a handy 3D scanner was proposed.

To construct a forearm model of each subject, an outline of the forearm cross-sectional area was obtained according to the subject's forearm geometry as shown in Fig. 5.2. The subject's arm was scanned with a handy 3D scanner (Sense, 3D System Inc., SC, USA) consisting of a CMOS camera, a color image CMOS camera and an infrared laser projector. During measurements, the subject sat on a chair with his arm extended away from the torso in supine position. The positions of the lateral epicondyle of the humerus, the lateral epeicondyle of the humerus and ulna were marked with color markers. An examiner held the 3D scanner and moved it around the subject to scan the whole subject's arm (Fig. 5.2a). The scan data points of subject's arm obtained from the 3D scanner numbered approximately 130,000 points at a resolution of a point-to-point space of approximately 0.6 mm with RGB color. The data points were cleaned, filtered and edited using computer program MeshLab (Version 1.3.3, Visual Computing Lab, Italian National Research Council, Italy) than the subject's forearm geometry was reconstructed from the cleaned data (Fig. 5.2b). The forearm geometry was exported into MATLAB (version R2014a, Mathworks, USA) for further processing.

The forearm axis was drawn by connecting points between two anatomical landmarks: the lateral epicondyle of the humerus and the radial styloid. The points within ± 2-mm interval from EMG–CT analyzed section which perpendiculars to the forearm axis were projected to a plane (Fig. 5.3a). An outline of the forearm cross-sectional area was thus created by connecting the points using a simple convex polygonal approximation method (Fig. 5.3b).

An EMG conduction model was constructed using the outline of the forearm cross-sectional area (Fig. 5.4a). Muscle element nodes were distributed across the entire cross-sectional with an element size of 1 mm at the surface and 5 mm for the inside region using Delaunay triangulation method. Delaunay triangulations maximize the minimum angle of all the angles of the triangles in the triangulation; they tend to avoid skinny triangles in order to get well distributed nodes within the forearm area (Fig. 5.4b). The boundary of each muscle element was divided using Voronoi tessellation (Fig. 5.4c). The area of each muscle element was calculated and used in muscle stress estimation. The surface electrodes were placed around the outline of the forearm model. The conduction distance of each muscle element was the distance between the muscle element and the surface electrode (Fig. 5.4d). The real shape EMG conduction model was constructed and used in calculating muscle activation using EMG-CT method.

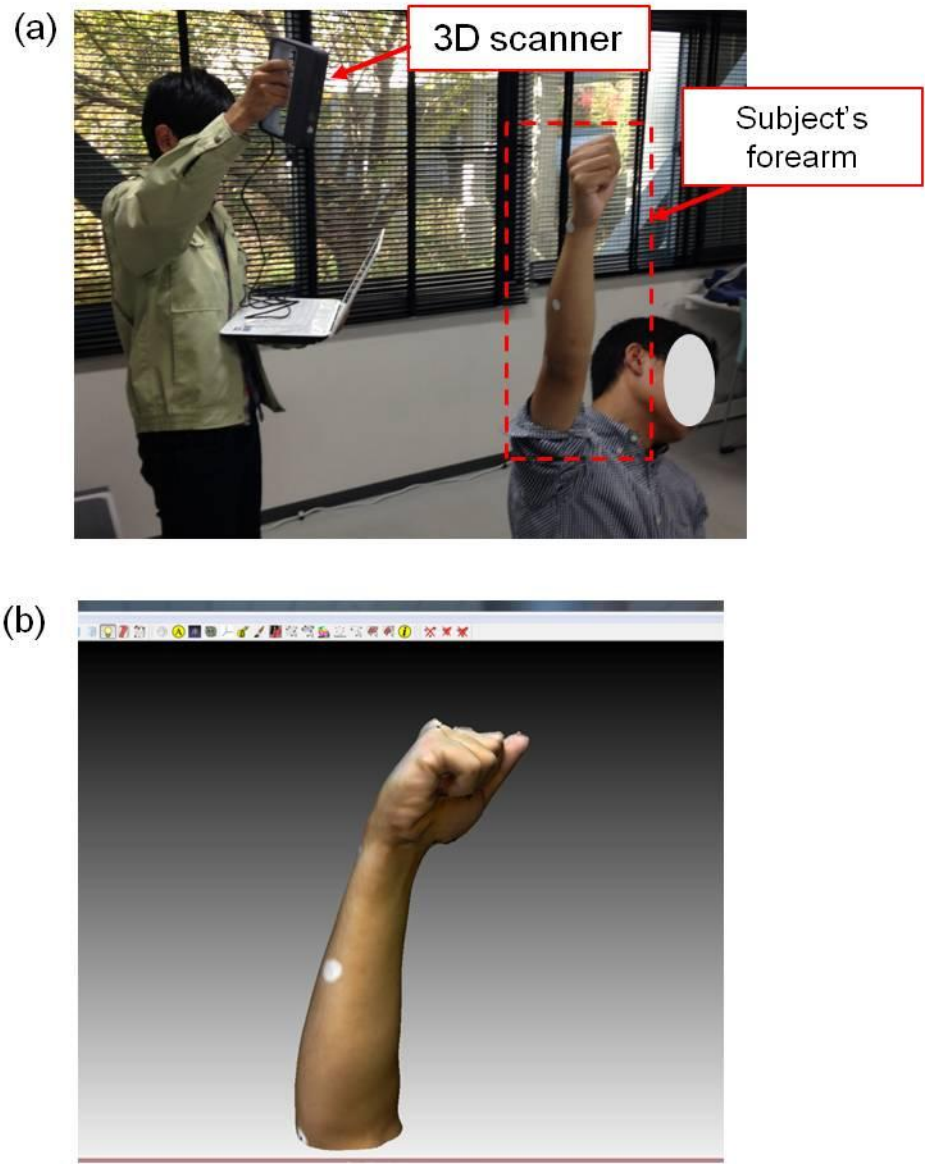

Figure 5.2 Subject's forearm scanning process. (a) The subject sat and extended his arm during the scanning process. (b) Subject's forearm was reconstructed from scanned data point.

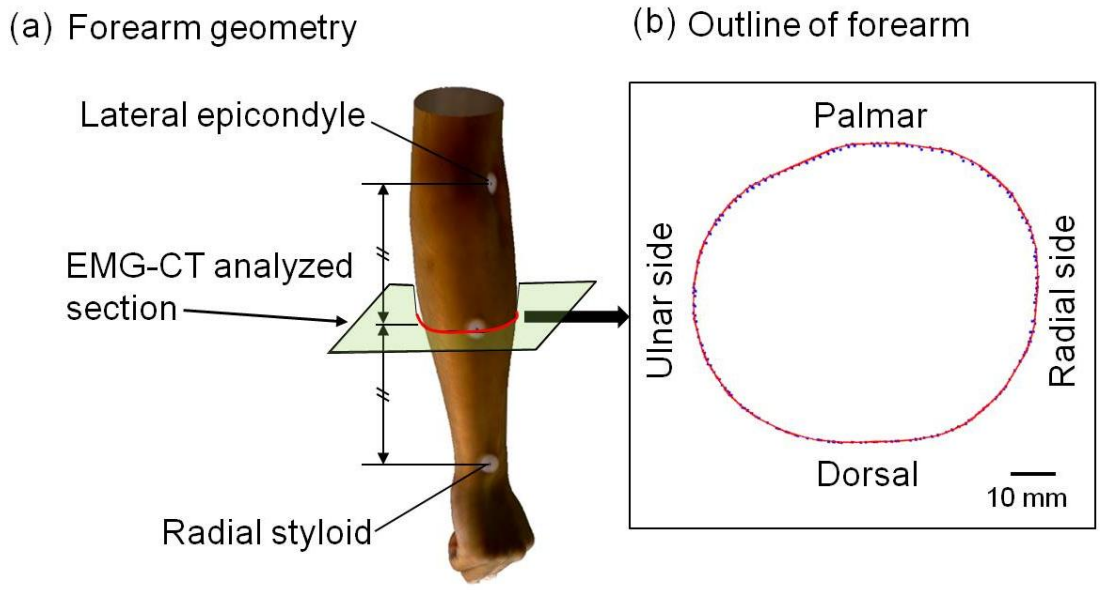

Figure 5.3 (a) Subject's forearm geometry based on 3D scan data. (b) Forearm cross-sectional area outline extracted from the EMG-analyzed section.

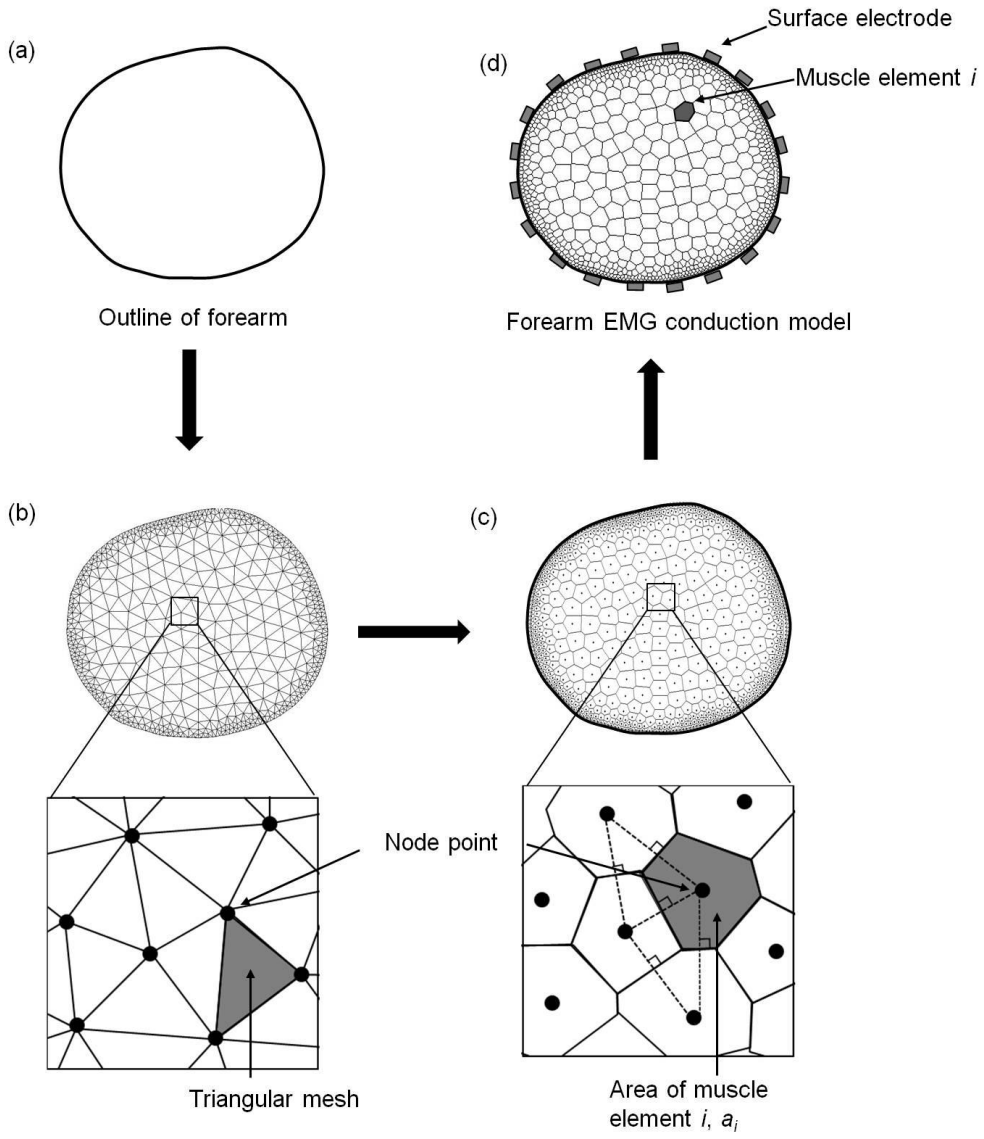

Figure 5.4 Forearm EMG conduction model construction. (a) Forearm cross-sectional area obtained from 3D scanner. (b) Nodes of muscle element were distributed within the muscle region. (c) The muscle region within the forearm outline was divided into small elements using Voronoi tessellation. (d) Surface electrodes were placed around the outline of the forearm.

5.1.2 Muscle activity calculation

The attenuation of the action potential depends on tissue conductivity and the distance between a muscle element and the surface electrode (Nakajima, et al., 2014). EMG-CT method as described in Chapter 4 was used in this study. It is considered that each muscle element was activated independently. Thus, the statistical summation of power of the EMG signals was possible. The mean square value of EMG from all muscle elements i detected by bipolar electrodes j, V_j can be simply expressed by the following equation:

$$\bar{V}_j^2 = V_0(d_j)^2 \sum_i m_i^2 \left(\frac{l_{ij}}{l_0} \right)^{2b(d_j)} \tag{5.4}$$

where $V_0(d_j)$ (mV·s/(mA dipole)) is a transformation coefficient that depends on the distance between the pair of bipolar electrodes d_j, m_i (mA dipole/s) is the muscle activity of the element i, l_{ij} (mm) is the conduction distance between the muscle element i and a pair of bipolar electrodes j, l_0 is the unit length (1 mm), and $b(d_j)$ is the power exponent of the attenuation under the distance d_j. In this study, d_j was 15 and 45 mm. V_0 and b were 162 mV·s/mA dipole and -2.12 at d_j = 15 mm and 115 mV·s/mA dipole and -1.74 at d_j = 45 mm (Nakajima, et al., 2014).

The activity of each muscle element m_i was calculated using a sequential quadratic programming method to minimize the objective function (OF), which was defined as the sum of the power of the differences between the measured EMG V_{Mj} and the calculated EMG V_j, as shown by the following equation:

$$OF = \sum_j (V_{Mj} - V_j)^2 \tag{5.5}$$

The optimization was calculated using the Optimization Toolbox in MATLAB (Mathworks, USA).

5.1.3 Stress calculation

When external forces are applied to the fingers, the muscles of the forearm generate reaction forces to maintain a static equilibrium. Total muscle activity Σm_i is defined as the sum of muscle activity within the forearm cross-sectional area calculated by EMG-CT method which reflects the amount of force generated by the muscles during contraction. The muscle force required to maintain a static equilibrium increased with the increase in gripping force. During gripping, all muscles within the forearm work together to generate gripping force. A linear relationship between F and Σm_i was assumed in this study. The muscle activity-force coefficient α (N·s/mA dipole) was defined as shown by the following equation:

$$F = \alpha \sum_i m_i \tag{5.6}$$

Here, the muscle force generated by each element can be calculated from the stress within each element multiplied by its area, as shown by the following equation:

$$f_i = \sigma_i a_i \tag{5.7}$$

where f_i (N) is the force generated by muscle element i, σ_i (MPa) is the stress in muscle element i, and a_i (mm^2) is the area of a muscle element i. Thus, F is equal to the sum of the force generated by all elements within the forearm and can be expressed by the following equation:

$$F = \sum_i f_i = \sum_i \sigma_i a_i = \alpha \sum_i m_i \tag{5.8}$$

The stress of each element within forearm EMG conduction model can be calculated from the following equation:

$$\sigma_i = \alpha \frac{m_i}{a_i} \tag{5.9}$$

Thus, the stress distribution in the forearm muscles can be calculated using muscle activity measured by EMG–CT and Equation (5.9).

5.2 Experimental procedure

Three male subjects (age, 23 ± 0 years; height, 169.7 ± 4.5 cm; weight, 65 ± 5.0 kg; mean ± SD) participated in this study. Table 5.1 shows the subject's specific data. The subjects sat on a chair with their dominant arm placed on a horizontal table. The upper arm was at approximately 0° of abduction, the elbow joint was flexed at approximately 90°, and the wrist was placed in supine position (Fig. 5.5).

The gripping force of each hand grip was measured using a testing machine (Model 3365, INSTRON Co., USA) by pressing a load cell (± 500 N) against the handle of a hand grip to measure resistance force. The probe head that used to press against hand grip has a diameter of 50 mm. A point of applied force on the handle of a hand grip was at the middle of gripping length (Fig. 5.6). Table 5.2 shows the specifications of three hand grips used in the experiment. For each gripping trial, the subject held a hand grip between the middle phalanges of fingers and palm and then squeezed the handles to full grip position and held for 5 seconds, three trials per load with 5 seconds of relaxation between trials.

EMG signals from the forearm were recorded using an EMG band, consisting of 40 pairs of bipolar surface electrodes (3-mm diameter disciform stainless steel electrodes). Each four electrodes were placed on a custom-built electrode plate. The inter-electrode distances of the bipolar electrodes of narrow and wide pairs are 15 and 45 mm respectively (Fig. 5.7a). EMG signals are detected from each electrode plate then amplified and sent to computer via connection port at electrode plate No. 3. The middle point of the EMG band was positioned at the middle point of the forearm lengthwise, between the lateral epicondyle of the humerus and the radial styloid. Before attachment of the EMG band, the subject's forearm skin was cleaned with an alcohol swab. Fat and skin thickness were measured using a skinfold caliper (Marutech, Japan). The position of the electrode plate No.1 was arranged to be at subject's ulna position.

The EMG data was collected for 30 seconds per trial using a custom program (LabVIEW 8.5, National Instruments, TX, USA). The collected raw EMG data were exported into MATLAB (version R2014a, Mathworks, USA) for further processing. The raw EMG data were filtered with a second-order Butterworth high- pass filter followed by a second-order Butterworth low-pass filter. The root mean square (RMS) value and mean power of each channel were calculated from the recorded signals in 500-ms windows. The average data were calculated from three trials for each load condition.

Magnetic Resonance Imaging (MRI) of each subject was taken using MRI scanning machine at Hokkaido University hospital. The cross-sectional area at EMG-CT analysis plane was marked using a marker. The subjects lie down, extend their right arm in MRI scanning machine and took the MRI. The scan MRIs were import to image processing program (ImageJ 1.48v, National Institutes of Health, USA) for contrast adjustment.

In order to compare the result with anatomical information, Figure 5.8 shows typical pattern of muscle alignment in the middle part of forearm obtained from a MR image. There are thirteen muscles in the cross section: the extensor carpi ulnaris (ECU), extensor digiti minimi (EDM), extensor digitorum communis (EDC), extensor pollicis longus (EPL), abductor pollicis longus (APL), extensor carpi radialis longus (ECRL), extensor carpi radialis brevis (ECRB), flexor digitorum profundus (FDP), flexor pollicis longus (FPL), brachioradialis (BR), flexor carpi ulnaris (FCU), flexor digitorum superficialis (FDS), and flexor carpi radialis (FCR) [Nakajima, et al., 2014].

Table 5.1 Subjects specific data.

	Age (year)	Height (cm)	Weight (kg)	Average fat and skin thickness (mm)
Subject A	23	165	60	1.2
Subject B	23	174	70	1.6
Subject C	23	170	65	1.3
Mean ± SD	23 ± 0.0	170 ± 4.5	65 ± 5	1.7 ± 0.2

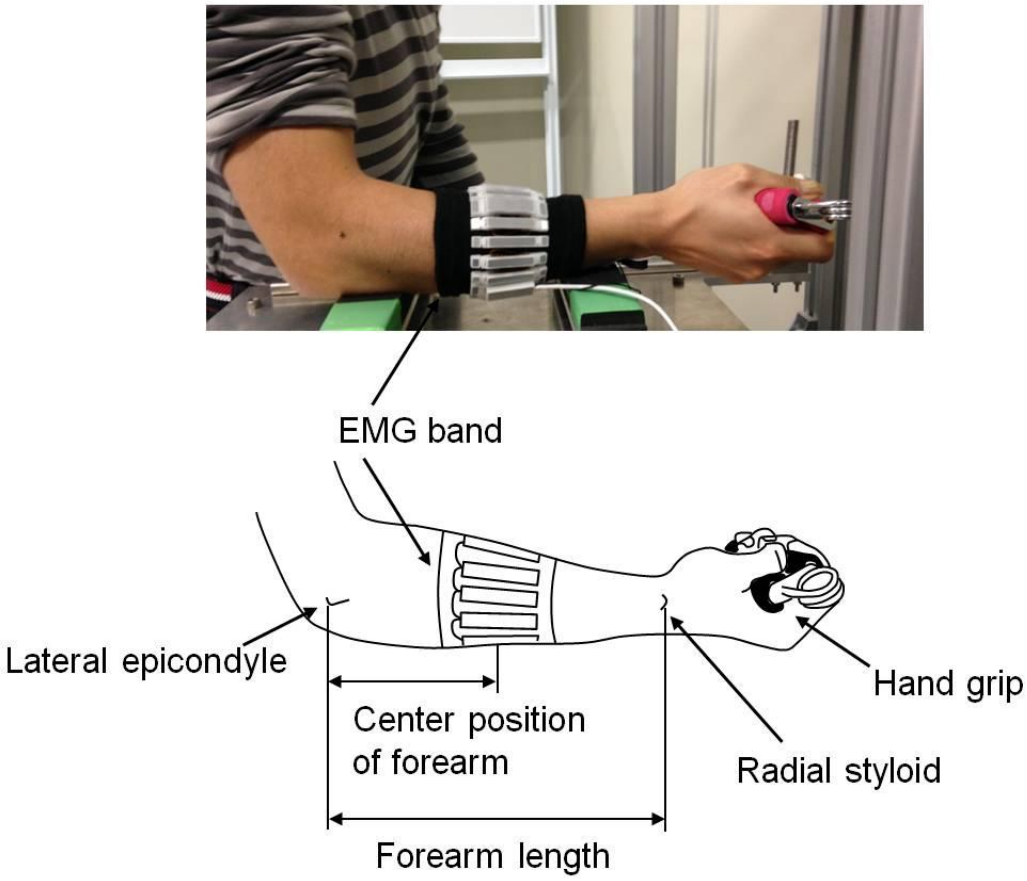

Figure 5.5 Experimental setup. The upper right arm of a subject was placed on a table, holding a hand grip in supinate position. An EMG band was bound around the forearm to detect the EMG signals. The position of the EMG band is at the middle point of forearm length; between lateral epicondyle and radial styolid. Subject gripped and held the hand grip in full grip position.

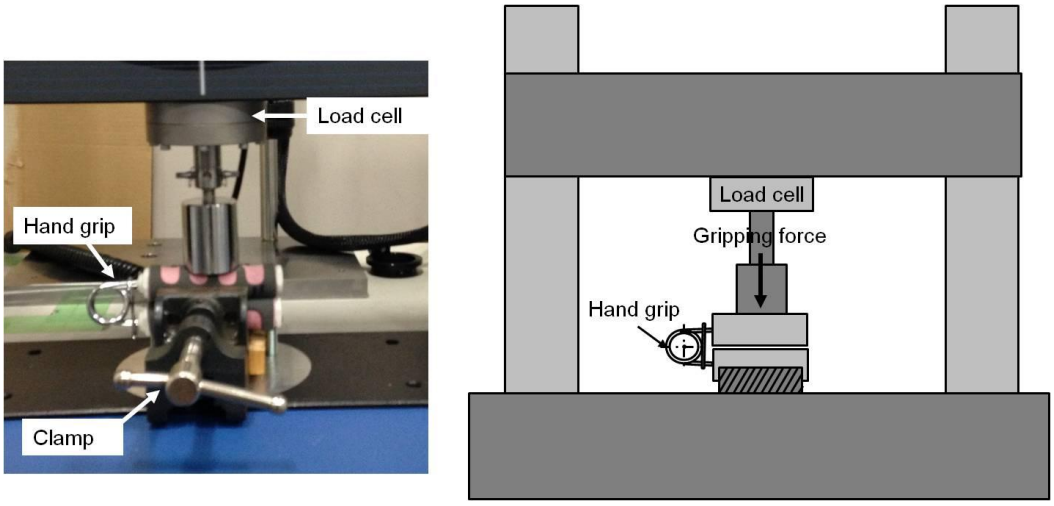

Figure 5.6 Gripping force measurement. Load cell was press against a fixed hand grip to measure gripping force required to hold a hand grip at full grip position.

Table 5.2 Specification of the three hand grips used in the experiment. k is the measured torsion spring constant, T_{max} is the measured maximum torque generated by the hand grip at the full grip position, and F is maximum gripping force as defined in Equation (5.1).

No. Hand grip	k (N·m/degree)	T_{max} (N·m)	F (N)
A	0.21	5.01	77
B	0.37	8.06	124
C	0.61	15.73	242

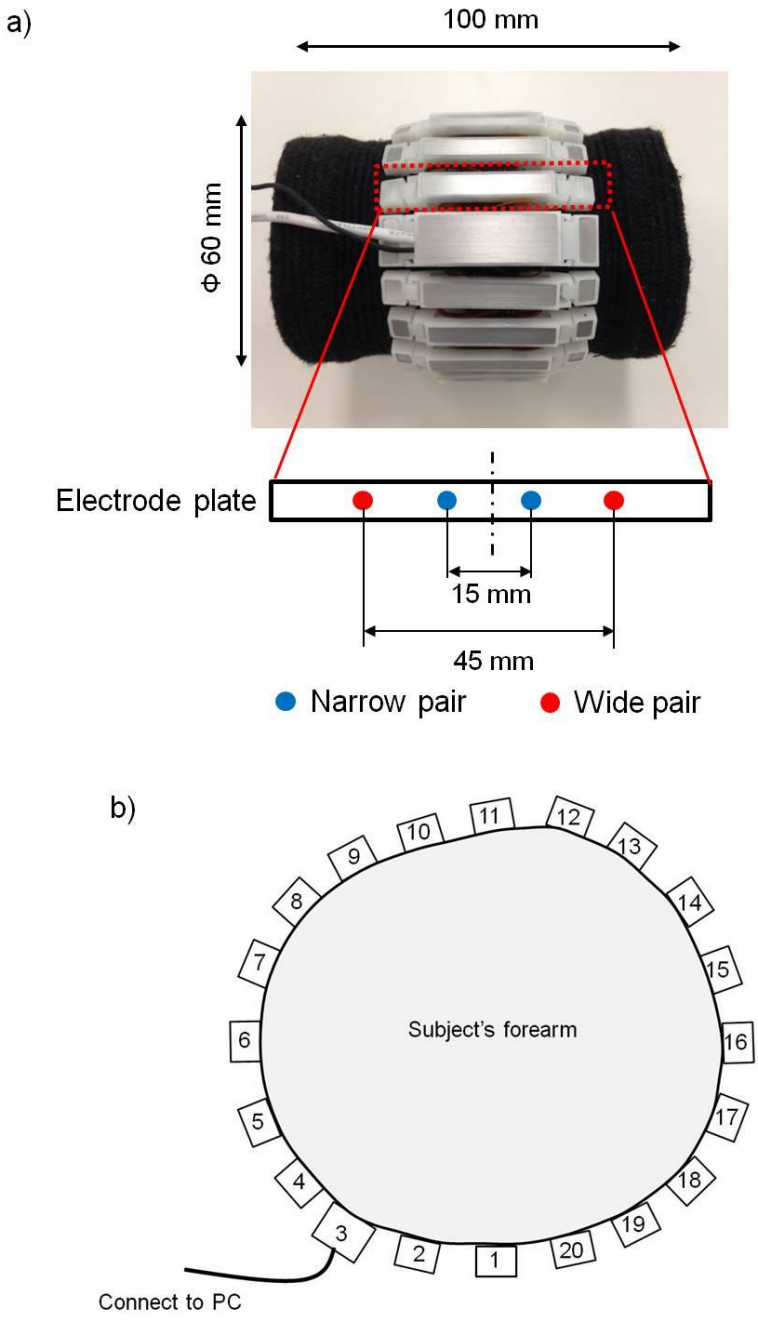

Figure 5.7 a) The EMG band consists of 20 electrode plates in which two bipolar electrode pairs were constructed. The inter-electrode distances in the differential bipolar electrode were 15 and 45 mm. b) schematic diagram of EMG band. The numbers indicate electrode plate. EMG band connect to PC via electrode plate No.3.

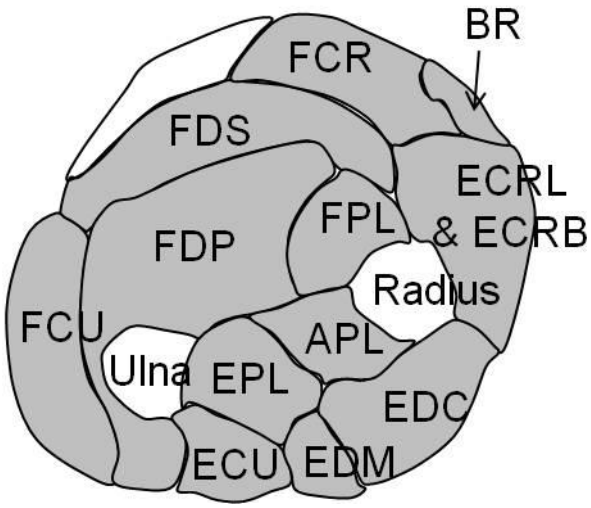

Figure 5.8 Typical alignment of muscles in the middle part of forearm, by tracing from the cross-sectional area of a MR image. There are thirteen muscles in the cross section: the extensor carpi ulnaris (ECU), extensor digiti minimi (EDM), extensor digitorum communis (EDC), extensor pollicis longus (EPL), abductor pollicis longus (APL), extensor carpi radialis longus (ECRL), extensor carpi radialis brevis (ECRB), flexor digitorum profundus (FDP), flexor pollicis longus (FPL), brachioradialis (BR), flexor carpi ulnaris (FCU), flexor digitorum superficialis (FDS), and flexor carpi radialis (FCR) [reprinted from Nakajima, et al., 2014].

5.3 Results

Figure 5.9 shows example of raw EMG data obtained by EMG band of Subject A during 124 N gripping force. The timing and amplitude of narrow pair and wide pair were in consistent with subject's gripping action. EMG data obtained from EMG band was used to analyze muscle activation within the forearm using EMG-CT method. Figure 5.10 shows the processed RMS value that used in calculation of muscle activity.

Figure 5.11a shows an example of EMG–CT result of subject A for the first trial using 124 N of gripping force. The distribution of muscle activity can be observed. The intensity measured for each muscle element represents the level of muscle activity. The result provides an outline of the subject's forearm geometry in a supine position. The palmar side is represented at the upper side of the image, and the radial side can be found at the right-hand side of the image.

Figure 5.12 shows the relationship between F and the total muscle activity within the forearm of all subjects. Total muscle activities were plotted against gripping force, and the relationship was described by a linear regression (R^2 = 0.97 ± 0.04). The mean of the total muscle activity of all subjects increased from 1626 ± 344 to 3878 ± 170 mA dipole/s when the gripping force increased from 77 to 242 N. α of subjects A, B, and C were 0.054, 0.060, and 0.062 N·s/mA dipole, respectively.

An example of stress distribution within the forearm muscle of subject A was calculated from α and Equation (5.9). During gripping, muscle activity was distributed across the entire cross-sectional area, indicating the cooperative activity of forearm muscles (Fig. 5.11a). Stress was calculated by the method described and is shown in Fig 5.11b. Stress distribution showed a trend consistent with the muscle activity pattern, although significant stress at the surface region was detected. The position of maximum activity is different from

that of maximum muscle stress, because stress calculation considers the area of muscle elements unlike muscle activity calculation.

Figure 5.13 shows tomographic images representing stress distribution within the forearm muscles during gripping in all subjects. Patterns of stress distribution could be observed under all investigated conditions. The results showed a change in level and area for all conditions, and an increase in stress concomitant with load increase was observed. A MRI of the forearm cross-sectional area of each subject is shown in the top row for anatomical comparison (Fig. 5.13a). The activated area and the maximum value of muscle stress increased with gripping force in all subjects. Under the 77 and 124 N load conditions, muscles in ulnar region and radial–dorsal region were active in all subjects. Under the 242 N load condition, muscles in the palmar region were active in subjects A and B. The average maximum stresses in all subjects under 77, 124, and 242 N load conditions were 0.08 ± 0.01, 0.11 ± 0.01, and 0.18 ± 0.02 MPa, respectively. In subject A, the maximum stress was found in the ulnar region under all load conditions, whereas in subject B and C, the maximum stress was found in the radial–dorsal region under all load conditions.

Figure 5.14 to 5.16 show muscle stress distribution during gripping of all subjects. Muscle stress from three trials of every loading condition was presented in tomographic image. The maximum stress for each trial was indicated by an arrow as shown in the figures. The difference of muscle stress distribution can be observed individually. Figure 5.17 shows average maximum stress within FDP, FDS, EDC and FCR muscle of all subjects. Maximum stress of all muscles increased as gripping force increased.

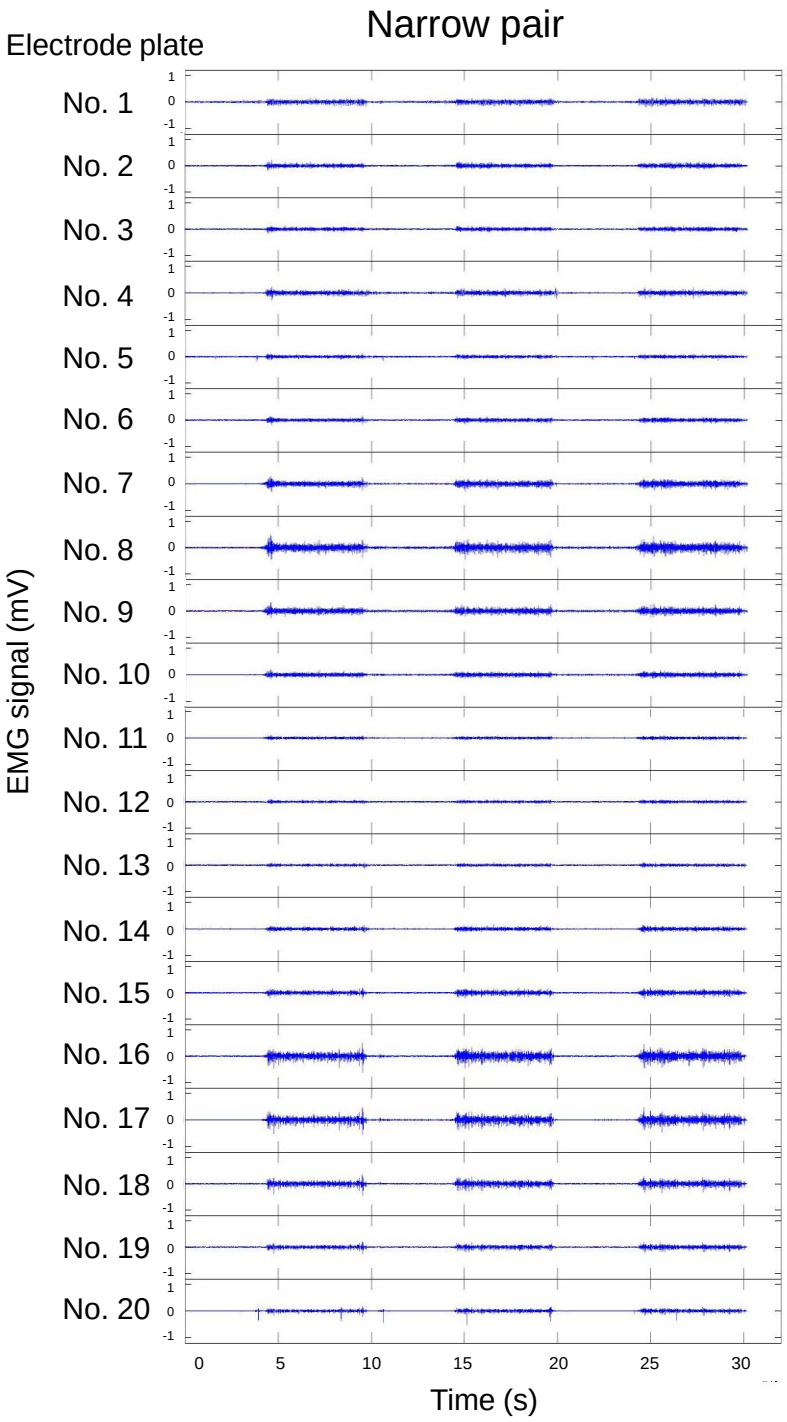

Figure 5.9 (continue)

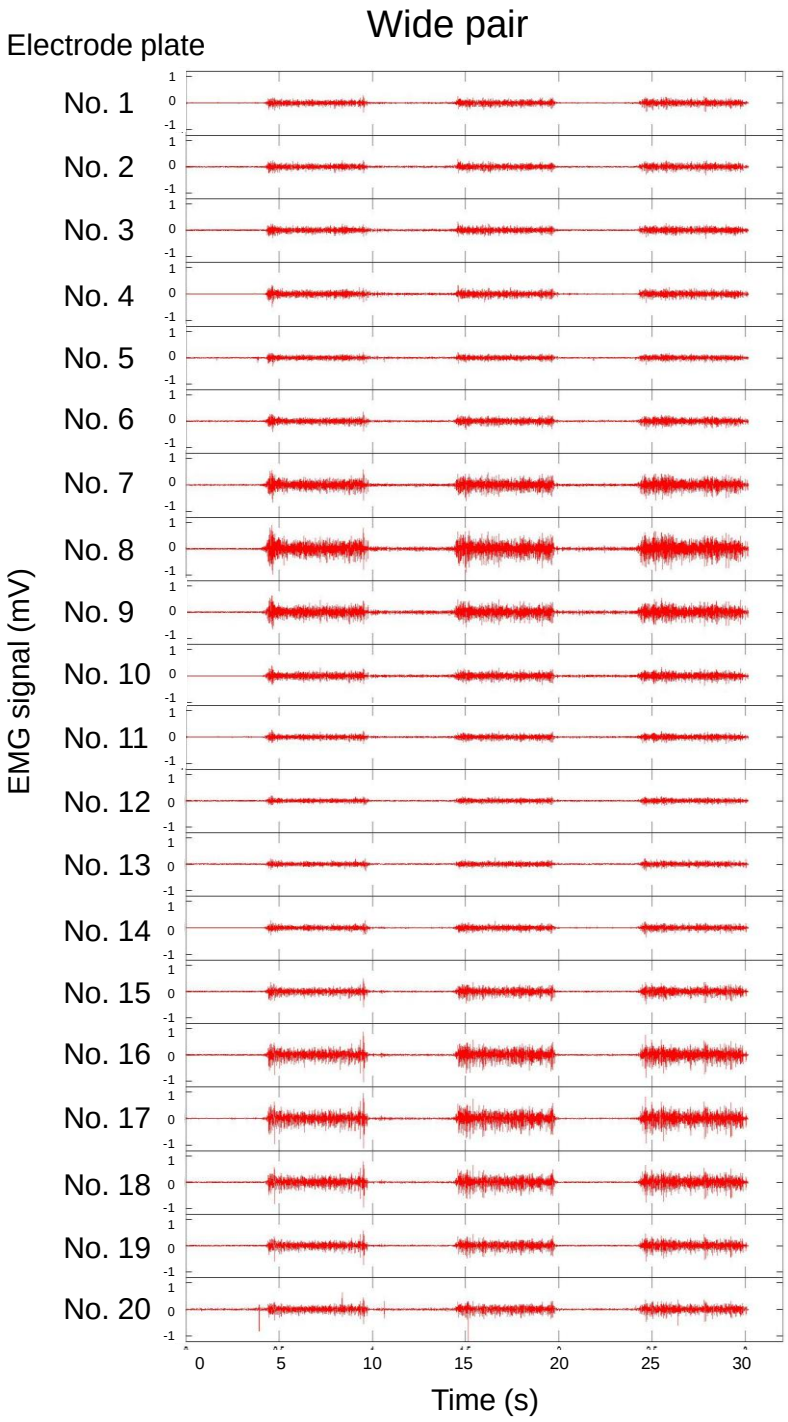

Figure 5.9 Raw EMG signal obtained by EMG band of subject A during 124 N gripping force. The EMG band is consisted of 20 electrode plates. The distance between bipolar electrode of narrow pair and wide pair are 15 mm and 45 mm respectively.

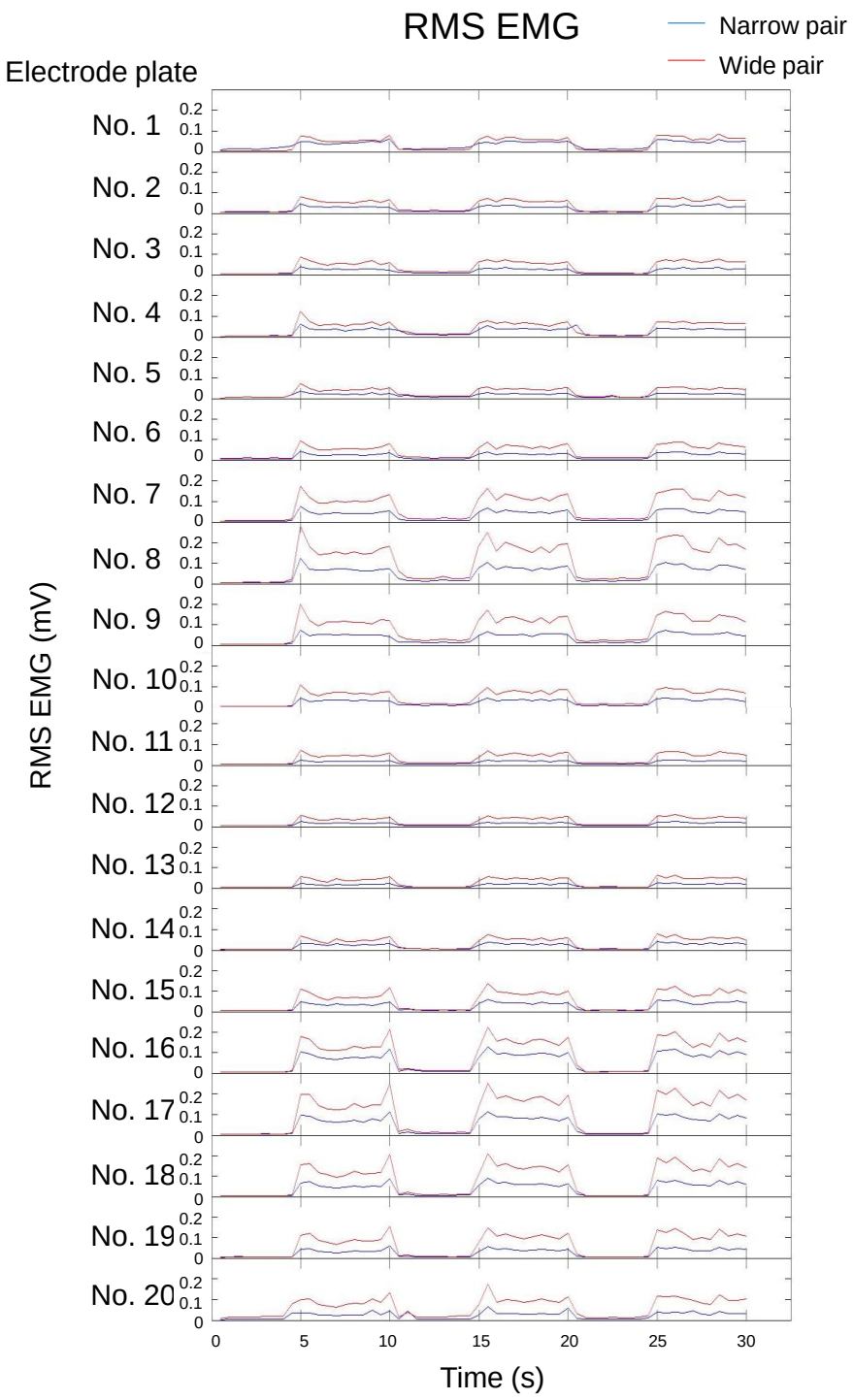

Figure 5.10 Processed RMS of EMG signal of subject A during 124 N gripping force. The RMS EMG from 20 electrode plate of narrow pair (blue line) and wide pair (red line) were used as input to calculate muscle activation using EMG-CT.

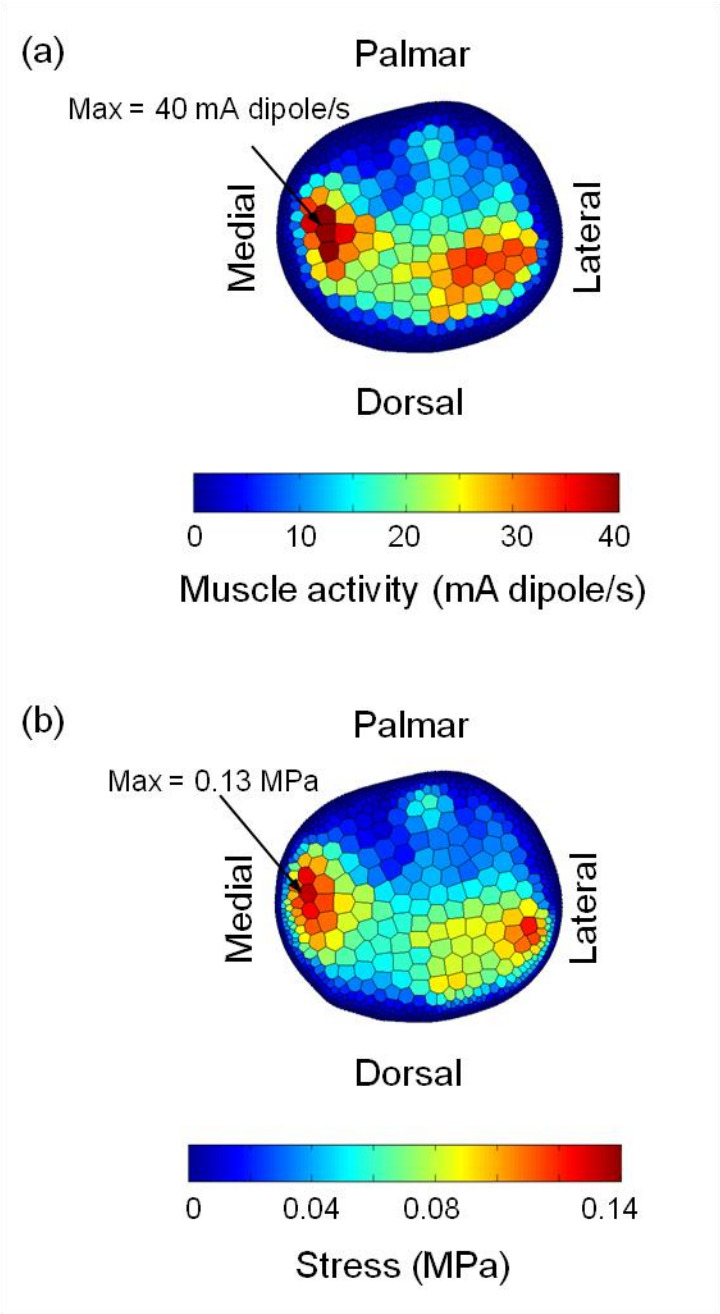

Figure 5.11 (a) Typical muscle activity distribution of subject A during 124 N of gripping force. (b) The stress distribution within the forearm was calculated from the muscle activity distribution as shown in (a).

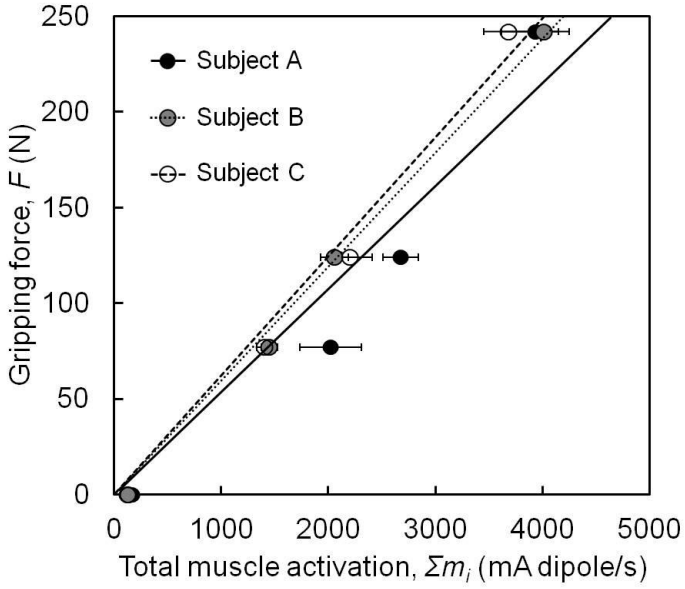

Figure 5.12 Relationship between gripping force F and total muscle activity Σm_i within the forearm during gripping.

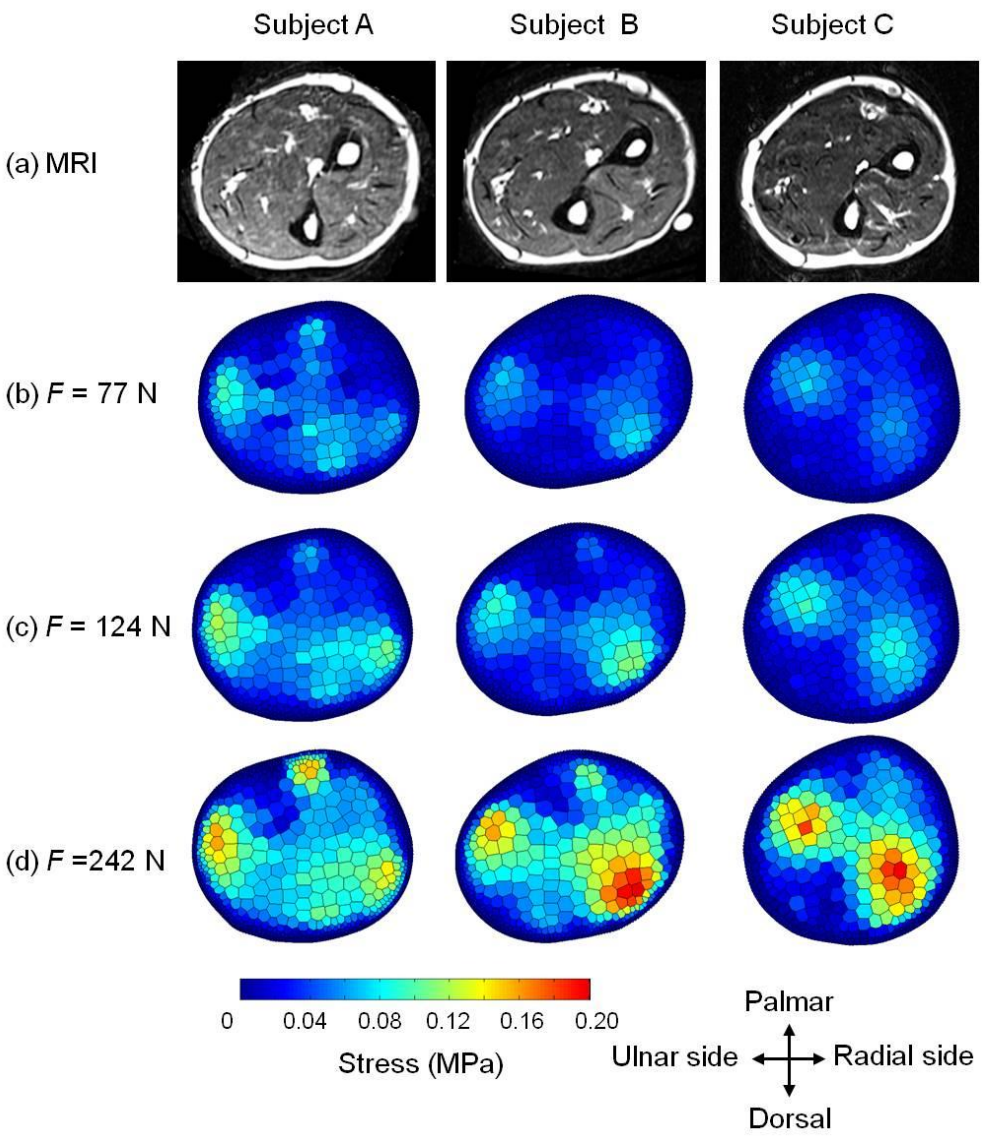

Figure 5.13 (a) Magnetic resonance image of forearm cross-sectional area. Stress distribution generated in the forearm muscle during gripping (b) 77 N, (c) 124 N, and (d) 242 N.

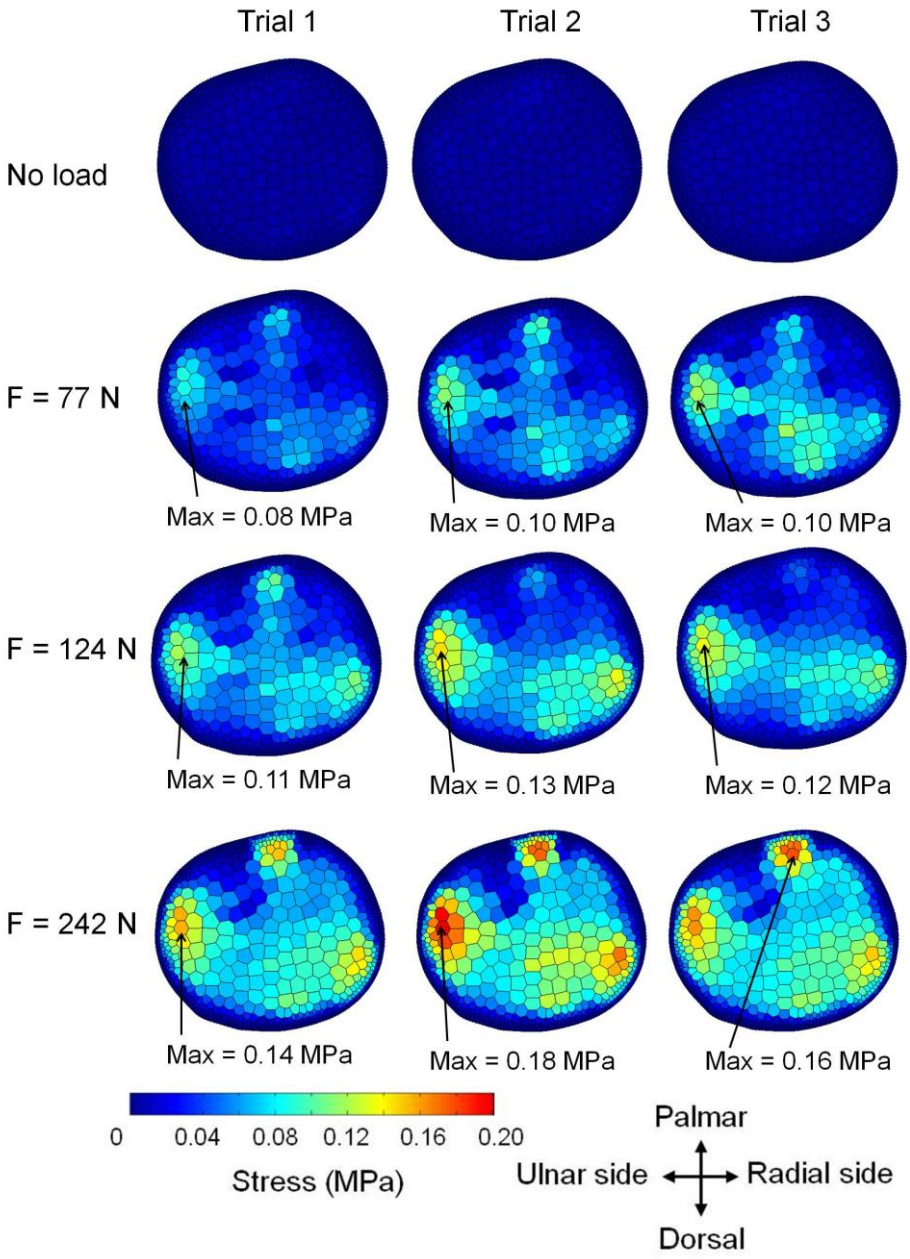

Figure 5.14 Stress distribution during gripping of subject A in all testing condition. The arrows indicate maximum stress within the forearm cross-sectional area.

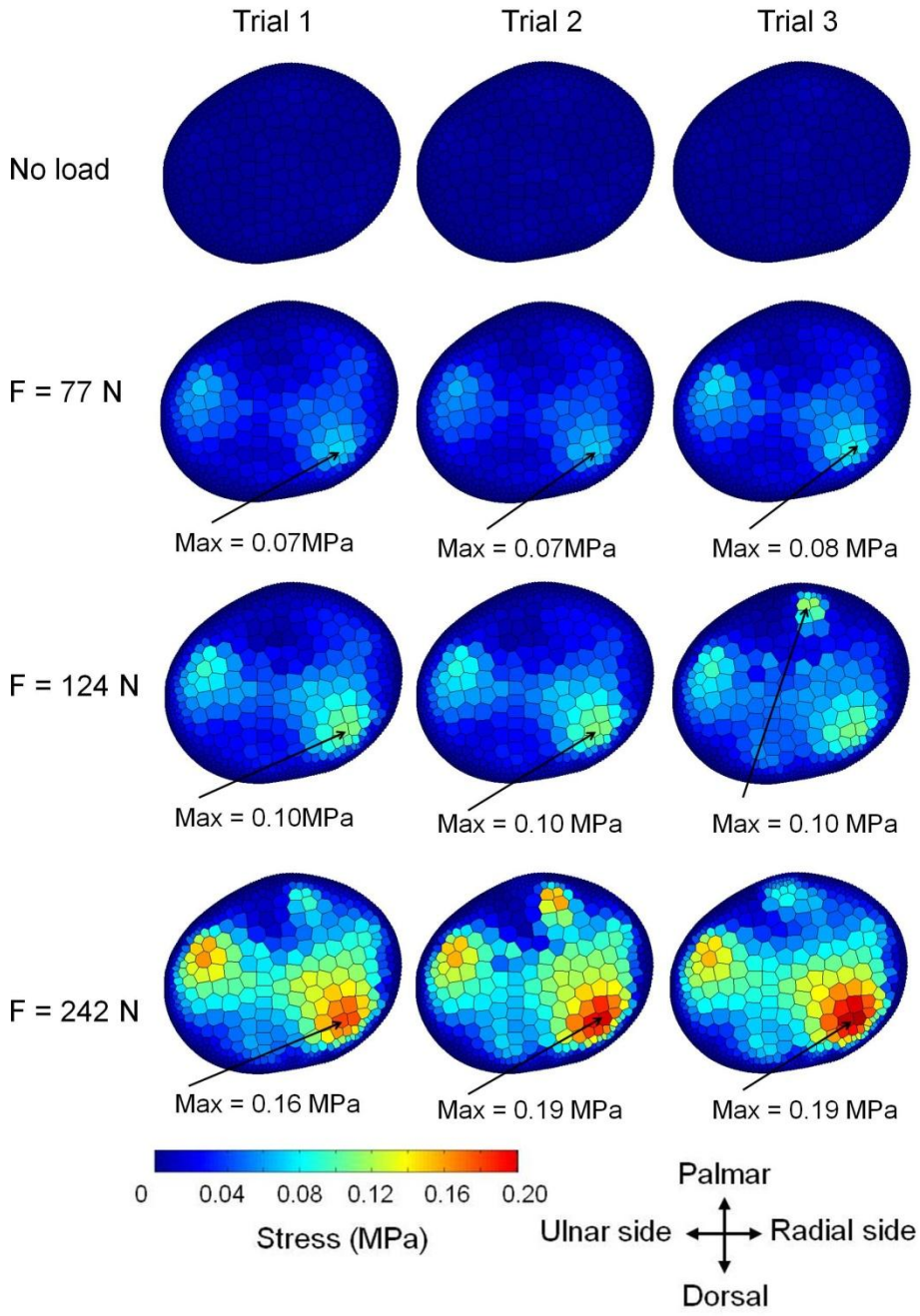

Figure 5.15 Stress distribution during gripping of subject B in all testing condition. The arrows indicate maximum stress within the forearm cross-sectional area.

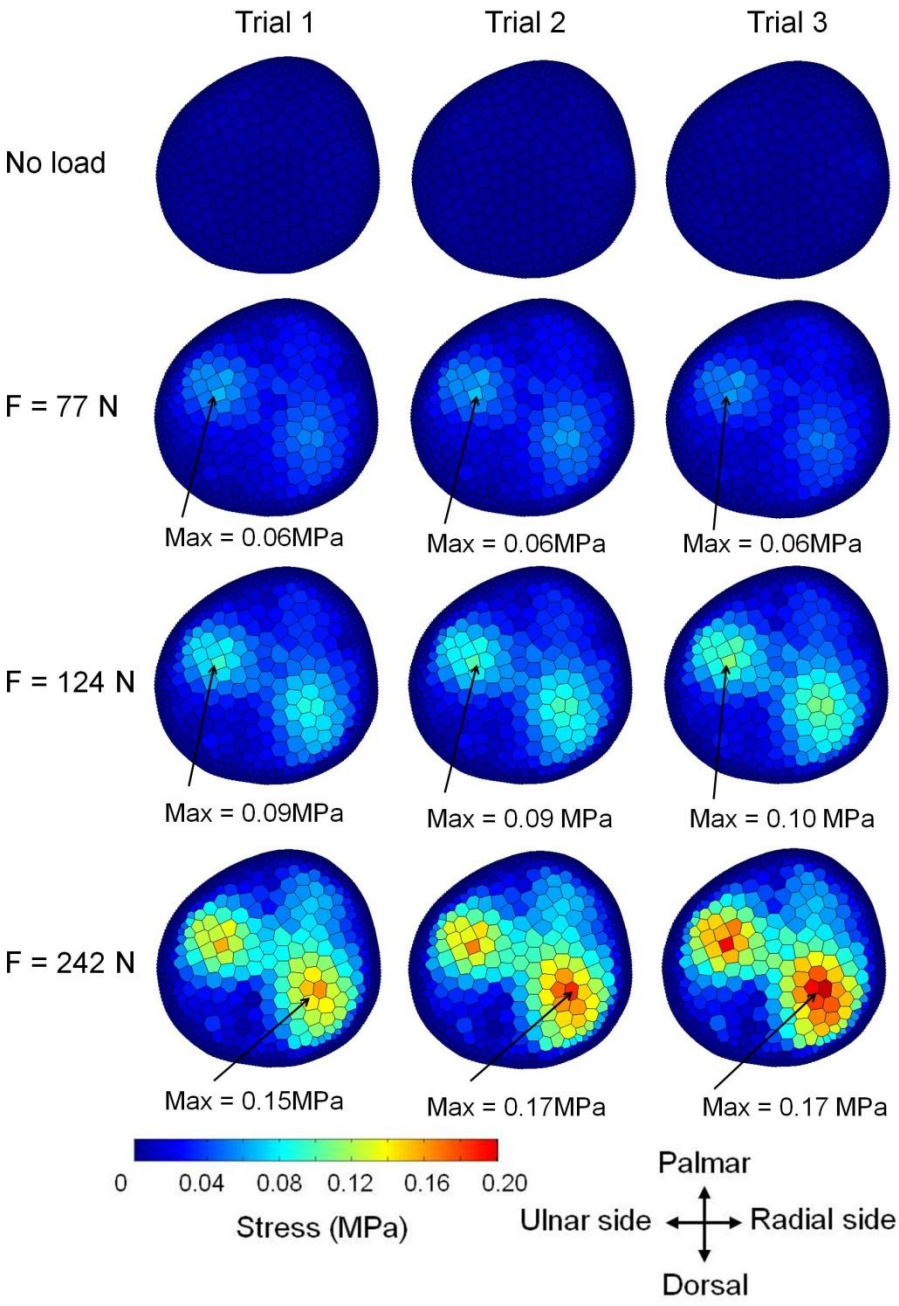

Figure 5.16 Stress distribution during gripping of subject C in all testing condition. The arrows indicate maximum stress within the forearm cross-sectional area.

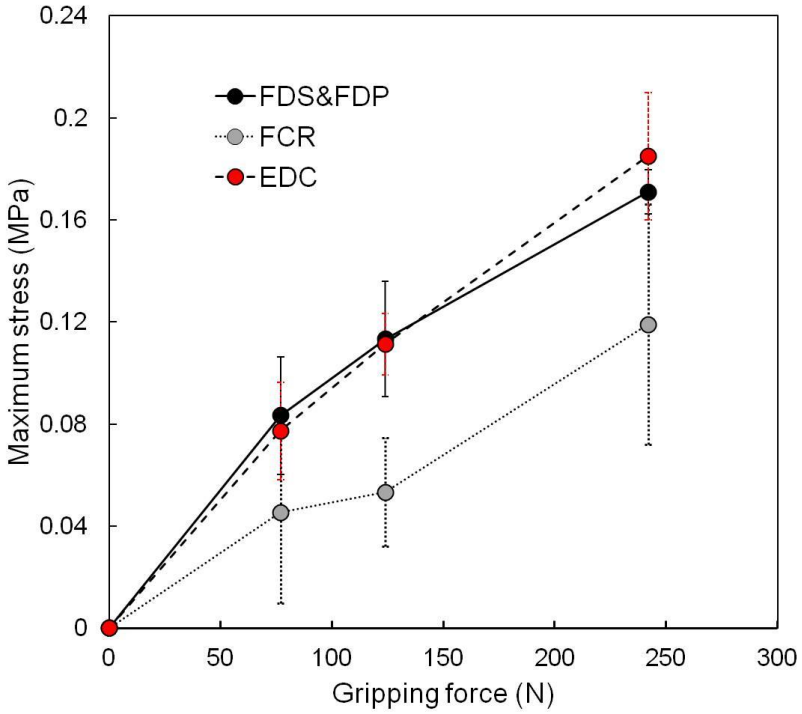

Figure 5.17 Maximum stress of three muscle region during hand grip.

5.3.1 Relationship between muscle force and muscle activity

In this study, we investigated the relationship between external force and muscle activity during gripping. EMG band which consisted of 40 pairs of bipolar electrode was used to detect muscle activity of the whole subject's forearm during hand gripping. The muscle activation of muscle detected by both narrow and wide pair was in consistent as shown in Fig. 5.9. The amplitude of detected EMG from the wide pairs was higher than that of the narrow pair. Since the wide pair can detect deeper muscle region while narrow pair can detect only at superficial muscle. The use of two different pair of electrode to detect EMG signal from the same cross section make it possible to estimate muscle activity from different depth. The detected surface EMG signal from EMG band seems consistent with the timing of gripping action and relaxing time. The raw EMG signals were processed and the RMS values of each electrode plate (Fig.5.10) were used as input to EMG-CT method.

We used a linear relationship between total muscle activity within the forearm and F at various gripping forces to estimate α of each subject. The muscle force required to maintain a static equilibrium increased with the gripping force. Generally, muscles increase their force output by recruiting more motor units or by increasing the muscle firing rate, resulting in an increase in EMG signals. The muscle activity calculated by EMG-CT method is based on the detected surface EMG signal. The increase in total muscle activity with increasing in load is shown in Fig 5.12. Nakajima et al. (2014) noted that muscle activity during finger motion increases with the external load. The results from the present study agree with the previously reported trends. Many studies reported a linear relationship between EMG and external force (torque) under isometric conditions (Messier, et al., 1971; Pruim, et al., 1980; Hof, 1984; Karlsson and Gerdle, 2001; Del Santo, et al., 2007). A linear model appears to offer a good approximation of the relationship between muscle activity and force under isometric conditions.

It has to be noted that muscle force at a given level of muscle activity is affected by many factors that not reflect in EMG signal, such as muscle length, rate of length change, and fatigue (Hof, 1997). In this study, during isometric hand gripping, muscle length was the same thus there is no rate of length change. Fatigue is defined as the decline in the ability of an individual to maintain a level of performance. Fatigue also affects the detected EMG signal (Dimitrova and Dimitrov, 2003). The duration gripping time in this study was 5 seconds. When analyzing the EMG signal during the experiment, the pattern of EMG signal was stable during recording time (30 seconds). Since the gripping force in this study was about 30% of maximum gripping force. It seems that the effect of fatigue might be small. However, the effect of fatigue on EMG signals when load is heavy and long period of contraction should be further studied and considered in the future work.

5.3.2 Muscle stress within the forearm

Stress levels in forearm muscles of all subjects can be measured by the method we have described. Stress in each muscle element did not increase linearly with load. More muscles were active when load increased. It appears that the human hand has a mechanism that distributes load between muscles so that the stress is not concentrated in only one portion. In previous studies, values for maximum muscle stress of individual muscle fibers in mammals were measured and found to vary between 0.06 and 0.38 MPa (Close, 1969; Burke and Tsairis, 1973; Lannergren and Westerblad, 1987; Kanda and Hashizume, 1992; Buchanan, 1995). The results obtained in our study were within the range of the reported data.

The pattern of stress distribution within the forearm muscles during gripping is shown in Figure 5.13. The shape of forearm model of every subject seems consistent with the MRI image. The comparison between real shape forearm model and MRI makes it possible to indentify muscle location. Under 77 and 124 N gripping load conditions (Fig. 5.13b and c), the stress is concentrated in two muscle groups: on the ulnar side, which may include the flexor digitorum superficialis (FDS) and the flexor digitorum profundus (FDP), and on the radial–dorsal side, which may include the extensor digitorum communis (EDC). Subject A appeared to use more muscles during gripping, resulting in less stress concentration than the other subjects. Under the 242 N load condition (Fig. 5.13d), stress was distributed across the whole area. Additional stress concentration was found in subjects A and B on the palmar side which may include the flexor carpi radialis. The basic gripping function involves finger flexion generated by muscle forces from the finger flexor muscles in the forearm. This mechanism is shown by the finding that both the FDS and FDP generate stress during gripping. It is also consistent with results of previous studies that used wire electrodes to study finger motion, finding that the FDP is responsible for synchronous flexion of finger joints (Johanson, et al., 1990; Darling, et al., 1994). The maximum stress was found in the extensor

region of subject B and C under the 242 N load condition (Fig. 5.13d). The stress appearing in the extensor might be explained by the co-contraction of the muscles to counteract the wrist flexion torque caused by the finger flexor. Many studies also found strong surface EMG signals from the extensor muscle during gripping (Hagg and Milerad, 1997; Johanson, et al., 1998; Hoozemans and van Dieen, 2005). It appears that extensors play an important role under high gripping load.

Pattern of stress distribution within the forearm of each subject can be analyzed. Figure 5.14 shows muscle stress distribution of subject A in all loading conditions. The pattern of every trials of the same loading condition was similar. The results show good repeatability of the method. It seems that the Subject A used the same muscle during gripping at low loading condition. During 77 N and 124N loading condition, Stress was distribute in FDP, FDS and EDC area. The maximum stress appears in muscle area at outer ulnar side which is the location of FDP and FDS muscle. The value of maximum stress increases as gripping load increases. When gripping load increase to 242 N, stress was distributed across the forearm cross-sectional area, there is stress concentration in palmar side of forearm which is the location of the FCR muscle. It is possible that during high grip load, Subject A use muscle to resist wrist motion.

Figure 5.15 shows muscle stress distribution of subject B in all loading conditions. Subject B seems to use different muscles from subject A during gripping. Maximum stress appears in EDC muscle which used in finger extension. During 242 N loading condition, subject B has the maximum stress in EDC area. It is possible that EDC was used to stabilize hand when high force from FDP and FDS was generated during high load grip.

Figure 5.16 shows muscle stress distribution of subject C in all loading conditions. During 77 N and 124 N loading conditions, maximum stress appears in FDP and FDS muscle area but during 242 N loading condition, maximum stress change to EDC muscle. Subject C seems to use different

muscle pattern from subject A and B. The difference pattern observed in individual subject might be caused by many factors such as the different in muscles size, the location of muscles within the forearm, and strength of individual muscles.

Figure 5.17 show maximum force within muscle region. It seems that the magnitude of maximum stress appears in FDS and FDP muscles are similar to maximum stress in EDC muscle. It seems that during gripping both flexors and extensor exert force to generate gripping force. The maximum stress within FCR region seems to increase when gripping force increase especially during high gripping force. This might be caused by the fact that FCR has to generate force to counter wrist motion generated by FDS, FDP and EDC.

When increase external load, muscles generate more force to maintain the static equilibrium. This reflects in increasing in active area and higher stress. The muscle stress presents in tomographic image are nonnegative value, because a muscle can only generate tensile force. Increasing in muscle stress is consistent with increasing in external load. Each muscle force acts through a moment arm to generate joint moment. Thus, the role of muscle as agonist or antagonist depends on the direction of moment arm that cross the joint. In this study, we assumed that during gripping task only agonist muscles are active to generate force. In order to implement this method to the other posture, the role of muscle should be considered.

Muscles that move fingers can be divided into two groups e.g. extrinsic and intrinsic groups. The extrinsic muscles originate primarily in the forearm, while the intrinsic muscles originate primarily in the hand. Therefore, the extrinsic muscles are large and provide strength, while the intrinsic muscles are small and provide precise coordination for the fingers. Each finger is innervated by both sets of muscles, requiring good coordination for hand movement. This study considered only force that generated by extrinsic muscles. Thus the results might be overestimate since force generated from intrinsic muscles did not consider in the calculation.

The change in arm posture may affect the muscle stress distribution. The load conditions in this study were limited to only forearm in supination posture. When forearm changes posture, the muscle length and moment arm also change. The future works aim to study the muscle cooperative activities in various forearm postures. In addition, the muscle stress during finger synchrony action such as grasping, gripping and pinching, are also interesting. The information of these studies will be very important in developing rehabilitation procedure which requires finger function for daily activities.

5.4 Discussion

We demonstrated that the stress distribution within the forearm muscles during gripping can be estimated and presented by the EMG–CT method. We constructed an EMG conduction model based on subjects' forearm geometry. We developed a mathematical model relating muscle activity and force to calculate stress distribution. To the best of our knowledge, this is the first method that allows measuring stress distribution within the forearm muscles in a non-invasive manner.

The key to understanding muscle cooperation is to observe the distribution of muscle activities during contraction. In general, to obtain deep muscle activity, the needle electrode was used. The current knowledge of how muscles work together results from the measurement with needle electrodes or surface electrodes (Maier and Hepp-Reymond, 1995; Johanson, et al., 1998; Kilbreath, et al., 2002). However, tests using a needle electrode are invasive and traumatic, and the reliability of an EMG signal depends on the physician's skill of inserting the needles. In addition, a needle electrode detects only a small area of muscle around the needle, which limits the potential to understand the mechanism underlying muscle cooperative activities for whole muscles. Whilst, the limitation of the surface electrode method is that the active muscle location is difficult to observe. Surface EMG cannot access deep muscles, and the detected signals are distorted by noise from nearby muscles. Researches attempted to understand muscle cooperative activities in forearm using cadaveric models (Garcia-Elias, et al., 1991; Haugstvedt, et al., 2001) and implanted force transducers in vivo (Schuind, et al., 1992; Dennerlein, 2005). Garcia-Elias et al. (1991) used stereophotogrammetric measurement system to study extensor mechanism of the fingers in human forearm specimens. Change in length and orientation of different zones of the extensor mechanism at different finger configurations were reported. Haugstvedt et al. (2001) used human cadaveric upper extremity specimens to determine torque generated by the muscles rotating the forearm at various pronation/supination. The

relationships between moment arm and angle of the flexor carpi ulnaris, extensor carpi ulnaris, supinator, biceps, pronator teres and the pronator quadrates were reported. Studying from cadaveric model gain us insights of anatomical aspect of muscles, but the effects of physiologic forces such as muscle contraction cannot be considered by this approach. Furthermore, Schuind et al. (1992) applied force transducers to the flexor pollicis longus and flexor digitorum superficialis and produndus tendons of the index finger of patients. The tendon forces generated during passive and active motion of the wrist and fingers were recorded and reported. Dennerlein et al. (2005) measured the *in vivo* tendon force of the flexor digitorum superficialis of the long finger during open carpal tunnel release surgery using force transducer. Forces were measured during isometric pinch and dynamic tapping of the finger. The results showed that tendon forces were a complicated function of fingertip force and motion. These studies provide insight of how forearm muscles generate force during contraction. However, the measurements using force transducer was invasive and cannot provide the distribution of muscle activity within the whole cross-section in detail. The developed muscle stress distribution estimation using EMG-CT method can solve the problems and will provide new information regarding the muscle cooperative activity within the forearm cross-sectional area.

Many studies used biomechanical model of hand and fingers to estimate muscle force from external load and kinematics data (An, et al., 1979; Sancho-Bru, et al., 2001; Fok and Chou, 2010). The muscle force can be estimated by inverse-dynamic calculation. Muscle force-external force value is equal 1 in this study, whereas previously studies report values range from 1 to 7 (Chao, et al., 1976; Fok and Chou, 2010; Goislard de Monsabert, et al., 2012). Biomechanical model usually uses anatomical segment length and many musculoskeletal parameters. However, these musculoskeletal parameters are uncertainty and vary among subject. In addition, biomechanical model of hand is very complex; when considering that there are many muscles within the forearm, difference in muscle force pattern can be used to produce a similar

external force (Kursa, et al., 2005). There are more unknown parameters than equilibrium equations. Make it difficult to estimate muscle force distribution correctly.

A 3D scanner was used to obtain forearm geometry of each subject. The scanning time took approximately 1 min at a resolution of point-to-point space of approximately 0.6 mm, comprising 250,000 triangles. Using a 3D scanner to construct a forearm model is very practical for clinical application. Body segment geometry data are generally obtained from medical imaging methods such as MRI and gamma-ray scanning (Martin, et al., 1989; Cheng, et al., 2000; Dumas, et al., 2005). However, these methods are expensive and require long measurement times. The advantages of the 3D scanner method over MRI and gamma-ray scanning are low cost and rapid measurement. Comparison of the forearm model constructed from 3D scanner data with the MRI image suggests that the resolution was sufficient to accurately outline the forearm from the geometry obtained. The shapes of the forearm cross-sectional area differed markedly among subjects. The development of a forearm model using a 3D scanner allows comparison with anatomical information.

The conduction model was based on an assumption that the live muscle tissue between source and surface electrode was like ground bovine muscle. In order to quantitatively discuss about muscle cooperative activity, it will be required to consider muscle properties of human living muscle. In addition, the muscle activity was represented as mA dipole/s which passes normally through the cross-sectional area, although muscle fibers are not exactly aligned to the longitudinal direction of the forearm. The subjects in this study were young. It is known that age is also affect muscle function. To gain more understanding regarding ageing and pathology in live human, a various range of the subject's age should be consider. This study measured activity only in extrinsic muscles within the forearm. It seems that during finger motion, intrinsic muscles also work during finger motion. Measuring intrinsic muscle activity will also improve our understanding of finger function.

In the study, we did not include the bone region in the forearm model; however, when our results were compared with MRI of each subject's forearm, the expected bone area showed very low activity. The prospect of further study to detect the bone region using the EMG–CT method is interesting and important. It was also assumed that force exerted by fingers was equal to total muscle force generated by forearm muscles. However, there are many factors such as wrist and arm posture and the position of applied load on fingers that can affect the muscle force generation mechanism. Gripping may be usable as a calibration process when this method is applied to estimate stress in other hand and finger motions. This method is also limited to static isometric conditions. The relationship between muscle activity and muscle stress was assumed to be linear, an assumption that might not apply under dynamic conditions. During dynamic movement, many factors such as muscle length, velocity and type of movement also affect the relationship between EMG signal and muscle force. Further studies are thus required to establish the effects of dynamic conditions on muscle activity and stress.

In summary, this study has shown high potential for estimating stress distribution generated in the forearm muscles using an EMG–CT band and a 3D scanner. The use of a new EMG conduction model devised from subjects' forearm geometry and a model for calculating stress from muscle activity represent an improvement in the EMG–CT method and make it more clinically applicable. This improvement allows visualizing stress within the forearm muscles, a capability that may advance the development of diagnostic tools.

Chapter 6 Conclusions

6.1 Summary

In this study, methods to estimate muscle force from surface electromyography (EMG) signal were developed. Muscle forces generated during upper and lower limb movement were estimated using the developed methods.

EMG-driven model was developed and used to estimate muscle forces in elbow and knee joint during flexion/extension motion. Body kinematic data and EMG signal were measured and used to estimate individual muscle force. The results show that there is the relationship between movement speed and EMG signal. The EMG-driven model using surface EMG is very useful in estimating muscle force in elbow or knee joint which is moved by large muscles. However, the limitations of conventional surface EMG signal prevent the possibility of using this system to estimate force in human forearm which many small muscles are deeply reside within.

A novel method called EMG-CT was developed to estimate muscle activities within the forearm. Surface EMG signals within the forearm region were detected by multiple surface electrodes. EMG conduction model was formulated for reverse-estimation of muscle activities using detected surface EMG signals. The individual muscle activities in the deep region were estimated and present in EMG tomographic image. It is demonstrated that EMG-CT allows the investigation of the activity of the MU within the muscle region. This makes the activated muscles to be located non-invasively from the skin surface possible. This method opens a new window to EMG study, forearm which could be potentially used for studying of muscle mechanism and diagnostic tool for rehabilitation evaluation in the future.

A method for estimating muscle force in the forearm region based on EMG-CT was developed. The study has shown high potential for estimating stress distribution generated in the forearm muscles using an EMG band and a handy 3D scanner. The use of a new EMG conduction model devised from subjects' forearm geometry and a model for calculating stress from muscle

activity represent an improvement in the EMG–CT method and make it more clinically applicable. This improvement allows visualizing stress within the forearm muscles, a capability that may advance the development of diagnostic tools.

In this study, two methods for estimating muscle force were developed: EMG-driven model which uses surface EMG signals and kinematic data as inputs is useful to estimate muscle force in major link like elbow and knee during dynamic movement. For forearm region, a method for estimating muscle force based on EMG-CT was developed. To the best of our knowledge, this is the first time that we can measure stress distribution within the forearm in a non-invasive way. The ultimate goal of this research is to develop a measurement method that can be used in clinical application. The current state of study is the first step to achieve that goal. Further study and research are required to improve the method which is discussed in the Future work section.

6.2 Future work

The developed muscle stress estimation method based on EMG-CT is very useful in studying hand and finger motion. Upper arm is also important during human locomotion. Currently, only biceps and triceps muscle activity can be detected using conventional surface EMG. Using EMG-CT method to measure forces of both upper arm and forearm muscles simultaneously will help us understand upper limb mechanism and function. The EMG-CT method also has high potential to be used in lower-limb. However, the human leg is larger than the forearm. To implement EMG-CT to lower limb, more electrodes are required to achieve the accuracy as in forearm region.

The study of fatigue during muscle contraction is also important in ergonomic design. Understand how human muscle respond to fatigue is an interesting issue. The developed stress estimation method can be used to observed change in muscle force generation pattern during long period contraction. However, the effect of fatigue on EMG signal is complicated. In order to implement EMG-CT to study muscle fatigue, more studies on fatigue and EMG relationship is required to interpret muscle activation correctly.

Some aspects that required future work to improve muscle stress estimation using EMG-CT method should be mention. First, currently the bone region was not included in the forearm model. However, when compare the results with anatomical information of muscles in the forearm; the expected bone area has quite low activity. The effect of bone on conductivity of muscle action potential might be higher in the part with large bone region and may affect the accuracy of the results. A method to estimate bones location and implement to the conduction model will be very useful in developing this method in the future. Secondly, the validation of the results is difficult since there is no practical way to measure muscle stress in vivo. One way to validate the obtained results is to compare between mechanical work and metabolic energy cost, since the energy consumption depends on muscular activation and

muscle contraction (Bisi, et al., 2011). Further study on work and energy of muscle during contraction might be benefit for validation aspect.

The method developed in this study provides both quantitative values of stress levels and a distribution pattern in a non-invasive manner. This information is very useful for medical diagnosis, given that muscle force generation can be affected by muscular diseases or injury, resulting in abnormalities in stress level and distribution pattern. For example, in a patient with muscle pain, the pattern of muscle distribution might change to avoid excessive stress on the painful muscle. In a patient with muscular disease, some muscles may be affected by paralysis and not generate force properly. A clinician can use the method to observe muscle function in more detail. Thus, diseased or injured muscles can be detected and treated more accurately. In addition, this proposed method is very useful for designing ergonomic gripping hand tools. To prevent injury under high work-load condition, the design of gripping hand tools should consider load sharing among muscles, taking care not to overuse one muscle. In addition, the accessibility of deep muscle activity can provide a more delicate control of a prosthetic arm using the pattern of muscle activity from EMG-CT. This will help in developing more advance prosthesis that can control complex movement.

Reference

Adrian, E. D. and Bronk, D. W., The discharge of impulses in motor nerve fibres: Part II. The frequency of discharge in reflex and voluntary contractions, The Journal of physiology, Vol.67, No.2 (1929), pp.i3-151.

Amarantini, D. and Martin, L., A method to combine numerical optimization and EMG data for the estimation of joint moments under dynamic conditions, Journal of biomechanics, Vol.37, No.9 (2004), pp.1393-1404.

Amis, A. A., Dowson, D. and Wright, V., Analysis of elbow forces due to high-speed forearm movements, Journal of biomechanics, Vol.13, No.10 (1980), pp. 825-831.

An, K. N., Chao, E. Y., Cooney, W. P., 3rd and Linscheid, R. L., Normative model of human hand for biomechanical analysis, Journal of biomechanics, Vol.12, No.10 (1979), pp.775-788.

An, K. N., Hui, F. C., Morrey, B. F., Linscheid, R. L. and Chao, E. Y., Muscles across the elbow joint: a biomechanical analysis, Journal of biomechanics, Vol.14, No.10 (1981), pp.659-669.

Bisi, M. C., Stagni, R., Houdijk, H. and Gnudi, G., An EMG-driven model applied for predicting metabolic energy consumption during movement, Journal of electromyography and kinesiology : official journal of the International Society of Electrophysiological Kinesiology, Vol.21, No.6 (2011), pp.1074-1080.

Blok, J. H., van Dijk, J. P., Drost, G., Zwarts, M. J. and Stegeman, D. F., A high-density multichannel surface electromyography system for the characterization of single motor units, Review of Scientific Instruments, Vol.73, No.4 (2002), pp.1887-1897.

Bodine, S. C., Roy, R. R., Eldred, E. and Edgerton, V. R., Maximal force as a function of anatomical features of motor units in the cat tibialis anterior, Journal of neurophysiology, Vol.57, No.6 (1987), pp.1730-1745.

Bottinelli, R., Canepari, M., Pellegrino, M. A. and Reggiani, C., Force-velocity properties of human skeletal muscle fibres: myosin heavy chain isoform and temperature dependence, The Journal of physiology, Vol.495 (Pt 2), (1996), pp. 573-586.

Bottinelli, R., Pellegrino, M. A., Canepari, M., Rossi, R. and Reggiani, C., Specific contributions of various muscle fibre types to human muscle

performance: an in vitro study, Journal of electromyography and kinesiology, Vol.9, No.2 (1999), pp.87-95.

Bouisset, S., EMG and muscle force in normal motor activities, New Developments in Electromyography and Clinical Neurophysiology Switzerland: Kargel, Besel, (1973).

Brindle, T. J., Nitz, A. J., Uhl, T. L., Kifer, E. and Shapiro, R., Kinematic and EMG characteristics of simple shoulder movements with proprioception and visual feedback, Journal of electromyography and kinesiology, Vol.16, No.3 (2006), pp.236-249.

Buchanan, T. S., Evidence that maximum muscle stress is not a constant: differences in specific tension in elbow flexors and extensors, Medical engineering & physics, Vol.17, No.7 (1995), pp.529-536.

Buchanan, T. S., Lloyd, D. G., Manal, K. and Besier, T. F., Neuromusculoskeletal modeling: estimation of muscle forces and joint moments and movements from measurements of neural command, Journal of applied biomechanics, Vol.20, No.4 (2004), pp.367-395.

Buchanan, T. S., Moniz, M. J., Dewald, J. P. and Zev Rymer, W., Estimation of muscle forces about the wrist joint during isometric tasks using an EMG coefficient method, Journal of biomechanics, Vol.26, No.4-5 (1993), pp.547-560.

Buchthal, F. and Schmalbruch, H., Motor unit of mammalian muscle, Physiological reviews, Vol.60, No.1 (1980), pp.90-142.

Burger, H. C. and van, D., Specific electric resistance of body tissues, Physics in medicine and biology, Vol.5, (1961), pp.431-447.

Burke, R. E., Levine, D. N., Tsairis, P. and Zajac, F. E., 3rd. Physiological types and histochemical profiles in motor units of the cat gastrocnemius, The Journal of physiology, Vol.234, No.3 (1973), pp.723-748.

Burke, R. E. and Tsairis, P., Anatomy and innervation ratios in motor units of cat gastrocnemius, The Journal of physiology, Vol.234, No.3 (1973), pp.749-765.

Busse, M. E., Wiles, C. M. and van Deursen, R. W. M., Muscle co-activation in neurological conditions, Physical Therapy Reviews, Vol.10, No.4 (2005), pp. 247-253.

Butler, T. J., Kilbreath, S. L., Gorman, R. B. and Gandevia, S. C., Selective recruitment of single motor units in human flexor digitorum superficialis muscle during flexion of individual fingers, The Journal of physiology, Vol.567 (Pt 1), (2005), pp.301-309.

Carpentier, A., Duchateau, J. and Hainaut, K., Velocity-dependent muscle strategy during plantarflexion in humans, Journal of electromyography and kinesiology, Vol.6, No.4 (1996), pp.225-233.

Chao, E. Y., Opgrande, J. D. and Axmear, F. E., Three-dimensional force analysis of finger joints in selected isometric hand functions, Journal of biomechanics, Vol.9, No.6 (1976), pp.387-396.

Cheney, M., Isaacson, D. and Newell, J. C., Electrical impedance tomography, SIAM Review, Vol.41 (1999), pp.85-101.

Cheng, C.-K., Chen, H.-H., Chen, C.-S., Lee, C.-L. and Chen, C.-Y., Segment inertial properties of Chinese adults determined from magnetic resonance imaging, Clinical biomechanics, Vol.15, No.8 (2000), pp.559-566.

Close, R., Dynamic properties of fast and slow skeletal muscles of the rat after nerve cross-union, The Journal of physiology, Vol.204, No.2 (1969), pp.331-346.

Close, R. I., Dynamic properties of mammalian skeletal muscles, Physiological reviews, Vol.52, No.1 (1972), pp.129-197.

Darling, W. G., Cole, K. J. and Miller, G. F., Coordination of index finger movements, Journal of biomechanics, Vol.27, No.4 (1994), pp.479-491.

De Luca, C. J. and Merletti, R., Surface myoelectric signal cross-talk among muscles of the leg, Electroencephalography and clinical neurophysiology, Vol.69, No.6 (1988), pp.568-575.

Del Santo, F., Gelli, F., Ginanneschi, F., Popa, T. and Rossi, A., Relation between isometric muscle force and surface EMG in intrinsic hand muscles as function of the arm geometry, Brain research, Vol.1163, (2007), pp.79-85.

Delp, S. L., Anderson, F. C., Arnold, A. S., Loan, P., Habib, A., John, C. T., Guendelman, E. and Thelen, D. G., OpenSim: open-source software to create and analyze dynamic simulations of movement, IEEE transactions on bio-medical engineering, Vol.54, No.11 (2007), pp.1940-1950.

den Otter, A. R., Geurts, A. C. H., Mulder, T. and Duysens, J., Speed related changes in muscle activity from normal to very slow walking speeds, Gait & posture, Vol.19, No.3 (2004), pp.270-278.

Dennerlein, J. T., Finger flexor tendon forces are a complex function of finger joint motions and fingertip forces, Journal of hand therapy : official journal of the American Society of Hand Therapists, Vol.18, No.2 (2005), pp.120-127.

Dennerlein, J. T., Diao, E., Mote, C. D., Jr. and Rempel, D. M., Tensions of the flexor digitorum superficialis are higher than a current model predicts, Journal of biomechanics, Vol.31, No.4 (1998), pp.295-301.

Dimitrova, N. A. and Dimitrov, G. V., Interpretation of EMG changes with fatigue: facts, pitfalls, and fallacies, Journal of electromyography and kinesiology, Vol.13, No.1 (2003), pp.13-36.

Disselhorst-Klug, C., Schmitz-Rode, T. and Rau, G., Surface electromyography and muscle force: limits in sEMG-force relationship and new approaches for applications, Clinical biomechanics, Vol.24, No.3 (2009), pp.225-235.

Drost, G., Stegeman, D. F., van Engelen, B. G. and Zwarts, M. J., Clinical applications of high-density surface EMG: a systematic review, Journal of electromyography and kinesiology, Vol.16, No.6 (2006), pp.586-602.

Du, Q., Faber, V. and Gunzburger, M., Centroidal Voronoi tessellations: Applications and algorithms, Siam Rev, Vol.41, No.4 (1999), pp.637-676.

Dum, R. P., Burke, R. E., O'Donovan, M. J., Toop, J. and Hodgson, J. A., Motor-unit organization in flexor digitorum longus muscle of the cat, Journal of neurophysiology, Vol.47, No.6 (1982), pp.1108-1125.

Dumas, R., Aissaoui, R., Mitton, D., Skalli, W. and de Guise, J. A., Personalized body segment parameters from biplanar low-dose radiography, IEEE transactions on bio-medical engineering, Vol.52, No.10 (2005), pp.1756-1763.

Duque, J., Masset, D. and Malchaire, J., Evaluation of handgrip force from EMG measurements, Applied ergonomics, Vol.26, No.1 (1995), pp.61-66.

Erdemir, A., McLean, S., Herzog, W. and van den Bogert, A. J., Model-based estimation of muscle forces exerted during movements, Clinical biomechanics, Vol.22, No.2 (2007), pp.131-154.

Faes, T. J., van der Meij, H. A., de Munck, J. C. and Heethaar, R. M., The electric resistivity of human tissues (100 Hz-10 MHz): a meta-analysis of review studies, Physiological measurement, Vol.20, No.4 (1999), pp.R1-10.

Fee Jr, J. W., Miller, F. and Lennon, N., EMG reaction in muscles about the knee to passive velocity, acceleration, and jerk manipulations, Journal of Electromyography and Kinesiology, Vol.19, No.3 (2009), pp.467-475.

Feng, C. J., Mak, A. F. T. and Koo, T. K. K., A surface EMG driven musculoskeletal model of the elbow flexion-extension movement in normal subjects and in subjects with spasticity, Journal of Musculoskeletal Research, Vol.03, No.02 (1999), pp.109-123.

Finni, T., Komi, P. V. and Lukkariniemi, J., Achilles tendon loading during walking: application of a novel optic fiber technique, European journal of applied physiology and occupational physiology, Vol.77, No.3 (1998), pp.289-291.

FitzHugh, R., A model of optimal voluntary muscular control, Journal of mathematical biology, Vol.4, No.3 (1977), pp.203-236.

Fok, K. S. and Chou, S. M., Development of a finger biomechanical model and its considerations, Journal of biomechanics, Vol.43, No.4 (2010), pp.701-713.

Freivalds, A. Biomechanics of the Upper Limbs: Mechanics, Modeling and Musculoskeletal Injuries, Second Edition, Taylor & Francis, (2011).

Fukashiro, S., Komi, P. V., Jarvinen, M. and Miyashita, M., Comparison between the directly measured achilles tendon force and the tendon force calculated from the ankle joint moment during vertical jumps, Clinical biomechanics, Vol.8, No.1 (1993), pp.25-30.

Gabriel, S., Lau, R. W. and Gabriel, C., The dielectric properties of biological tissues: II. Measurements in the frequency range 10 Hz to 20 GHz, Physics in medicine and biology, Vol.41, No.11 (1996), pp.2251-2269.

Gallucci, J. G. and Challis, J. H., Examining the role of the gastrocnemius during the leg curl exercise, J Appl Biomech, Vol.18, No.1 (2002), pp.15-27.

Garcia-Elias, M., An, K. N., Berglund, L., Linscheid, R. L., Cooney, W. P., 3rd and Chao, E. Y., Extensor mechanism of the fingers. I. A quantitative geometric study, The Journal of hand surgery, Vol.16, No.6 (1991), pp.1130-1136.

Garcia, G. A., Okuno, R. and Akazawa, K., A decomposition algorithm for surface electrode-array electromyogram. A noninvasive, three-step approach to analyze surface EMG signals, IEEE engineering in medicine and biology magazine, Vol.24, No.4 (2005), pp.63-72.

Geddes, L. A. and Baker, L. E., The specific resistance of biological material--a compendium of data for the biomedical engineer and physiologist, Medical & biological engineering, Vol.5, No.3 (1967), pp.271-293.

Goislard de Monsabert, B., Rossi, J., Berton, E. and Vigouroux, L., Quantification of hand and forearm muscle forces during a maximal power grip task, Medicine and science in sports and exercise, Vol.44, No.10 (2012), pp.1906-1916.

Hagg, G. M. and Milerad, E., Forearm extensor and flexor muscle exertion during simulated gripping work -- an electromyographic study, Clinical biomechanics, Vol.12, No.1 (1997), pp.39-43.

Hale, R., Dorman, D. and Gonzalez, R. V., Individual muscle force parameters and fiber operating ranges for elbow flexion-extension and forearm pronation-supination, Journal of biomechanics, Vol.44, No.4 (2011), pp.650-656.

Harridge, S. D. R., Bottinelli, R., Canepari, M., Pellegrino, M. A., Reggiani, C., Esbjornsson, M. and Saltin, B., Whole-muscle and single-fibre contractile properties and myosin heavy chain isoforms in humans, Pflug Arch Eur J Phy, Vol.432, No.5 (1996), pp.913-920.

Haugstvedt, J. R., Berger, R. A. and Berglund, L. J., A mechanical study of the moment-forces of the supinators and pronators of the forearm, Acta orthopaedica Scandinavica, Vol.72, No.6 (2001), pp.629-634.

Heintz, S. and Gutierrez-Farewik, E. M., Static optimization of muscle forces during gait in comparison to EMG-to-force processing approach, Gait & posture, Vol.26, No.2 (2007), pp.279-288.

Hill, A. V., The Heat of Shortening and the Dynamic Constants of Muscle, Proceedings of the Royal Society of London. Series B, Biological Sciences, Vol.126, No.843 (1938), pp.136-195.

Hof, A. L., EMG and muscle force: An introduction, Human Movement Science, Vol.3, No.1–2 (1984), pp.119-153.

Hof, A. L., The relationship between electromyogram and muscle force, Sportverletzung Sportschaden : Organ der Gesellschaft fur Orthopadisch-Traumatologische Sportmedizin, Vol.11, No.3 (1997), pp.79-86.

Hof, A. L., Elzinga, H., Grimmius, W. and Halbertsma, J. P., Speed dependence of averaged EMG profiles in walking, Gait & posture, Vol.16, No.1 (2002), pp.78-86.

Hof, A. L. and Van den Berg, J., EMG to force processing I: An electrical analogue of the Hill muscle model, Journal of biomechanics, Vol.14, No.11 (1981), pp.747-758.

Hoozemans, M. J. and van Dieen, J. H., Prediction of handgrip forces using surface EMG of forearm muscles, Journal of electromyography and kinesiology, Vol.15, No.4 (2005), pp.358-366.

Huxley, H. and Hanson, J., Changes in the cross-striations of muscle during contraction and stretch and their structural interpretation, Nature, Vol.173, No.4412 (1954), pp.973-976.

Hwang, I. S. and Abraham, L. D., Quantitative EMG analysis to investigate synergistic coactivation of ankle and knee muscles during isokinetic ankle movement. Part 2: time frequency analysis, Journal of electromyography and kinesiology, Vol.11, No.5 (2001), pp.327-335.

Johanson, M. E., James, M. A. and Skinner, S. R., Forearm muscle activation during power grip and release, The Journal of hand surgery, Vol.23, No.5 (1998), pp.938-944.

Johanson, M. E., Skinner, S. R., Lamoreux, L. W., St Helen, R., Moran, S. A. and Ashley, R. K., Phasic relationships of the extrinsic muscles of the normal hand, The Journal of hand surgery, Vol.15, No.4 (1990), pp.587-594.

Kanda, K. and Hashizume, K., Factors causing difference in force output among motor units in the rat medial gastrocnemius muscle, The Journal of physiology, Vol.448, (1992), pp.677-695.

Karlsson, S. and Gerdle, B., Mean frequency and signal amplitude of the surface EMG of the quadriceps muscles increase with increasing torque--a study using the continuous wavelet transform, Journal of electromyography and kinesiology, Vol.11, No.2 (2001), pp.131-140.

Kilbreath, S. L., Gorman, R. B., Raymond, J. and Gandevia, S. C., Distribution of the forces produced by motor unit activity in the human flexor digitorum profundus, The Journal of physiology, Vol.543 (Pt 1) (2002), pp.289-296.

Kingma, I., Toussaint, H. M., De Looze, M. P. and Van Dieen, J. H., Segment inertial parameter evaluation in two anthropometric models by application of a dynamic linked segment model, Journal of biomechanics, Vol.29, No.5 (1996), pp.693-704.

Kumar, S. and Mital, A. Electromyography in ergonomics, CRC Press, (1996).

Kursa, K., Diao, E., Lattanza, L. and Rempel, D., In vivo forces generated by finger flexor muscles do not depend on the rate of fingertip loading during an isometric task, Journal of biomechanics, Vol.38, No.11 (2005), pp.2288-2293.

Lannergren, J. and Westerblad, H., The temperature dependence of isometric contractions of single, intact fibres dissected from a mouse foot muscle, The Journal of physiology, Vol.390, (1987), pp.285-293.

Larsson, L. and Moss, R. L., Maximum Velocity of Shortening in Relation to Myosin Isoform Composition in Single Fibers from Human Skeletal-Muscles, J Physiol-London, Vol.472, (1993), pp.595-614.

Laursen, B., Jensen, B. R. and Sjogaard, G., Effect of speed and precision demands on human shoulder muscle electromyography during a repetitive task, European journal of applied physiology and occupational physiology, Vol.78, No.6 (1998), pp.544-548.

Le Bozec, S., Evans, O. M. and Maton, B., Long-latency stretch reflexes of the human elbow extensors during voluntary relaxation: Differences between agonistic muscles, Experimental Neurology, Vol.96, No.3 (1987), pp.516-527.

Lindström, L. and Magnusson, R., Interpretation of myoelectric power spectra: a model and its applications. Proceedings of the IEEE Vol.65 (1977), pp.653-62.

Lloyd, D. G. and Besier, T. F., An EMG-driven musculoskeletal model to estimate muscle forces and knee joint moments in vivo, J Biomech, Vol.36, No.6 (2003), pp.765-776.

Loren, G. J., Shoemaker, S. D., Burkholder, T. J., Jacobson, M. D., Friden, J. and Lieber, R. L., Human wrist motors: biomechanical design and application to tendon transfers, Journal of biomechanics, Vol.29, No.3 (1996), pp.331-342.

Lowery, M. M., Stoykov, N. S. and Kuiken, T.A., A simulation study to examine the use of cross-correlation as an estimate of surface EMG cross talk. Journal of Applied Physiology, Vol. 94 (2003), pp.1324-34.

Lucas, K., On the relation between the electric disturbance in muscle and the propagation of the excited state, The Journal of physiology, Vol.39, No.3 (1909), pp.207-227.

Maier, M. A. and Hepp-Reymond, M. C., EMG activation patterns during force production in precision grip. II. Muscular synergies in the spatial and temporal domain, Experimental brain research, Vol.103, No.1 (1995), pp.123-136.

Martin, P. E., Mungiole, M., Marzke, M. W. and Longhill, J. M., The use of magnetic resonance imaging for measuring segment inertial properties, Journal of biomechanics, Vol.22, No.4 (1989), pp.367-376.

Merletti, R., Farina, D. and Gazzoni, M., The linear electrode array: a useful tool with many applications, Journal of Electromyography and Kinesiology, Vol.13, No.1 (2003), pp.37-47.

Messier, R. H., Duffy, J., Litchman, H. M., Paslay, P. R., Soechting, J. F. and Stewart, P. A., The electromyogram as a measure of tension in the human biceps and triceps muscles, International Journal of Mechanical Sciences, Vol.13, No.7 (1971), pp.585-598.

Metral, S. and Cassar, G., Relationship between force and integrated EMG activity during voluntary isometric anisotonic contraction, European journal of applied physiology and occupational physiology, Vol.46, No.2 (1981), pp.185-198.

Murray, W. M., Buchanan, T. S. and Delp, S. L., The isometric functional capacity of muscles that cross the elbow, J Biomech, Vol.33, No.8 (2000), pp.943-952.

Nakajima, Y., Yoshinari, S. and Tadano, S., Surface conduction analysis of EMG signal from forearm muscles. Proceedings of 13th International Congress on Biological and Medical Engineering, (2008), pp.1904–07.

Nakajima, Y., Yoshinari, S. and Tadano, S., An experimental model on the activity of forearm muscles using surface electromyography. Journal of Biomechanical Science and Engineering, Vol.4 (2009), pp.212-20.

Nakajima, Y., Keeratihattayakorn, S., Yoshinari, S. and Tadano, S., An EMG-CT method using multiple surface electrodes in the forearm, Journal of electromyography and kinesiology, Vol.24, No.6 (2014), pp.875-880.

Nakamura, H., Yoshida, M., Kotani, M., Akazawa, K. and Moritani, T., The application of independent component analysis to the multi-channel surface electromyographic signals for separation of motor unit action potential trains: part II-modelling interpretation, Journal of electromyography and kinesiology, Vol.14, No.4 (2004), pp.433-441.

Nene, A., Mayagoitia, R. and Veltink, P., Assessment of rectus femoris function during initial swing phase, Gait & Posture, Vol.9, No.1 (1999), pp.1-9.

Neptune, R. R., Kautz, S. A. and Hull, M. L., The effect of pedaling rate on coordination in cycling, Journal of biomechanics, Vol.30, No.10 (1997), pp.1051-1058.

Perry, J., Easterday, C. S. and Antonelli, D. J., Surface versus intramuscular electrodes for electromyography of superficial and deep muscles, Physical therapy, Vol.61, No.1 (1981), pp.7-15.

Plonsey, R., The active fiber in a volume conductor, IEEE transactions on bio-medical engineering, Vol.21, No.5 (1974), pp.371-381.

Pruim, G. J., de Jongh, H. J. and ten Bosch, J. J., Forces acting on the mandible during bilateral static bite at different bite force levels, Journal of biomechanics, Vol.13, No.9 (1980), pp.755-763.

R, L. d. N., Analysis of the distribution of the action currents of nerve in volume conductors, Studies from the Rockefeller institute for medical research. Reprints. Rockefeller Institute for Medical Research, Vol.132, (1947), pp.384-477.

Raikova, R., A general approach for modelling and mathematical investigation of the human upper limb, Journal of biomechanics, Vol.25, No.8 (1992), pp.857-867.

Ravary, B., Pourcelot, P., Bortolussi, C., Konieczka, S. and Crevier-Denoix, N., Strain and force transducers used in human and veterinary tendon and ligament biomechanical studies, Clinical biomechanics, Vol.19, No.5 (2004), pp.433-447.

Roberto, M., Marco, P. and Dario, F., Electromyography: Detection, Processing and Applications, Biomedical Technology and Devices Handbook, CRC Press, (2003).

Roeleveld, K., Sandberg, A., Stalberg, E. V. and Stegeman, D. F., Motor unit size estimation of enlarged motor units with surface electromyography, Muscle & nerve, Vol.21, No.7 (1998), pp.878-886.

Rome, L. C., Funke, R. P., Alexander, R. M., Lutz, G., Aldridge, H., Scott, F. and Freadman, M., Why animals have different muscle fibre types, Nature, Vol.335, No.6193 (1988), pp.824-827.

Sancho-Bru, J. L., Perez-Gonzalez, A., Vergara-Monedero, M. and Giurintano, D., A 3-D dynamic model of human finger for studying free movements, Journal of biomechanics, Vol.34, No.11 (2001), pp.1491-1500.

Schuind, F., Garcia-Elias, M., Cooney, W. P., 3rd and An, K. N., Flexor tendon forces: in vivo measurements, The Journal of hand surgery, Vol.17, No.2 (1992), pp.291-298.

Schutte, L. M., Using musculoskeletal models to explore strategies for improving performance in electrical stimulation-induced leg cycle ergometry. Pd.D., Stanford University, (1993).

Schwan, H. P. and Li, K., Capacity and conductivity of body tissues at ultrahigh frequencies. Proceedings of the Institute of Radio Engineers, Vol.41 (1953), pp. 1735-40.

Seireg, A. and Arvikar. The prediction of muscular lad sharing and joint forces in the lower extremities during walking, Journal of biomechanics, Vol.8, No.2 (1975), pp.89-102.

Shao, Q., Bassett, D. N., Manal, K. and Buchanan, T. S., An EMG-driven model to estimate muscle forces and joint moments in stroke patients, Comput Biol Med, Vol.39, No.12 (2009), pp.1083-1088.

Shiavi, R., Bugle, H. J. and Limbird, T., Electromyographic gait assessment, Part 1: Adult EMG profiles and walking speed, Journal of rehabilitation research and development, Vol.24, No.2 (1987), pp.13-23.

Silva, M. P. T. and Ambrósio, J. A. C., Kinematic Data Consistency in the Inverse Dynamic Analysis of Biomechanical Systems, Multibody System Dynamics, Vol.8, No.2 (2002), pp.219-239.

Stalberg, E. and Antoni, L., Electrophysiological cross section of the motor unit, Journal of neurology, neurosurgery, and psychiatry, Vol.43, No.6 (1980), pp.469-474.

Stančić, I., Musić, J. and Zanchi, V., Improved structured light 3D scanner with application to anthropometric parameter estimation, Measurement, Vol.46, No.1 (2013), pp.716-726.

Stone, R. J. and Stone, J. A., Atlas of Skeletal Muscles, McGraw-Hill, (2003).

Stoykov, N. S., Lowery, M. M., Taflove, A. and Kuiken, T. A., Frequency- and time-domain FEM models of EMG: capacitive effects and aspects of dispersion, IEEE transactions on bio-medical engineering, Vol.49, No.8 (2002), pp.763-772.

Sukumar, N., Voronoi cell finite difference method for the diffusion operator on arbitrary unstructured grids, Int J Numer Meth Eng, Vol.57, No.1 (2003), pp.1-34.

Suzuki, S., Watanabe, S. and Homma, S., EMG activity and kinematics of human cycling movements at different constant velocities, Brain research, Vol.240, No.2 (1982), pp.245-258.

Van den Herrewegen, I., Cuppens, K., Broeckx, M., Barisch-Fritz, B., Vander Sloten, J., Leardini, A. and Peeraer, L., Dynamic 3D scanning as a markerless method to calculate multi-segment foot kinematics during stance phase: methodology and first application, Journal of biomechanics, Vol.47, No.11 (2014), pp.2531-2539.

Vigouroux, L., Quaine, F., Labarre-Vila, A., Amarantini, D. and Moutet, F., Using EMG data to constrain optimization procedure improves finger tendon tension estimations during static fingertip force production, Journal of biomechanics, Vol.40, No.13 (2007), pp.2846-2856.

Walmsley, B., Hodgson, J. A. and Burke, R. E., Forces produced by medial gastrocnemius and soleus muscles during locomotion in freely moving cats, Journal of neurophysiology, Vol.41, No.5 (1978), pp.1203-1216.

White, S. C. and Winter, D. A., Predicting muscle forces in gait from EMG signals and musculotendon kinematics, Journal of Electromyography and Kinesiology, Vol.2, No.4 (1992), pp.217-231.

Winter, D. A., Fuglevand, A. J. and Archer, S. E., Crosstalk in surface electromyography: Theoretical and practical estimates, Journal of electromyography and kinesiology : official journal of the International Society of Electrophysiological Kinesiology, Vol.4, No.1 (1994), pp.15-26.

Winters, J. M. and Stark, L., Analysis of fundamental human movement patterns through the use of in-depth antagonistic muscle models, IEEE transactions on bio-medical engineering, Vol.32, No.10 (1985), pp.826-839.

Zajac, F. E., Muscle and tendon: properties, models, scaling, and application to biomechanics and motor control, Critical reviews in biomedical engineering, Vol.17, No.4 (1989), pp.359-411.

Zipp, P., Recommendations for the Standardization of Lead Positions in Surface Electromyography, Eur J Appl Physiol O, Vol.50, No.1 (1982), pp.41-54.

Acknowledgments

I would like to sincerely thank many kind people who help and support me during my graduate education.

This thesis would not have been possible without the help, support and patience of my supervisor, Professor Shigeru Tadano, Hokkaido University. I am extremely grateful for his kindness and appreciate his guidance. I would like to thank Associate Professor Masahiro Todoh, Hokkaido University, for kind advice which has been invaluable on my study. I am also thankful to Assistant Professor Satoshi Yamada, Hokkaido University, for his support and encouragement. Thank you for every useful comments and suggestions. My special thanks to Assistant Professor Ryo Takeda, Hokkaido University, for giving constructive advice during my study. My sincere thanks also go to Dr. Yasuhiro Nakajima, Hokkaido Research Organization, for his advice and inspiration. I also thank Dr. Remel Alingalan Salmingo who always support me and help me during my stay in Japan.

I wish to express my special thanks to Professor Itsuro Kajiwara, Professor Toshiro Ohashi, and Professor Yukinori Kobayashi of the Division of Human Mechanical Systems and Design, Hokkaido University for their efforts in the oral examination and for giving me many important advices that are very helpful in improving this thesis. I also would like to thank the professors who were the examiners during my defense, Professor Katsuhiko Sasaki, Professor Yoshihiro Narita, Professor Takashi Nakamura, Professor Osamu Fujita, Professor Kazutoshi Gohara, Professor Hideyuki Ogawa and Professor Michihiro Furusaka of Hokkaido University for valuable suggestions and feedbacks.

I also thank all the members in laboratory of Biomechanical Design, Dr. Hayato Suzuki and Dr. Kaori Endo for great support and friendship. I am also thankful to Mr. Yuuki Tonsho, Mr. Takashi Kurashima and Mr. Naoki Toyota for great support in EMG research team. I hope you all have a great success in

your life ahead. Special thank go to Mr. Toshiaki Takada for his technical support and Ms. Yumi Yamazaki for helping me a lot during my stay in Japan.

I want to thank all my friends who I have opportunity to meet during my stay in Japan. Living in foreign country is quite a challenge and many supports are required to pass-through. This can't be done without the support of all my friends who live in Japan. Thank you so much for making my life joyful and memorable.

I would like to acknowledge the financial support of the Monbukagakusho (MEXT) of the Japanese Government for providing me scholarship grant.

I am most grateful to my family, Dr. Chusak Keeratihattayakorn, Somchit Keeratihattayakorn and Dr. Pakorn Keeratihattayakorn for their love and absolute confidence in me. This work would be impossible without them.

Saran Keeratihattayakorn